

Supporting Materials for

Rate Constants of the Fulvenallenyl Recombination with Propargyl and Its Role in PAH Formation: A Theoretical and Kinetic Modeling Study

Alexander N. Morozov,¹ Luna Pratali Maffei,^{2*} Alexander M. Mebel,^{1*}

¹ Department of Chemistry and Biochemistry, Florida International University, Miami, Florida 33199, USA

² Department of Chemistry, Materials and Chemical Engineering “G. Natta”, Politecnico di Milano, P.zza Leonardo da Vinci 32, 20133 Milano, Italy

List of Contents

SM.pdf: detailed product branching fractions, lumped groups of isomers, results of kinetic simulations; inchiislist.txt: list of InChIs for the structures on the PES studied in this work;

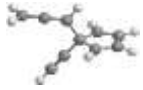
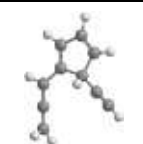
Compressed (zipped) SM folder: rates_lumped.txt, rates_pssa.txt, therm_lumped.txt: rate constants and thermochemistry in chemkin format (for details: see main text); BFs directory: temperature- and pressure-dependent branching fractions of the lumped groups of species.

* Corresponding authors. E-mail addresses: luna.pratali@polimi.it (Luna Pratali Maffei) and mebela@fiu.edu (Alexander M. Mebel).

Section S.1 T , p - dependent calculations of the rate constants and branching fractions for unimolecular reactions initiating from C_{10}H_8 wells

The results of the branching fraction calculations at $p = 1$ atm and $T = 1100, 1300$, and 1500 K for the main dissociation/isomerization reactions of the C_{10}H_8 , iR1 (head- C_3H_3 + tail- C_7H_5) adduct are shown in Table S1. The computed values of the total rate constant for the $\text{iR1} \rightarrow \text{products}$ reaction are 3.8×10^4 , 2.4×10^5 , and $7.2 \times 10^6 \text{ s}^{-1}$ at $p = 1$ atm and $T = 1100, 1300$, and 1500 K, respectively. Pressures higher than 1 atm can stabilize iR1 at T above 1500 K. For example, at 2000 K and 100 atm the computed rate constant for the $\text{iR1} \rightarrow \text{products}$ reaction is $1.2 \times 10^9 \text{ s}^{-1}$, while 99% of iR1 dissociates back to the fulvenallenyl and propargyl reactants.

Table S1. Branching fractions at pressure of 1 atm and temperatures of 1100, 1300, and 1500 K for the main dissociation/isomerization reactions of the C_{10}H_8 , iR1 (head- C_3H_3 + tail- C_7H_5) adduct.

	Reaction	Product	Branching Fraction		
			1100 K	1300 K	1500 K
R23	C_{10}H_8 , iR1 \rightarrow propargyl + fulvenallenyl	$\text{C}_3\text{H}_3 + \text{C}_7\text{H}_5$	68%	86%	92%
R24	C_{10}H_8 , iR1 \rightarrow C_{10}H_8 , fulvalene, iR9		6%	3%	2%
R25	C_{10}H_8 , iR1 \rightarrow C_{10}H_8 , iR6		6%	0%	0%
R26	C_{10}H_8 , iR1 \rightarrow C_{10}H_8 , iR7		15%	8%	6%
R27	C_{10}H_8 , iR1 \rightarrow 5-ethynyl-1-(propa-1,2-dienyl)cyclopenta-1,3-diene, C_{10}H_8 , iR15		5%	3%	0%

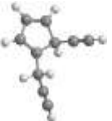
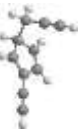
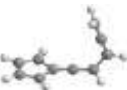
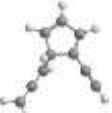
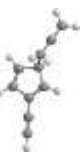
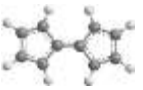
At $p = 1$ atm, the C_{10}H_8 , iR2 (head- C_3H_3 + *ipso*- C_7H_5) adduct does not stabilize collisionally at $T > 1400$ K. The computed branching fractions at $p = 1$ atm and $T = 1100$ and 1400 K for the kinetically significant dissociation/isomerization reactions of iR2 adduct are shown in Table S2. The computed values of the total rate constant for the $\text{iR2} \rightarrow \text{products}$ reaction are 3.2×10^6 , and $3.5 \times 10^7 \text{ s}^{-1}$ at $p = 1$ atm and $T = 1100$ and 1400 K, respectively. At $p = 100$ atm, iR2 can be stabilized by collisions up to 1900 K; at these conditions, the computed rate constant for the $\text{iR2} \rightarrow \text{products}$ reaction is $3.1 \times 10^9 \text{ s}^{-1}$, with 66% of the mass flowing back to the initial reactants and 19, 3, 1, and 11% converting to iR3, iR5, iR7, and iR8, respectively.

Table S2. Branching fractions at pressure of 1 atm and temperatures of 1100, and 1400 K for the main dissociation/isomerization reactions of the C₁₀H₈, iR2 (head-C₃H₃ + *ipso*-C₇H₅) adduct.

	Reaction	Product	Branching Fraction	
			1100 K	1400 K
R28	C ₁₀ H ₈ , iR2 → propargyl + fulvenallenyl	C ₃ H ₃ + C ₇ H ₅	18%	33%
R29	C ₁₀ H ₈ , iR2 → C ₁₀ H ₈ , 5-ethynyl-1-(prop-2-ynyl)cyclopenta-1,3-diene, iR14		11%	0%
R30	C ₁₀ H ₈ , iR2 → C ₁₀ H ₈ , iR3		14%	23%
R31	C ₁₀ H ₈ , iR2 → C ₁₀ H ₈ , iR5		11%	8%
R32	C ₁₀ H ₈ , iR2 → C ₁₀ H ₈ , 5-ethynyl-1-(propa-1,2-dienyl)cyclopenta-1,3-diene, iR15		1%	0%
R33	C ₁₀ H ₈ , iR2 → C ₁₀ H ₈ , iR7		3%	7%
R34	C ₁₀ H ₈ , iR2 → C ₁₀ H ₈ , iR8		42%	26%
R35	C ₁₀ H ₈ , iR2 → C ₁₀ H ₈ , fulvalene, iR9		0%	1%

At $p = 1$ atm, collisional stabilization of the C₁₀H₈, iR3 (head-C₃H₃ + *ortho*-C₇H₅) adduct is predicted up to $T = 1700$ K. The computed branching fractions at $p = 1$ atm and $T = 1100$, 1500, and 1700 K for the kinetically significant dissociation/isomerization reactions of iR3 are shown in Table S3. The rate constant for the iR3 → products reaction is 1.5×10^7 , 8.4×10^6 , and 2.5×10^7 s⁻¹ at $p = 1$ atm and $T = 1100$, 1500, and 1700 K, respectively. At $p = 100$ atm, the C₁₀H₈, iR3 is collisionally stabilized up to 2000 K and, at 2000 K and 100 atm, the rate constant for iR3 → products is 6×10^8 s⁻¹, with 72% of the mass dissociating back to the initial reactants and 20, 2, 1, and 7% isomerizing to iR4, iR5, iR7, and iR8, respectively.

Table S3. Branching fractions at pressure of 1 atm and temperatures of 1100, 1500, and 1700 K for the main dissociation/isomerization reactions of the C₁₀H₈, iR3 (head-C₃H₃ + *ortho*-C₇H₅) adduct.

	Reaction	Product	Branching Fraction		
			1100 K	1500 K	1700 K
R36	C ₁₀ H ₈ , iR3 → propargyl + fulvenallenyl	C ₃ H ₃ + C ₇ H ₅	0%	48%	62%
R37	C ₁₀ H ₈ , iR3 → C ₁₀ H ₈ , 5-ethynyl-1-(prop-2-ynyl)cyclopenta-1,3-diene, iR14		99.5%	0%	0%
R38	C ₁₀ H ₈ , iR3 → C ₁₀ H ₈ , iR4		0%	24%	19%
R39	C ₁₀ H ₈ , iR3 → C ₁₀ H ₈ , iR5		0%	7%	4%
R40	C ₁₀ H ₈ , iR3 → C ₁₀ H ₈ , iR7		0%	8%	16%
R41	C ₁₀ H ₈ , iR3 → C ₁₀ H ₈ , iR8		0%	12%	10%
R42	C ₁₀ H ₈ , iR3 → C ₁₀ H ₈ , fulvalene, iR9		0%	1%	1%

At $p = 1$ atm, the calculations predict collisional stabilization of the C₁₀H₈, iR4 (head-C₃H₃ + *meta*-C₇H₅) adduct up to $T = 1700$ K. The calculated branching ratios at $p = 1$ atm and $T = 1100$, 1500, and 1700 K for kinetically significant dissociation/isomerization reactions of iR4 are collected in Table S4. The total rate constant for the consumption of iR4 was estimated at 1.3×10^5 , 9.1×10^6 , and 2.7×10^7 s⁻¹ at $p = 1$ atm and $T = 1100$, 1500, and 1700 K, respectively. At $p = 100$ atm the C₁₀H₈, iR4 adduct can be collisionally stabilized up to 2000 K, with the computed rate constant for iR4 decomposition of 6.7×10^8 s⁻¹, where 59% of the mass dissociates back to the initial reactants and 22, 15, and 5% proceed to iR3, iR7, and iR8, respectively.

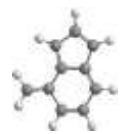
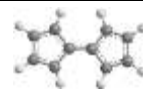
Table S4. Branching fractions at pressure of 1 atm and temperatures of 1100, 1500, and 1700 K for the main dissociation/isomerization reactions of the C₁₀H₈, iR4 (head-C₃H₃ + *meta*-C₇H₅) adduct.

	Reaction	Product	Branching Fraction		
			1100 K	1500 K	1700 K
R43	$\text{C}_{10}\text{H}_8, \text{iR4} \rightarrow \text{propargyl} + \text{fulvenallenyl}$	$\text{C}_3\text{H}_3 + \text{C}_7\text{H}_5$	8%	34%	47%
R44	$\text{C}_{10}\text{H}_8, \text{iR4} \rightarrow \text{C}_{10}\text{H}_8, 5\text{-ethynyl-1-(prop-2-ynyl)cyclopenta-1,3-diene, iR14}$		10%	0%	0%
R45	$\text{C}_{10}\text{H}_8, \text{iR4} \rightarrow \text{C}_{10}\text{H}_8, \text{iR3}$		16%	23%	20%
R46	$\text{C}_{10}\text{H}_8, \text{iR4} \rightarrow \text{C}_{10}\text{H}_8, \text{iR6}$		4%	0%	0%
R47	$\text{C}_{10}\text{H}_8, \text{iR4} \rightarrow \text{C}_{10}\text{H}_8, 5\text{-ethynyl-1-(propa-1,2-dienyl)cyclopenta-1,3-diene, iR15}$		10%	0%	0%
R48	$\text{C}_{10}\text{H}_8, \text{iR4} \rightarrow \text{C}_{10}\text{H}_8, \text{iR7}$		29%	28%	32%
R49	$\text{C}_{10}\text{H}_8, \text{iR4} \rightarrow \text{C}_{10}\text{H}_8, \text{iR8}$		23%	13%	0%

At $p = 1$ atm, collisional stabilization of the $\text{C}_{10}\text{H}_8, \text{iR5}$ (tail- $\text{C}_3\text{H}_3 +$ tail- C_7H_5) adduct can occur up to $T = 1800$ K. The calculated branching fractions at $p = 1$ atm and $T = 1000, 1400$, and 1800 K for the kinetically significant dissociation/isomerization reactions of iR5 are shown in Table S5. The total rate constant for the $\text{iR5} \rightarrow \text{products}$ reaction was estimated at $1.9 \times 10^5, 6.8 \times 10^6$, and $2.9 \times 10^7 \text{ s}^{-1}$ at 1 atm and 1100, 1500, and 1800 K, respectively. At $p = 100$ atm the iR5 can collisionally stabilize up to 2250 K. At $T = 2250$ K and $p = 100$ atm, the rate constant for iR5 consumption is $1.7 \times 10^9 \text{ s}^{-1}$, with 93% of the mass dissociating back to the fulvenallenyl + propargyl, 6% isomerizing to fulvalene, and 1% going to iR4.

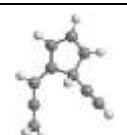
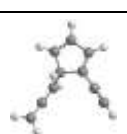
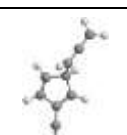
Table S5. Branching fractions at pressure of 1 atm and temperatures of 1100, 1500, and 1800 K for the main dissociation/isomerization reactions of the $\text{C}_{10}\text{H}_8, \text{iR5}$ (tail- $\text{C}_3\text{H}_3 +$ tail- C_7H_5) adduct.

	Reaction	Product	Branching Fraction		
			1100 K	1500 K	1800 K

R50	$\text{C}_{10}\text{H}_8, \text{iR5} \rightarrow \text{propargyl} + \text{fulvenallenyl}$	$\text{C}_3\text{H}_3 + \text{C}_7\text{H}_5$	1%	23%	48%
R51	$\text{C}_{10}\text{H}_8, \text{iR5} \rightarrow \text{C}_{10}\text{H}_8, 4\text{-methylene-4H-indene, iR13}$		3%	4%	3%
R52	$\text{C}_{10}\text{H}_8, \text{iR5} \rightarrow \text{C}_{10}\text{H}_8, \text{fulvalene, iR9}$		95%	72%	48%

At $p = 1$ atm, the $\text{C}_{10}\text{H}_8, \text{iR6}$ (tail- $\text{C}_3\text{H}_3 + ipso\text{-C}_7\text{H}_5$) adduct cannot be collision-stabilized at T above 1100 K. The computed branching fractions at $p = 1$ atm and $T = 1100$ K for the kinetically significant dissociation/isomerization reactions of iR6 are presented in Table S6. The computed value of the total rate constant for the $\text{iR6} \rightarrow \text{products}$ reaction is $4.8 \times 10^7 \text{ s}^{-1}$ at $p = 1$ atm and $T = 1100$ K. At $p = 100$ atm the $\text{C}_{10}\text{H}_8, \text{iR6}$ adduct can be stabilized by collisions up to 1800 K. At 1800 K and 100 atm, the computed rate constant for the $\text{iR6} \rightarrow \text{products}$ reaction is $4.5 \times 10^9 \text{ s}^{-1}$, with 5% of the mass going back to the fulvenallenyl and propargyl reactants and 1, 2, 14, 75, and 2% proceeding to iR1, iR4, 5-ethynyl-1-(propa-1,2-dienyl)cyclopenta-1,3-diene, iR7, and iR8, respectively.

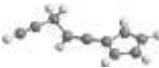
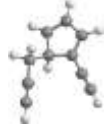
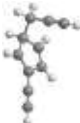
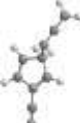
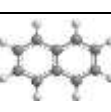
Table S6. Branching fractions at pressure of 1 atm and temperature of 1100 K for the main dissociation/isomerization reactions of the $\text{C}_{10}\text{H}_8, \text{iR6}$ (tail- $\text{C}_3\text{H}_3 + ipso\text{-C}_7\text{H}_5$) adduct.

	Reaction	Product	Branching Fraction
			1100 K
R53	$\text{C}_{10}\text{H}_8, \text{iR6} \rightarrow \text{propargyl} + \text{fulvenallenyl}$	$\text{C}_3\text{H}_3 + \text{C}_7\text{H}_5$	0%
R54	$\text{C}_{10}\text{H}_8, \text{iR6} \rightarrow \text{C}_{10}\text{H}_8, 5\text{-ethynyl-1-(propa-1,2-dienyl)cyclopenta-1,3-diene, iR15}$		11%
R55	$\text{C}_{10}\text{H}_8, \text{iR6} \rightarrow \text{C}_{10}\text{H}_8, \text{iR7}$		87%
R56	$\text{C}_{10}\text{H}_8, \text{iR6} \rightarrow \text{C}_{10}\text{H}_8, \text{iR8}$		2%

At $p = 1$ atm, collisional stabilization of the $\text{C}_{10}\text{H}_8, \text{iR7}$ (tail- $\text{C}_3\text{H}_3 + ortho\text{-C}_7\text{H}_5$) adduct is predicted to be possible up to $T = 1800$ K. The computed branching ratios at $p = 1$ atm and $T = 1100, 1500$, and

1800 K for the kinetically significant dissociation/isomerization reactions of iR7 are shown in Table S7. The computed rate constant for the decomposition/isomerization of iR7 is 5.5×10^6 , 1.1×10^7 , and 1.9×10^7 s⁻¹ at $p = 1$ atm and $T = 1100$, 1500 , and 1800 K, respectively. At $p = 100$ atm the iR7 can be collisionally stabilized up to 2500 K and at 2500 K and 100 atm the rate constant for the iR3 → products reaction is 1.9×10^9 s⁻¹, with nearly entire mass flow dissociating back to the initial reactants.

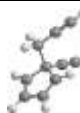
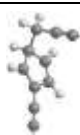
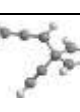
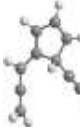
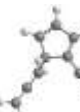
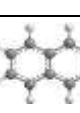
Table S7. Branching fractions at pressure of 1 atm and temperatures of 1100, 1500, and 1800 K for the main dissociation/isomerization reactions of the C₁₀H₈, iR7 (tail-C₃H₃ + *ortho*-C₇H₅) adduct.

	Reaction	Product	Branching Fraction		
			1100 K	1500 K	1800 K
R57	C ₁₀ H ₈ , iR7 → propargyl + fulvenallenyl	C ₃ H ₃ + C ₇ H ₅	0%	18%	95%
R58	C ₁₀ H ₈ , iR7 → C ₁₀ H ₈ , iR1		0%	2%	0%
R59	C ₁₀ H ₈ , iR7 → C ₁₀ H ₈ , iR3		0%	2%	0%
R60	C ₁₀ H ₈ , iR7 → C ₁₀ H ₈ , iR4		0%	6%	0%
R61	C ₁₀ H ₈ , iR7 → C ₁₀ H ₈ , iR6		11%	0%	0%
R62	C ₁₀ H ₈ , iR7 → C ₁₀ H ₈ , 5-ethynyl-1-(prop-1-en-1-yl)cyclopenta-1,3-diene, iR15		81%	0%	0%
R63	C ₁₀ H ₈ , iR7 → C ₁₀ H ₈ , 5-methylene-5H-indene		0%	2%	2.5%
R64	C ₁₀ H ₈ , iR7 → C ₁₀ H ₈ , iR8		7%	66%	0%
R65	C ₁₀ H ₈ , iR7 → C ₁₀ H ₈ , naphthalene, iR10		0%	2%	2.5%

At $p = 1$ atm, the calculations predict collisional stabilization of the C₁₀H₈, iR8 (tail-C₃H₃ + *meta*-

C_7H_5) adduct up to $T = 1600$ K. The branching ratios at $p = 1$ atm and $T = 1100, 1500$, and 1600 K for the dissociation/isomerization reactions of iR8 are illustrated in Table S8. The total rate constant for the $\text{iR8} \rightarrow \text{products}$ reaction was estimated at $8.7 \times 10^5, 2.0 \times 10^7$, and $3.2 \times 10^7 \text{ s}^{-1}$ at $p = 1$ atm and $T = 1100, 1500$, and 1600 K, respectively. At $p = 100$ atm, iR8 can be collisionally stabilized up to 2250 K. At $T = 2250$ K and $p = 100$ atm the rate constant for the $\text{iR8} \rightarrow \text{products}$ reaction is $2.0 \times 10^9 \text{ s}^{-1}$, with 58% of the mass dissociating back to the initial reactants and 3, 2, and 37% going to iR2, iR3, and iR7, respectively.

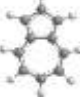
Table S8. Branching fractions at pressure of 1 atm and temperatures of 1100, 1500, and 1600 K for the main dissociation/isomerization reactions of the C_{10}H_8 , iR8 (tail- $\text{C}_3\text{H}_3 + meta\text{-C}_7\text{H}_5$) adduct.

	Reaction	Product	Branching Fraction		
			1100 K	1500 K	1600 K
R66	$\text{C}_{10}\text{H}_8, \text{iR8} \rightarrow \text{propargyl} + \text{fulvenallenyl}$	$\text{C}_3\text{H}_3 + \text{C}_7\text{H}_5$	0%	15%	19%
R67	$\text{C}_{10}\text{H}_8, \text{iR8} \rightarrow \text{C}_{10}\text{H}_8, \text{iR2}$		2%	0%	0%
R68	$\text{C}_{10}\text{H}_8, \text{iR8} \rightarrow \text{C}_{10}\text{H}_8, \text{iR3}$		1%	3%	4%
R69	$\text{C}_{10}\text{H}_8, \text{iR8} \rightarrow \text{C}_{10}\text{H}_8, \text{iR4}$		2%	4%	4%
R70	$\text{C}_{10}\text{H}_8, \text{iR8} \rightarrow \text{C}_{10}\text{H}_8, \text{iR6}$		2%	0%	0%
R71	$\text{C}_{10}\text{H}_8, \text{iR8} \rightarrow \text{C}_{10}\text{H}_8, 5\text{-ethynyl-1-(propa-1,2-dienyl)cyclopenta-1,3-diene, iR15}$		17%	0%	0%
R72	$\text{C}_{10}\text{H}_8, \text{iR8} \rightarrow \text{C}_{10}\text{H}_8, \text{iR7}$		76%	78%	73%
R73	$\text{C}_{10}\text{H}_8, \text{iR8} \rightarrow \text{C}_{10}\text{H}_8, \text{naphthalene, iR10}$		0%	0.5%	0.5%

The calculations predicted that at $p = 1$ atm the collisional stabilization of C_{10}H_8 , 4-methylene-4H-indene is possible up to 2500 K. At $p = 1$ atm and $T = 1500, 2000$, and 2500 K the total rate constant

for the 4-methylene-4H-indene → products reaction was estimated at 2.7×10^2 , 1.2×10^5 , and 2.8×10^6 s⁻¹. The predicted rate constants for the unimolecular dissociation/isomerization reactions of this molecule are too small below 1500 K to be of interest for kinetic modeling at combustion conditions. The calculated branching fractions at $p = 1$ atm and $T = 1500$, 2000, and 2500 K for the kinetically significant dissociation/isomerization reactions of 4-methylene-4H-indene is shown in Table S9. At $p = 100$ atm and $T = 2000$ K, the total rate constant for the consumption of 4-methylene-4H-indene is 1.5×10^5 s⁻¹, with 96% of the mass converting to azulene and 2 and 1% isomerizing to iR5 and 5-methylene-5H-indene, respectively.

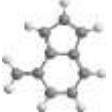
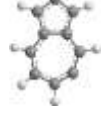
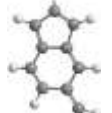
Table S9. Branching fractions at pressure of 1 atm and temperatures of 1500, 2000, and 2500 K for the main dissociation/isomerization reactions of C₁₀H₈, 4-methylene-4H-indene.

	Reaction	Product	Branching Fraction		
			1500 K	2000 K	2500 K
R74	C ₁₀ H ₈ , 4-methylene-4H-indene, iR13 → propargyl + fulvenallenyl	C ₃ H ₃ + C ₇ H ₅	0%	2.5%	6.5%
R75	C ₁₀ H ₈ , 4-methylene-4H-indene, iR13 → C ₁₀ H ₈ , 5-methylene-5H-indene, iR12		1%	13%	23%
R76	C ₁₀ H ₈ , 4-methylene-4H-indene, iR13 → C ₁₀ H ₈ , azulene, iR11		98.5%	76.5%	38%
R77	C ₁₀ H ₈ , 4-methylene-4H-indene, iR13 → C ₁₀ H ₇ + H, b20		0%	4%	16%
R78	C ₁₀ H ₈ , 4-methylene-4H-indene, iR13 → C ₁₀ H ₇ + H, b21		0%	3%	13.5%
R79	C ₁₀ H ₈ , 4-methylene-4H-indene, iR13 → C ₁₀ H ₇ + H, b22		0%	0%	2%

At $p = 1$ atm, the collisional stabilization of 5-methylene-5H-indene is possible up to $T = 2500$ K. At $p = 1$ atm and $T = 1500$, 2000, and 2500 K the total rate constant for the 5-methylene-5H-indene → products reaction was estimated at 1.3×10^2 , 9.4×10^4 , and 2.5×10^6 s⁻¹, respectively. The rate constants for the unimolecular dissociation/isomerization reactions of 5-methylene-5H-indene below 1500 K

are below 10^2 s⁻¹, which is too slow to be of interest in kinetic modeling at combustion conditions. The calculated branching fractions at $p = 1$ atm and $T = 1500$, 2000, and 2500 K for the dissociation/isomerization reactions of 5-methylene-5H-indene are shown in Table S10. At $p = 100$ atm and $T = 2000$ K, the computed rate constant for the 5-methylene-5H-indene → products reaction is 1.3×10^5 s⁻¹, with 92.5 % of the mass converting to azulene and 3, 0.5, 1.5, and 2.5% isomerizing to (Z)-1-allylidene-2-ethynylcyclopentane, 4-methylene-4H-indene, iR7, and b22, respectively.

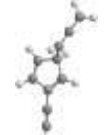
Table S10. Branching fractions at pressure of 1 atm and temperatures of 1500, 2000, and 2500 K for the main dissociation/isomerization reactions of C₁₀H₈, 5-methylene-5H-indene.

	Reaction	Product	Branching Fraction		
			1500 K	2000 K	2500 K
R80	C ₁₀ H ₈ , 5-methylene-5H-indene, iR12 → propargyl + fulvenallenyl	C ₃ H ₃ + C ₇ H ₅	0%	2%	5%
R81	C ₁₀ H ₈ , 5-methylene-5H-indene, iR12 → C ₁₀ H ₈ , 4-methylene-4H-indene		0.5%	10%	16%
R82	C ₁₀ H ₈ , 5-methylene-5H-indene, iR12 → C ₁₀ H ₈ , azulene, iR11		98%	76.5%	39%
R83	C ₁₀ H ₈ , 5-methylene-5H-indene, iR12 → C ₁₀ H ₇ + H, b20		0%	4%	15%
R84	C ₁₀ H ₈ , 5-methylene-5H-indene, iR12 → C ₁₀ H ₇ + H, b21		0%	3%	13%
R85	C ₁₀ H ₈ , 5-methylene-5H-indene, iR12 → C ₁₀ H ₇ + H, b22		0%	2%	7%

At $p = 1$ atm, collisional stabilization of C₁₀H₈, 5-ethynyl-1-(propa-1,2-dienyl)cyclopenta-1,3-diene can persist up to $T = 1300$ K. This intermediate is predicted to undergo isomerization back to the entrance channel adducts, mainly to iR7. The computed rate constant for the 5-ethynyl-1-(propa-1,2-dienyl)cyclopenta-1,3-diene → products reaction is 1.0×10^7 , 2.1×10^7 , and 3.7×10^7 s⁻¹ at $p = 1$ atm and $T = 1100$, 1200, and 1300 K, respectively. The branching fractions at $p = 1$ atm and $T = 1100$,

1200, and 1300 K for the kinetically significant dissociation/isomerization reactions of 5-ethynyl-1-(propa-1,2-dienyl)cyclopenta-1,3-diene are shown in Table S11. At $p = 100$ atm, 5-ethynyl-1-(propa-1,2-dienyl)cyclopenta-1,3-diene can be collisionally stabilized up to 1900 K and at 1900 K and 100 atm the rate constant for the 5-ethynyl-1-(propa-1,2-dienyl)cyclopenta-1,3-diene → products reaction is 2.1×10^9 s⁻¹, with 4% of the mass dissociating back to the initial reactants and 92 and 3% going to iR7, and iR8, respectively.

Table S11. Branching fractions at pressure of 1 atm and temperatures of 1100, 1200, and 1300 K for the main isomerization reactions of C₁₀H₈, 5-ethynyl-1-(propa-1,2-dienyl)cyclopenta-1,3-diene.

	Reaction	Product	Branching Fraction		
			1100 K	1200 K	1300 K
R86	C ₁₀ H ₈ , 5-ethynyl-1-(propa-1,2-dienyl)cyclopenta-1,3-diene, iR15 → C ₁₀ H ₈ , iR6		1.5%	0%	0%
R87	C ₁₀ H ₈ , 5-ethynyl-1-(propa-1,2-dienyl)cyclopenta-1,3-diene, iR15 → C ₁₀ H ₈ , iR7		96%	96%	94%
R88	C ₁₀ H ₈ , 5-ethynyl-1-(propa-1,2-dienyl)cyclopenta-1,3-diene, iR15 → C ₁₀ H ₈ , iR8		2%	3%	5%

The calculations showed that at $p = 1$ atm C₁₀H₈, 5-ethynyl-1-(prop-2-ynyl)cyclopenta-1,3-diene cannot be collisionally stabilized above 1100 K. The computed branching ratios at $p = 1$ atm and $T = 1100$ K for the dissociation/isomerization reactions of 5-ethynyl-1-(prop-2-ynyl)cyclopenta-1,3-diene are shown in Table S12. The computed value of the total rate constant for the 5-ethynyl-1-(prop-2-ynyl)cyclopenta-1,3-diene → products reaction is 3.1×10^7 s⁻¹ at $p = 1$ atm and $T = 1100$ K. At 100 atm, 5-ethynyl-1-(prop-2-ynyl)cyclopenta-1,3-diene can be collisionally stabilized up to 1600 K. The total rate constant at 1600 K and 100 atm for the 5-ethynyl-1-(prop-2-ynyl)cyclopenta-1,3-diene → products reaction is 2.3×10^9 s⁻¹, with 1% of the mass going back to the fulvenallenyl and propargyl reactants and 0.5, 98, and 0.5% to iR2, iR3, and iR4, respectively. Thus, 5-ethynyl-1-(prop-2-ynyl)cyclopenta-1,3-diene predominantly isomerizes to the iR3 adduct.

Table S12. Branching fractions at pressure of 1 atm and temperature of 1100 K for the main

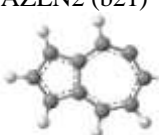
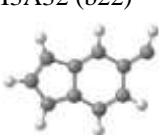
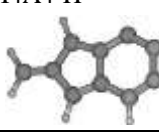
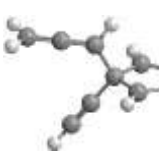
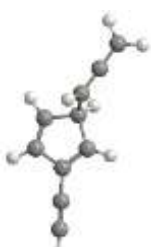
dissociation/isomerization reactions of C₁₀H₈, 5-ethynyl-1-(prop-2-ynyl)cyclopenta-1,3-diene.

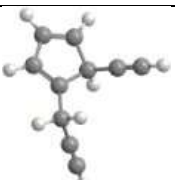
	Reaction	Product	Branching Fraction
			1100 K
R89	C ₁₀ H ₈ , 5-ethynyl-1-(prop-2-ynyl)cyclopenta-1,3-diene, iR14 → C ₁₀ H ₈ , iR2		0.1%
R90	C ₁₀ H ₈ , 5-ethynyl-1-(prop-2-ynyl)cyclopenta-1,3-diene, iR14 → C ₁₀ H ₈ , iR3		99.5%
R91	C ₁₀ H ₈ , 5-ethynyl-1-(prop-2-ynyl)cyclopenta-1,3-diene, iR14 → C ₁₀ H ₈ , iR4		0.2%

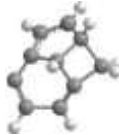
Section S.2 Lumped groups of species

Table S13: structures of lumped groups of species from C₇H₅ + C₃H₃ PES and corresponding InChIs.

Lumped name	Structures (as in PES and mess input; for bimolecular products: names correspond to fragment names in mess input file; bimol species in parentheses)	InChIs
C10H7	C10H7-1 (b18) 	InChI=1S/C10H7/c1-2-6-10-8-4-3-7-9(10)5-1/h1-7H
	C10H7-2 (b19) 	InChI=1S/C10H7/c1-2-6-10-8-4-3-7-9(10)5-1/h1-3,5-8H
FLV	FLV1 (b16) 	InChI=1S/C10H7/c1-2-6-9(5-1)10-7-3-4-8-10/h1-7H
	FLV2 (b17) 	InChI=1S/C10H7/c1-2-6-9(5-1)10-7-3-4-8-10/h1-3,5-8H
AZL	AZLN1 (b20)	InChI=1S/C10H7/c1-2-5-9-7-4-8-10(9)6-3-1/h1-5,7-8H

		
	AZLN2 (b21) 	InChI=1S/C10H7/c1-2-5-9-7-4-8-10(9)6-3-1/h1-2,4-8H
meth4Hind-H	I3A32 (b22) 	InChI=1S/C10H7/c1-8-5-6-9-3-2-4-10(9)7-8/h1-7H
meth2Hind-H	I4A4-H 	InChI=1S/C10H7/c1-8-6-9-4-2-3-5-10(9)7-8/h2-4,6-7H,1H2
C5H4C2HC3H3-p	iR7  iR6  iR15  iR8 	InChI=1S/C10H8/c1-3-6-10-8-5-7-9(10)4-2/h2,5-8,10H,1H2 InChI=1S/C10H8/c1-3-6-10-8-5-7-9(10)4-2/h2,5-9H,1H2 InChI=1S/C10H8/c1-3-7-10(4-2)8-5-6-9-10/h2,5-9H,1H2 InChI=1S/C10H8/c1-3-5-10-7-6-9(4-2)8-10/h2,5-8,10H,1H2
C5H4C2HC3H3-a1	iR14	InChI=1S/C10H8/c1-3-6-10-8-5-7-9(10)4-2/h1-2,5,7-9H,6H2

	 iR3  iR2 	InChI=1S/C10H8/c1-3-6-10-8-5-7-9(10)4-2/h1-2,5,7-8,10H,6H2 InChI=1S/C10H8/c1-3-7-10(4-2)8-5-6-9-10/h1-2,5-6,8-9H,7H2
C5H4C2HC3H3-a2	iR4 	InChI=1S/C10H8/c1-3-5-10-7-6-9(4-2)8-10/h1-2,6-8,10H,5H2
C5H4C5H4-p	iR5  i2  I5c2 	InChI=1S/C10H8/c1-2-3-4-7-10-8-5-6-9-10/h3-6,8-9H,1H2 InChI=1S/C10H8/c1-8-4-2-5-9-6-3-7-10(8)9/h2-4,6-7,10H,1H2 InChI=1S/C10H8/c1-2-7-4-5-9-6-8(3-1)10(7)9/h1,3-5,9-10H,6H2

		
C5H4C5H4-a	iR1  i3B 	InChI=1S/C10H8/c1-2-3-4-7-10-8-5-6-9-10/h1,4-6,8-9H,3H2 InChI=1S/C10H8/c1-2-6-9(5-1)10-7-3-4-8-10/h1-2,5-8H,3H2
5-methylene-5H-indene	iR13 	InChI=1S/C10H8/c1-8-4-2-5-9-6-3-7-10(8)9/h2-7H,1H2
4-methylene-4H-indene	iR12 	InChI=1S/C10H8/c1-8-5-6-9-3-2-4-10(9)7-8/h2-7H,1H2
2-methylene-2H-indene	i12 	InChI=1S/C10H8/c1-8-6-9-4-2-3-5-10(9)7-8/h2-7H,1H2
FULVALENE	fulvalene (iR9) 	InChI=1S/C10H8/c1-2-6-9(5-1)10-7-3-4-8-10/h1-8H
C10H8	naphthalene (iR10) 	InChI=1S/C10H8/c1-2-6-10-8-4-3-7-9(10)5-1/h1-8H

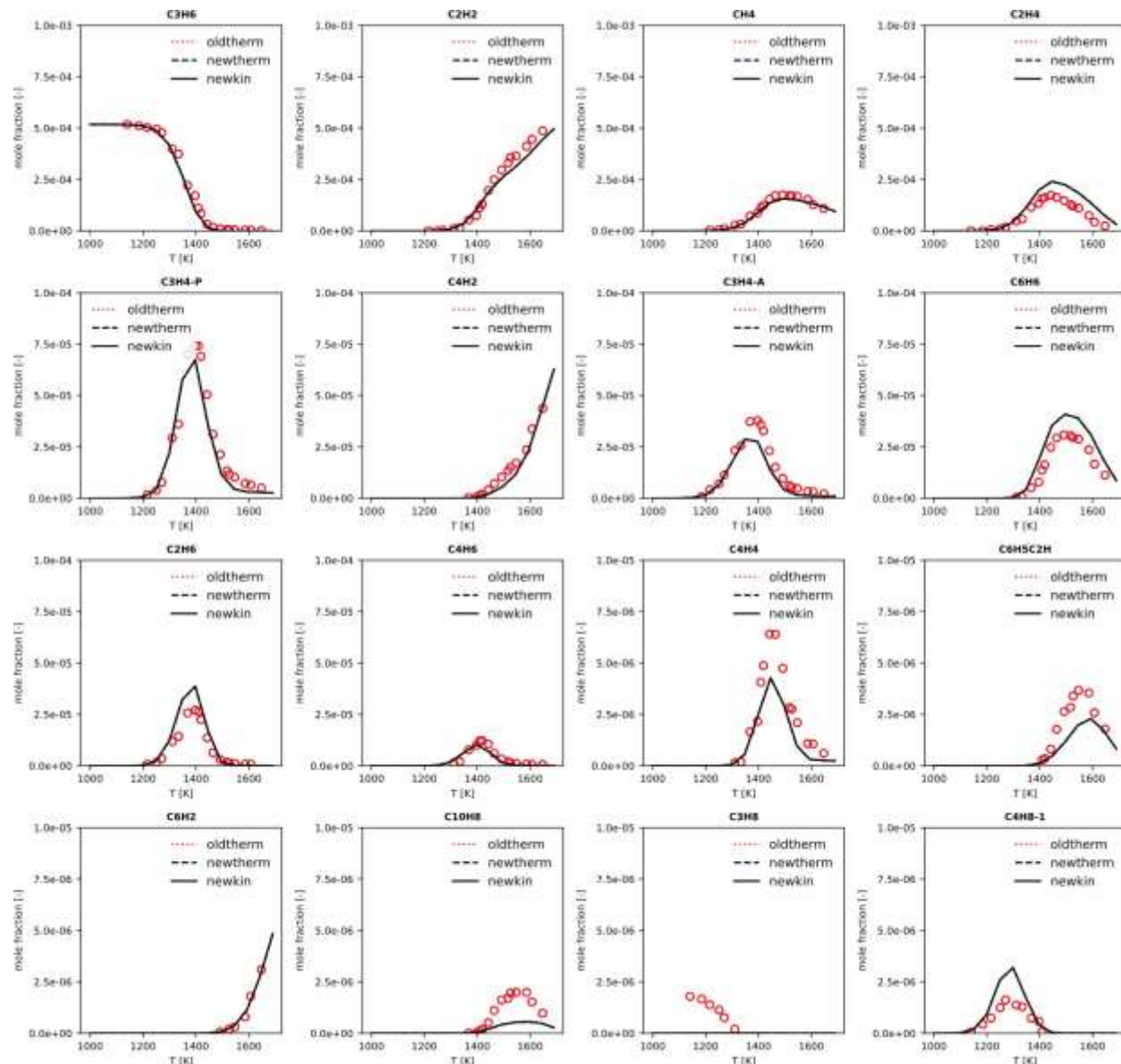
AZULENE	azulene (iR11) 	InChI=1S/C10H8/c1-2-5-9-7-4-8-10(9)6-3-1/h1-8H
---------	---	--

Section S.3 Kinetic simulations

Kinetic simulations of flow reactor and flames as listed in the tables in the main text. Figure headers report the reactor conditions and references according to the following layout:

Inlet	Reactor type	T [K]	P [atm]	ϕ	Reference
-------	--------------	-------	---------	--------	-----------

C3H4-P C3H6	ST	1000-1700	20	Inf	Sun et al. ¹
----------------	----	-----------	----	-----	-------------------------



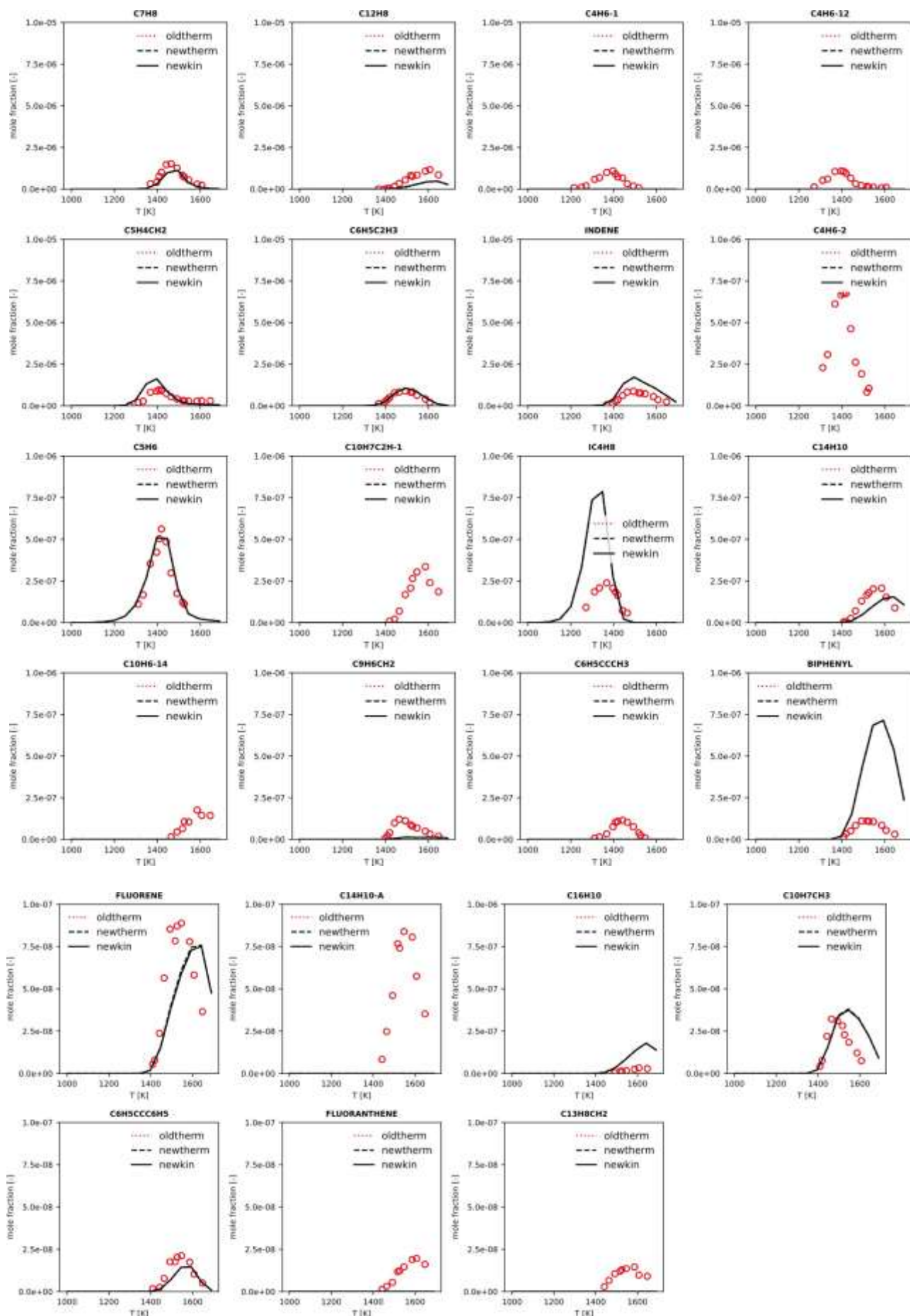
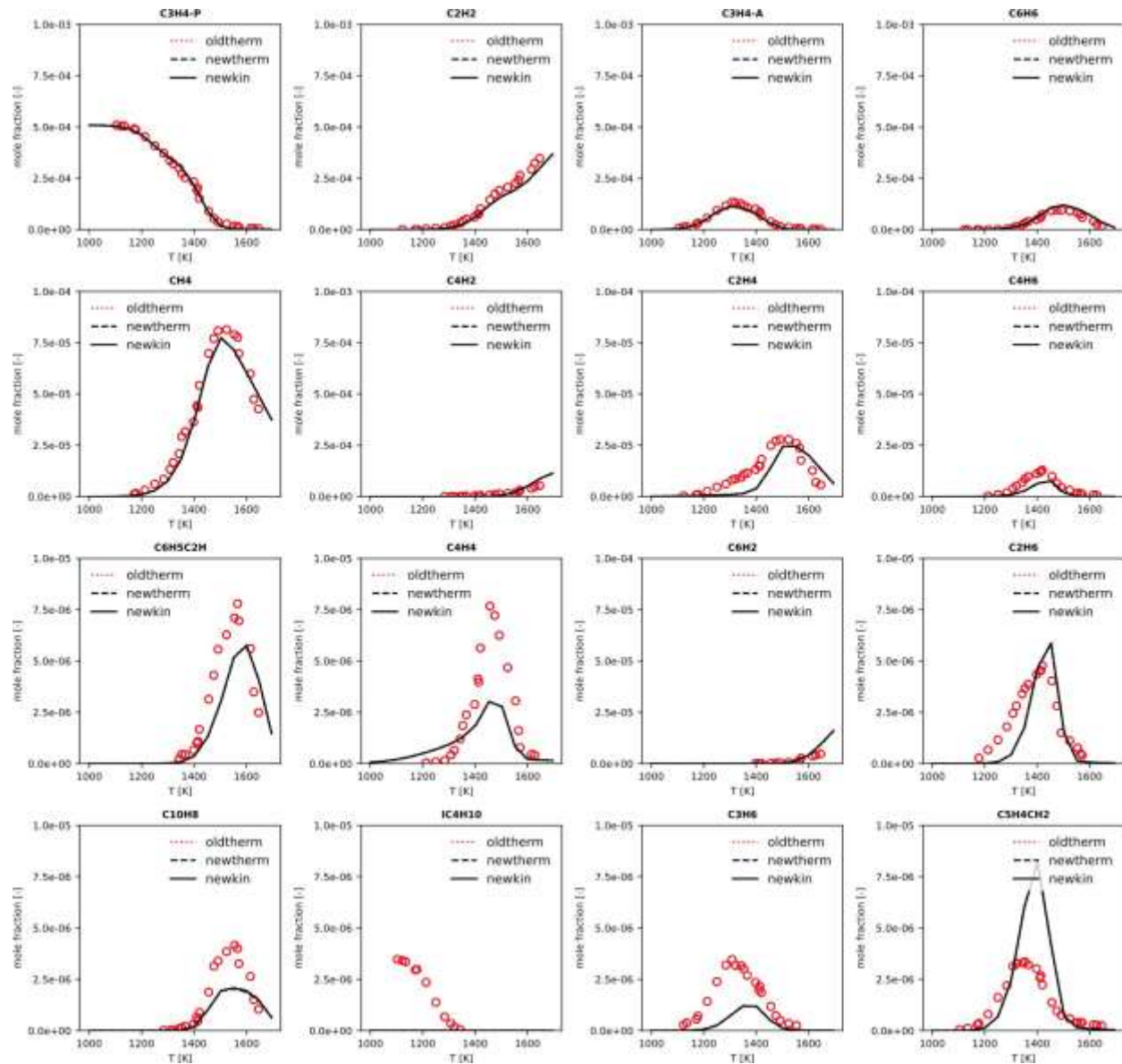
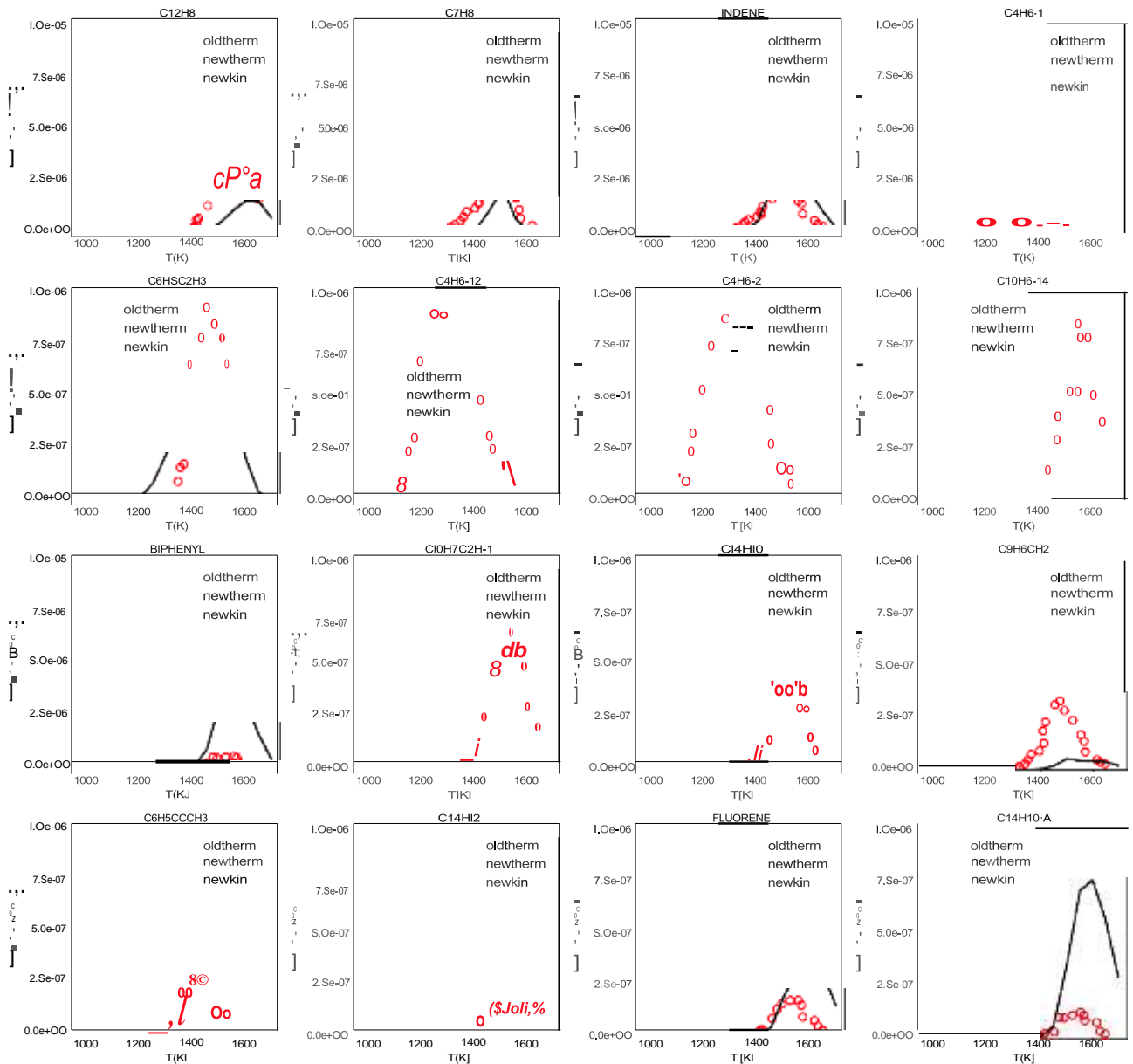


Figure S1: Experimental (points) and simulated (lines) mole fraction profiles of relevant detected products in the propene pyrolysis experiments of Sun et al.¹. Dotted red lines: starting model (oldtherm), dashed black lines: updated thermochemistry (newtherm), solid black lines: final model with updated kinetics (newkin). *plot generated automatically with SciExpeM post-processing tools.





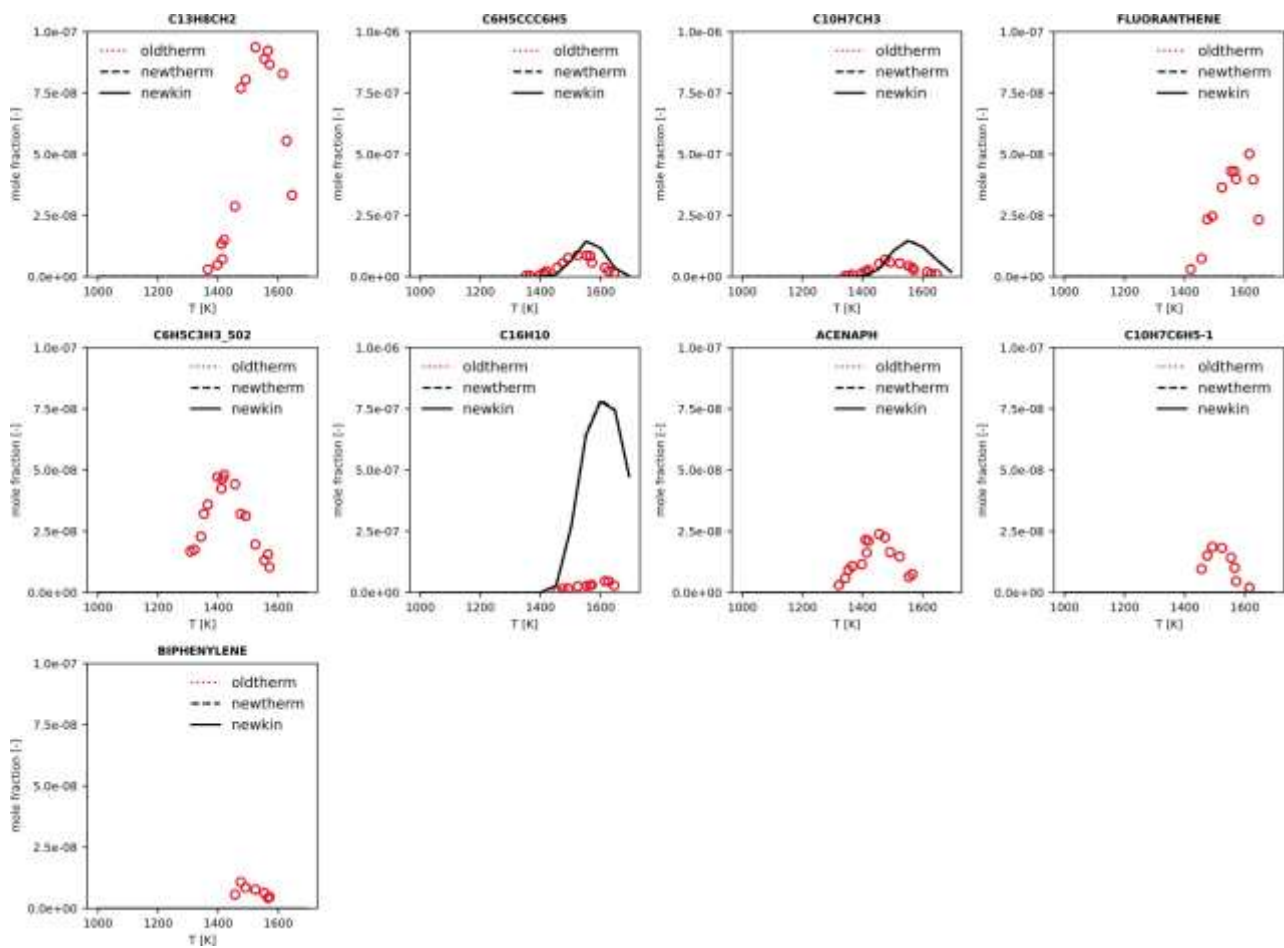


Figure S2: Experimental (points) and simulated (lines) mole fraction profiles of relevant detected products in the propyne pyrolysis experiments of Sun et al.¹. Dotted red lines: starting model (oldtherm), dashed black lines: updated thermochemistry (newtherm), solid black lines: final model with updated kinetics (newkin). *plot generated automatically with SciExpeM post-processing tools.

C5H6/C2H4	PFR	900-1200	1.7	inf	Vervust et al. ²
-----------	-----	----------	-----	-----	-----------------------------

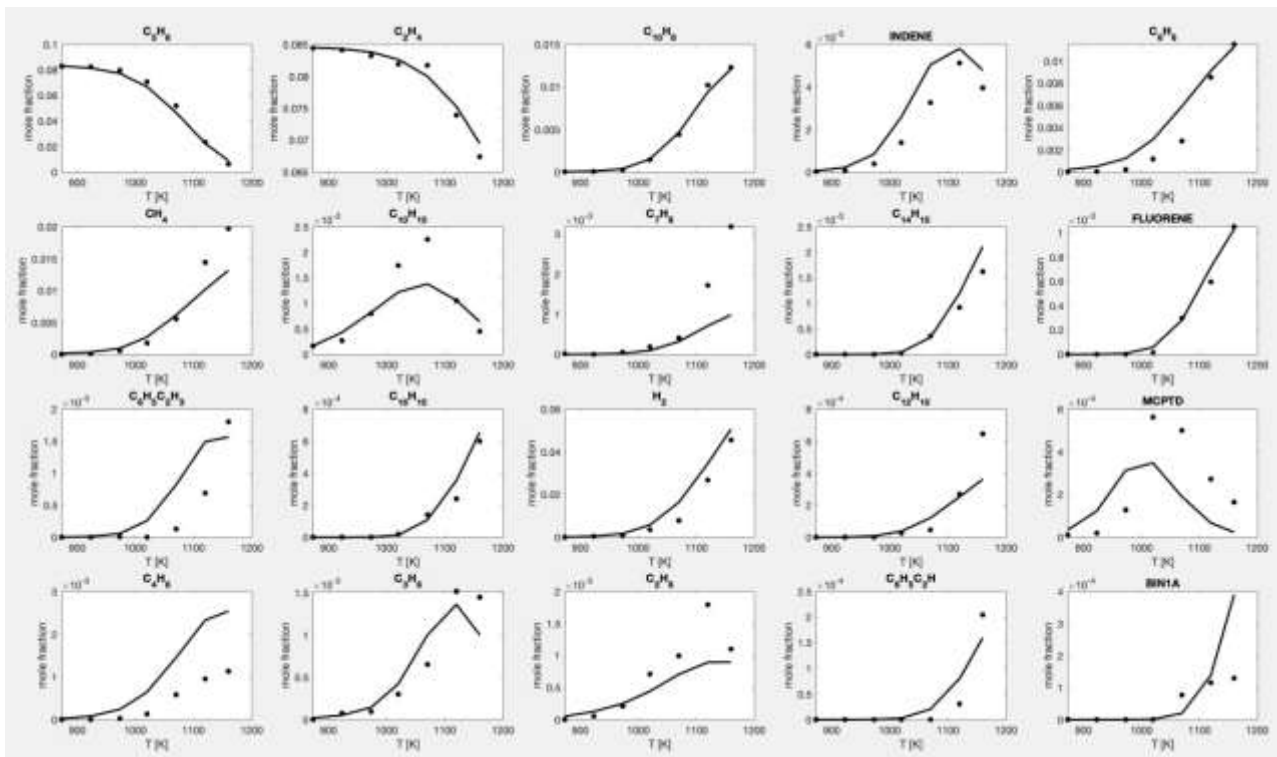


Figure S3: Experimental (points) and simulated (lines) mole fraction profiles of relevant detected products in the ethylene-doped cyclopentadiene pyrolysis experiments of Vervust et al.². Dotted red lines: starting model (oldtherm), dashed black lines: updated thermochemistry (newtherm), solid black lines: final model with updated kinetics (newkin)

C5H6	PFR	850-1150	1.7, 2.7	inf	Djokic et al. ³
------	-----	----------	----------	-----	----------------------------

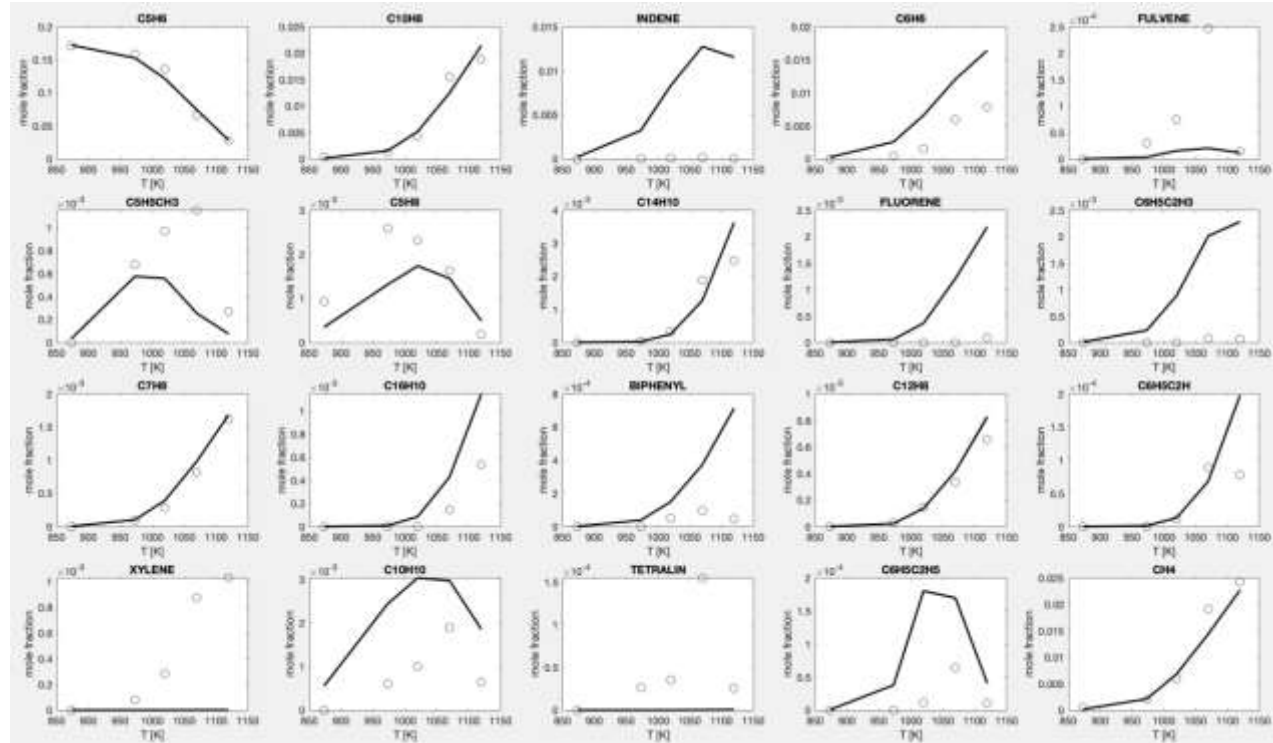


Figure S4: Experimental (points) and simulated (lines) mole fraction profiles of relevant detected products in the cyclopentadiene pyrolysis experiments of Djokic et al.³ in low dilution conditions. Dotted red lines: starting model (oldtherm), dashed black lines: updated thermochemistry (newtherm), solid black lines: final model with updated kinetics (newkin)

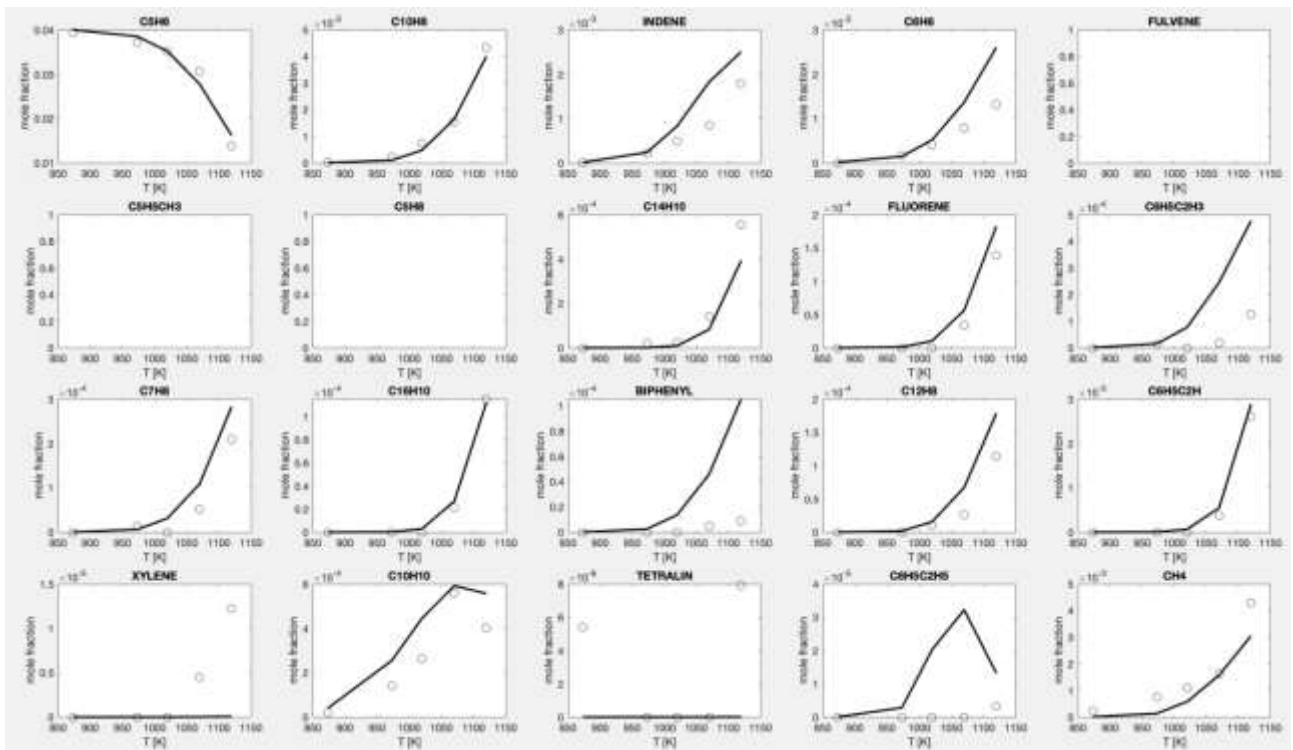
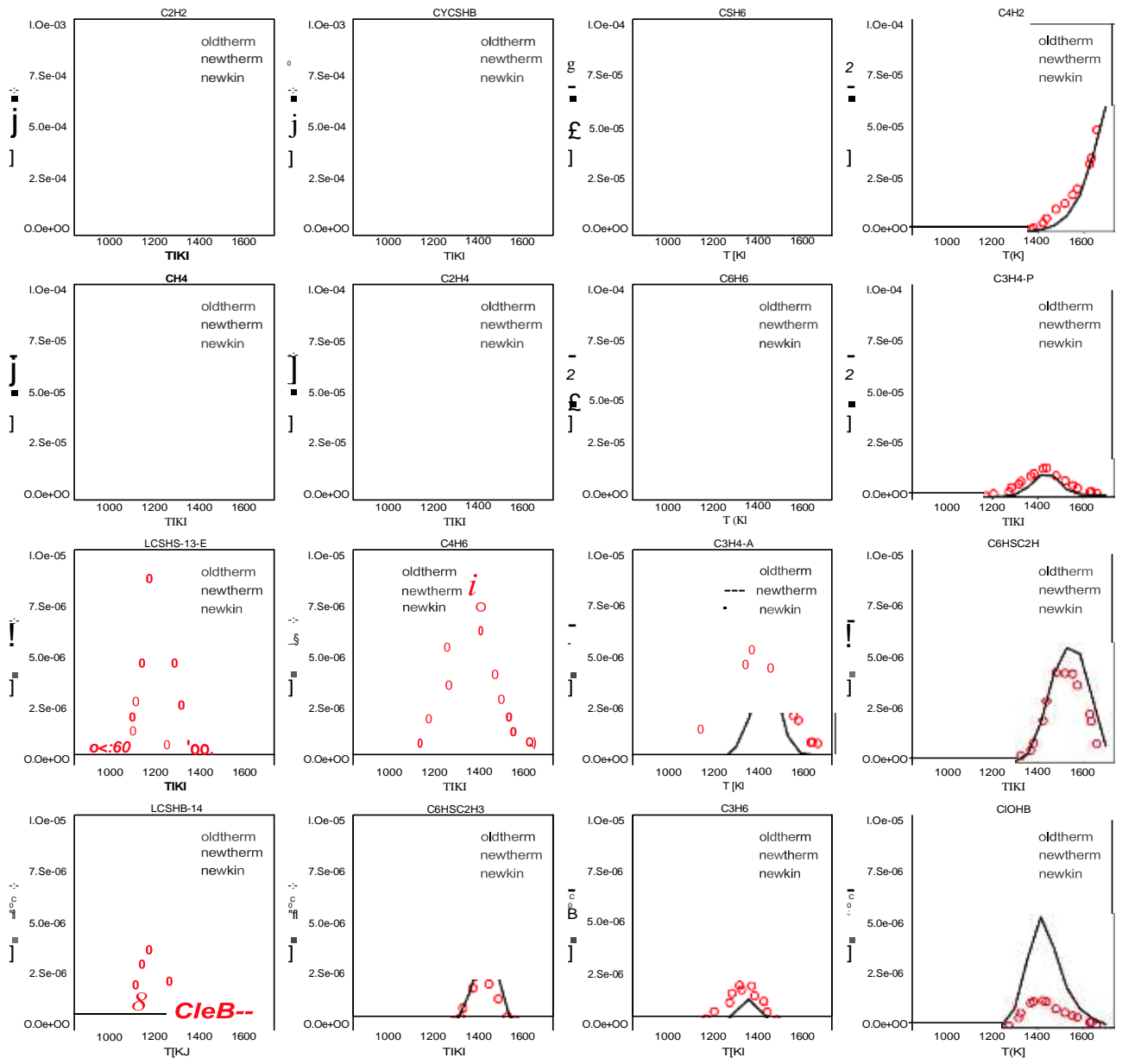


Figure S5: Experimental (points) and simulated (lines) mole fraction profiles of relevant detected products in the cyclopentadiene pyrolysis experiments of Djokic et al.³ in high dilution conditions. Dotted red lines: starting model (oldtherm), dashed black lines: updated thermochemistry (newtherm), solid black lines: final model with updated kinetics (newkin)

CYC5H8	ST	900-1700	20	Inf	Hamadi et al. ⁴
CYC5H8/C2H2					



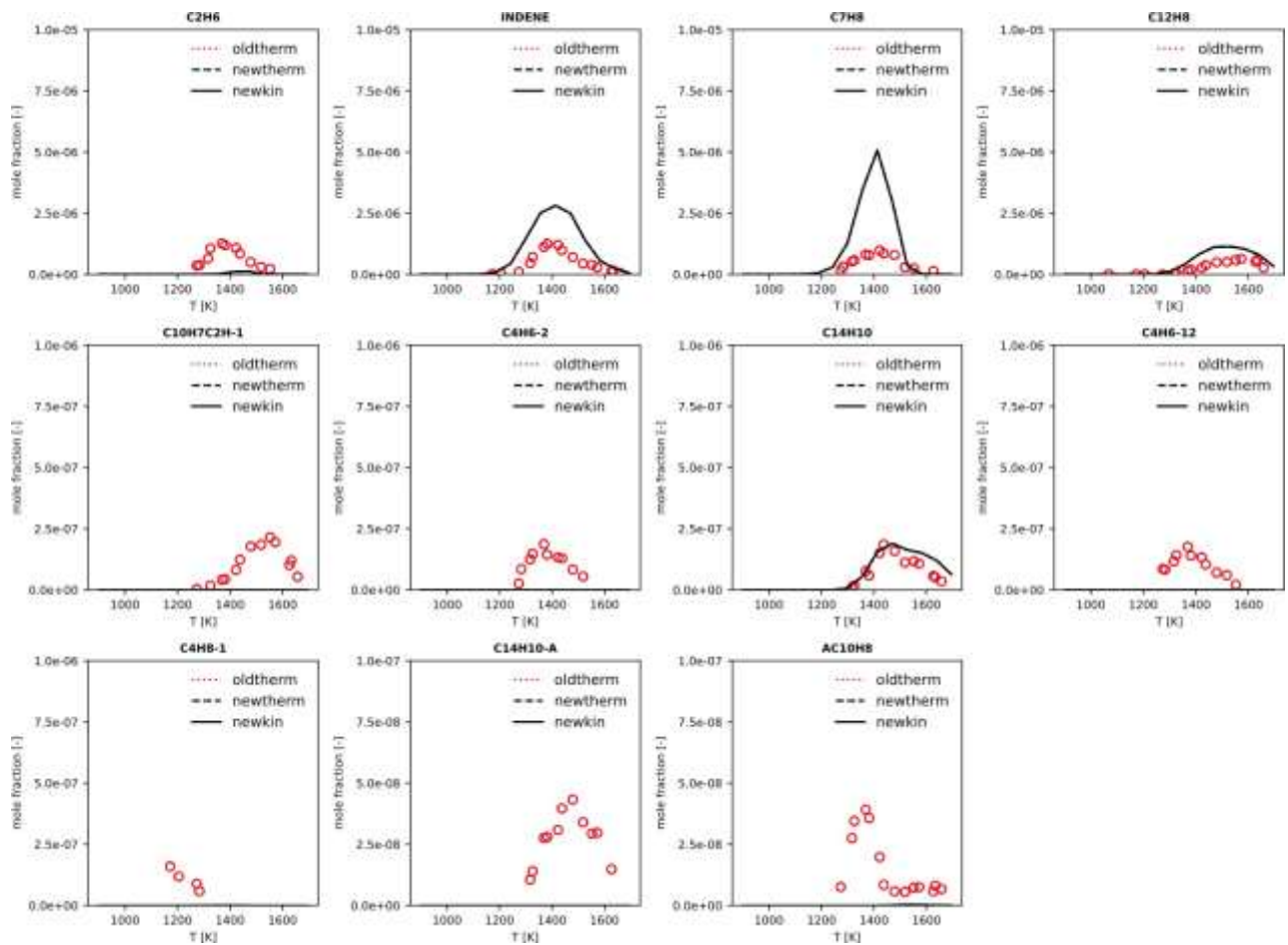
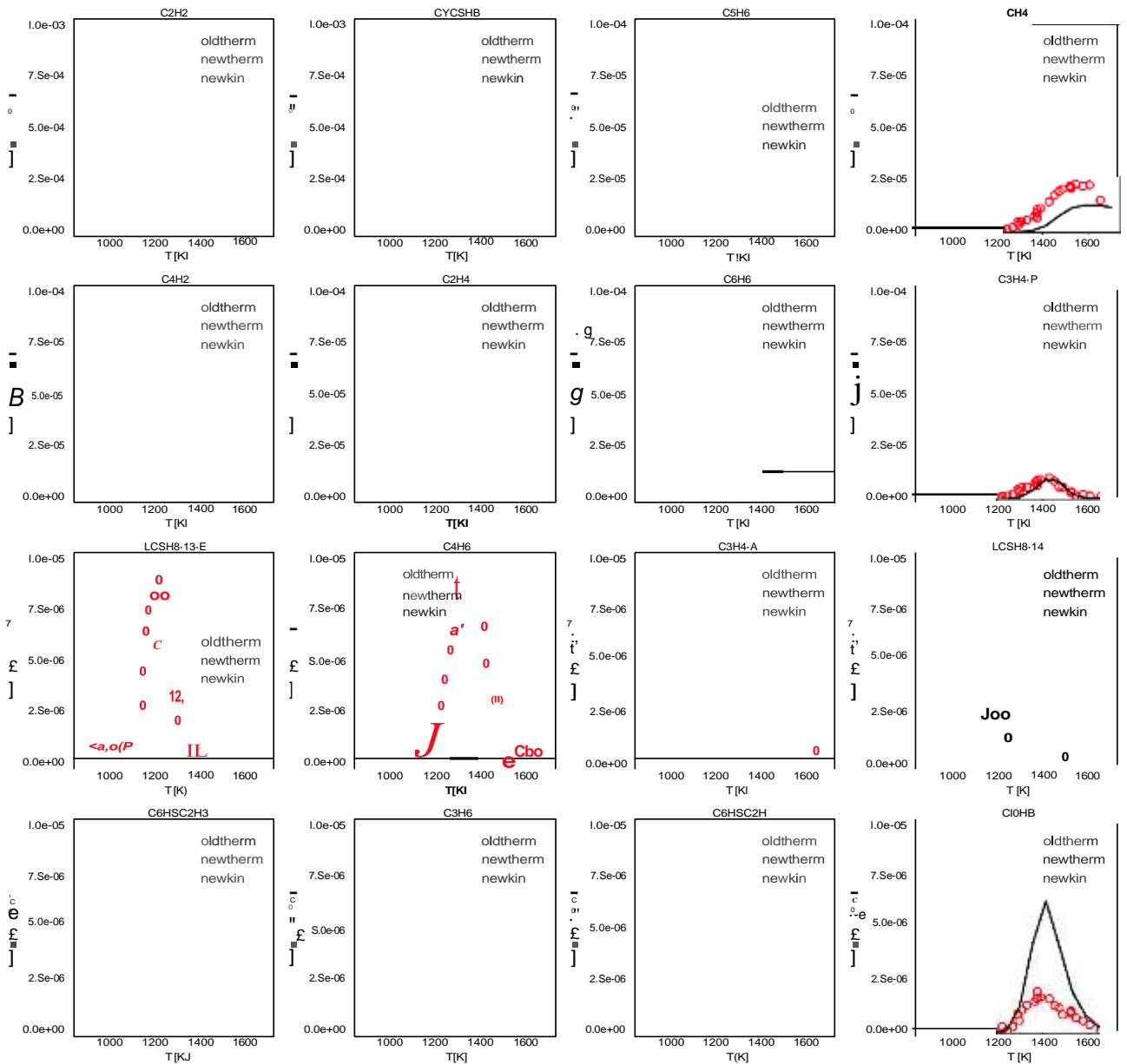


Figure S6: Experimental (points) and simulated (lines) mole fraction profiles of relevant detected products in the acetylene-doped cyclopentene pyrolysis shock tube experiments of Hamadi et al.⁴. Dotted red lines: starting model (oldtherm), dashed black lines: updated thermochemistry (newtherm), solid black lines: final model with updated kinetics (newkin). *plot generated automatically with SciExpeM post-processing tools.



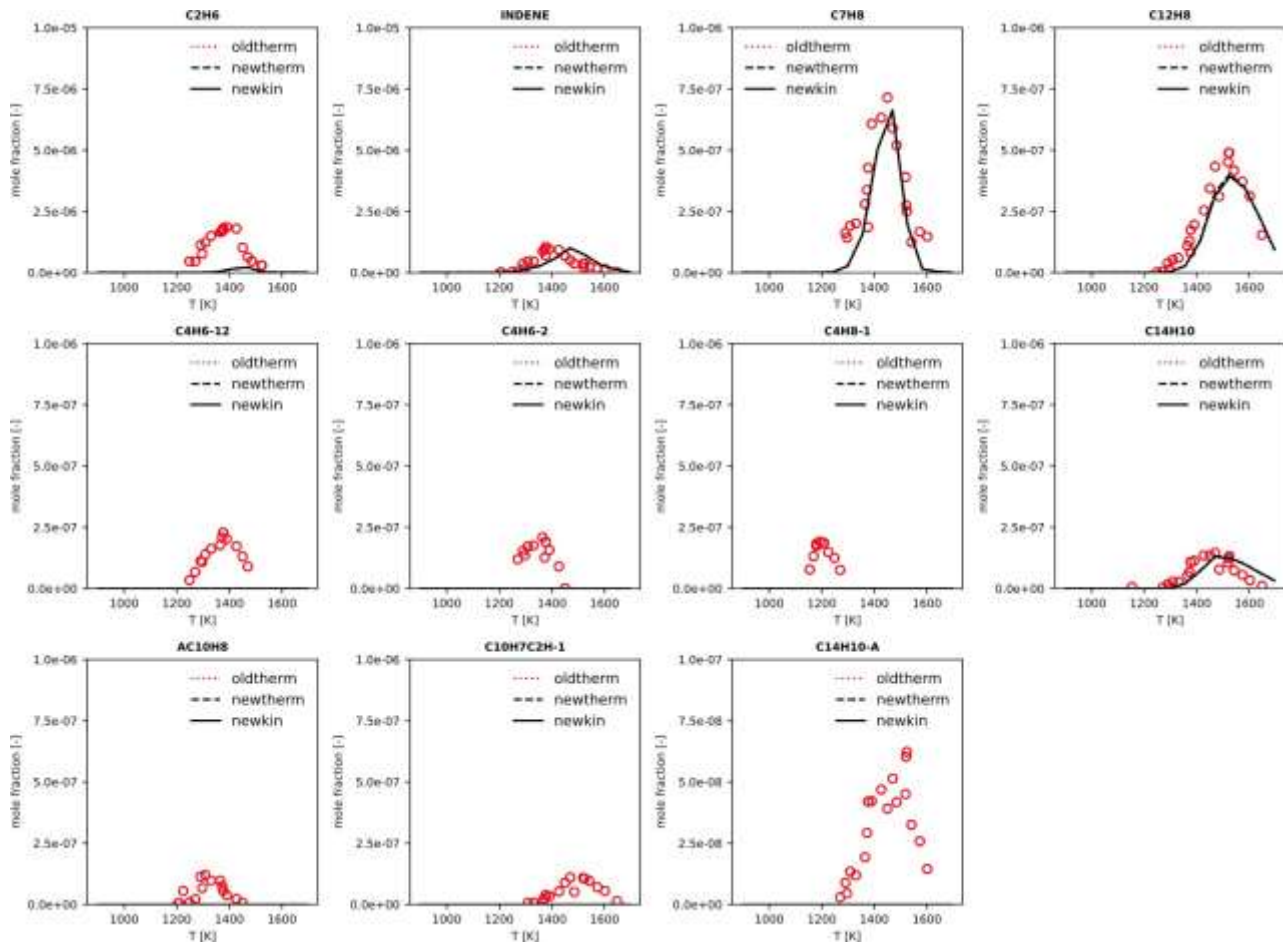


Figure S7: Experimental (points) and simulated (lines) mole fraction profiles of relevant detected products in the acetylene-doped cyclopentene pyrolysis shock tube experiments of Hamadi et al.⁴. Dotted red lines: starting model (oldtherm), dashed black lines: updated thermochemistry (newtherm), solid black lines: final model with updated kinetics (newkin). *plot generated automatically with SciExpeM post-processing tools

C7H8	ST	1100-1700	20	Inf	Sun et al. ⁵
------	----	-----------	----	-----	-------------------------

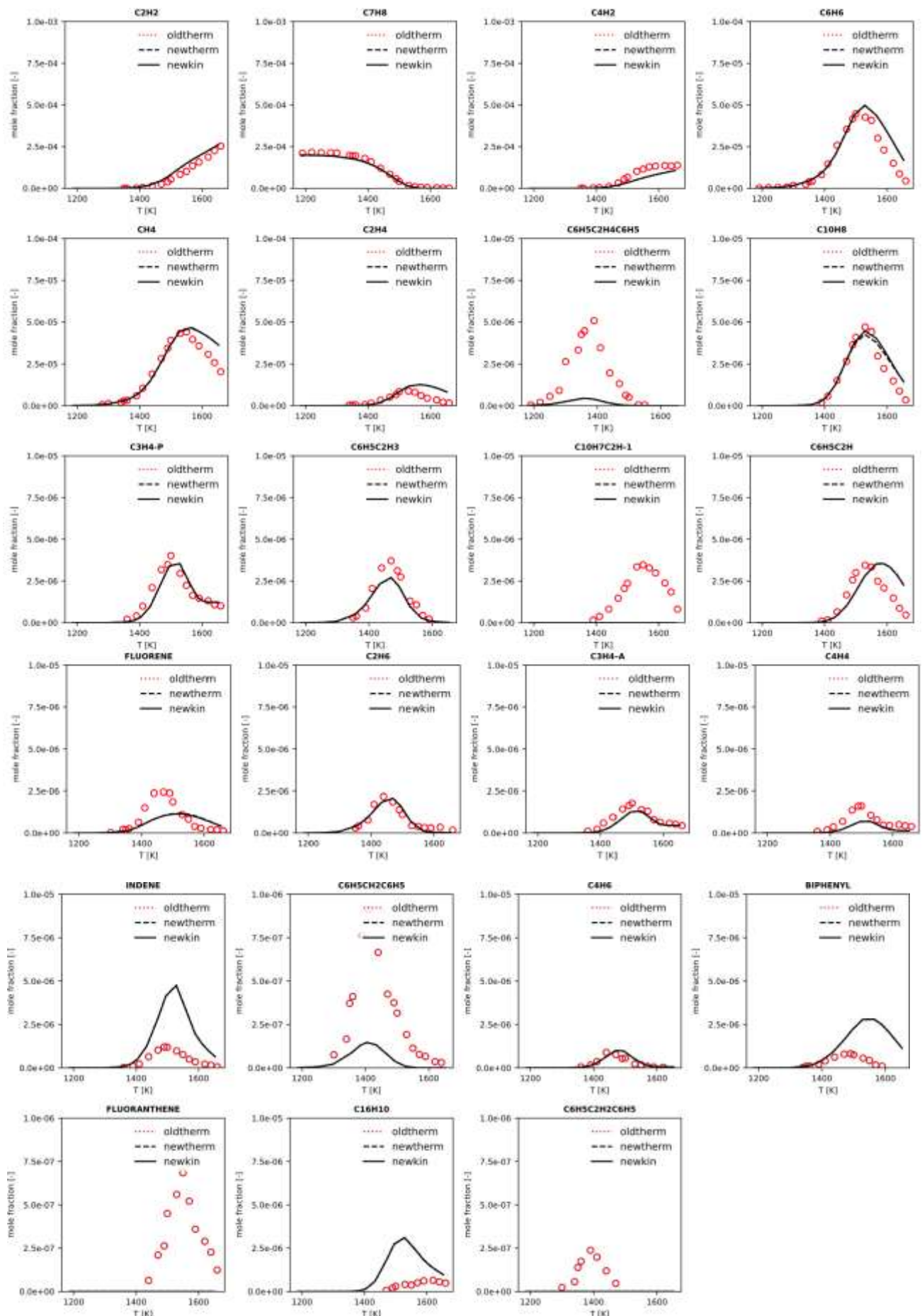
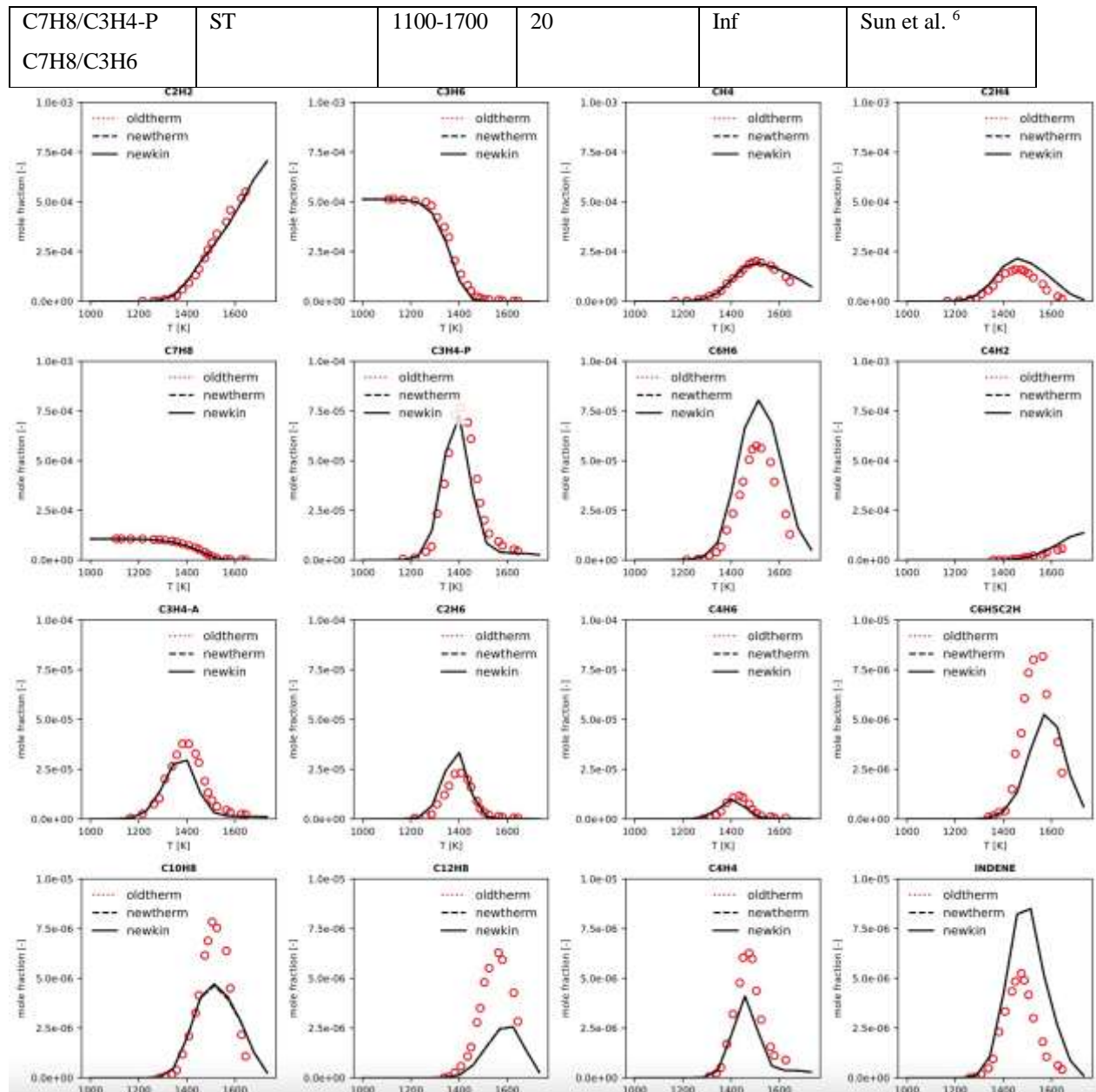
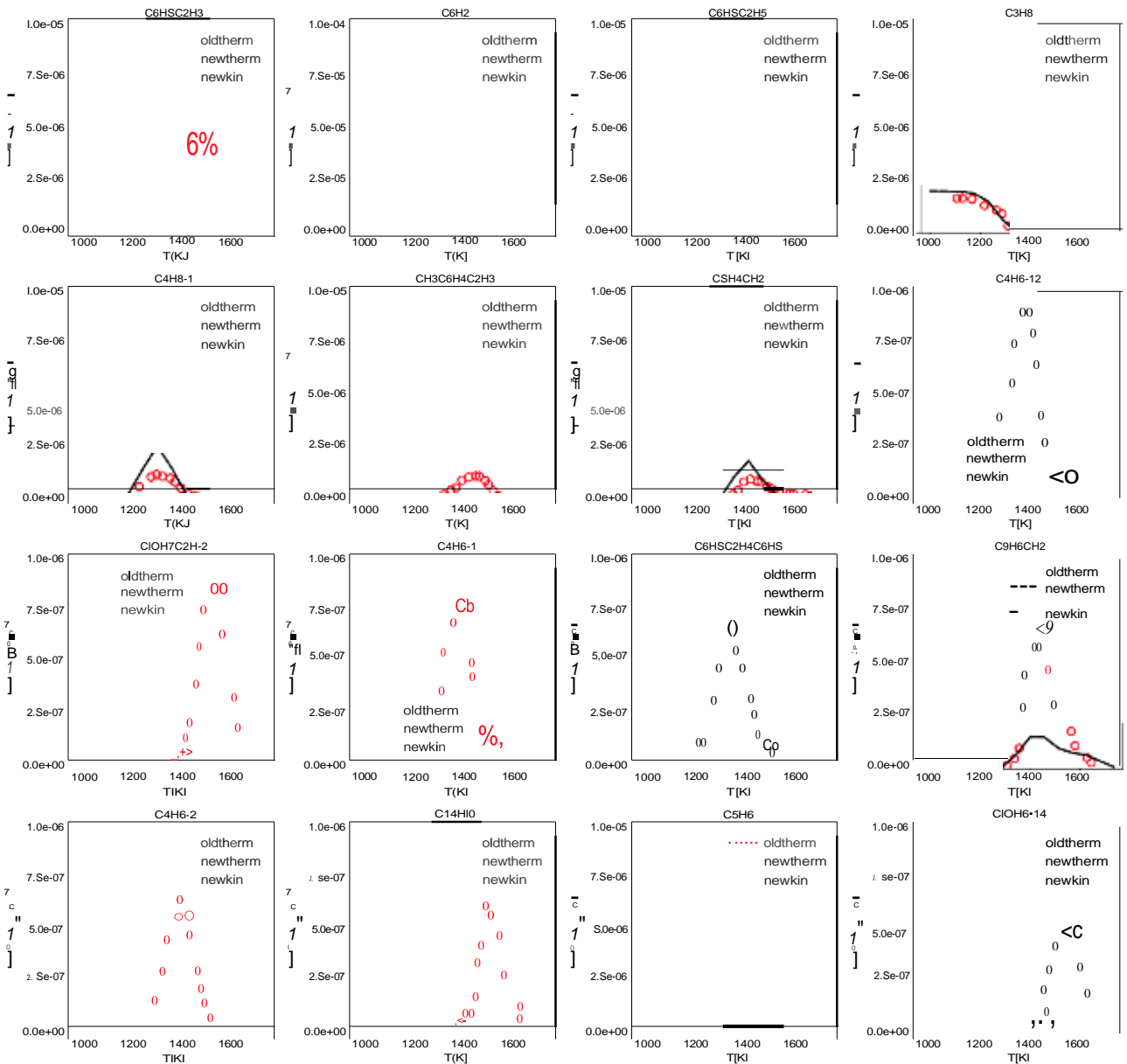


Figure S8: Experimental (points) and simulated (lines) mole fraction profiles of relevant detected products in the toluene pyrolysis experiments of Sun et al.⁵. Dotted red lines: starting model (oldtherm), dashed black lines: updated thermochemistry (newtherm), solid black lines: final model with updated kinetics (newkin). *plot generated automatically with SciExpeM post-processing tools.





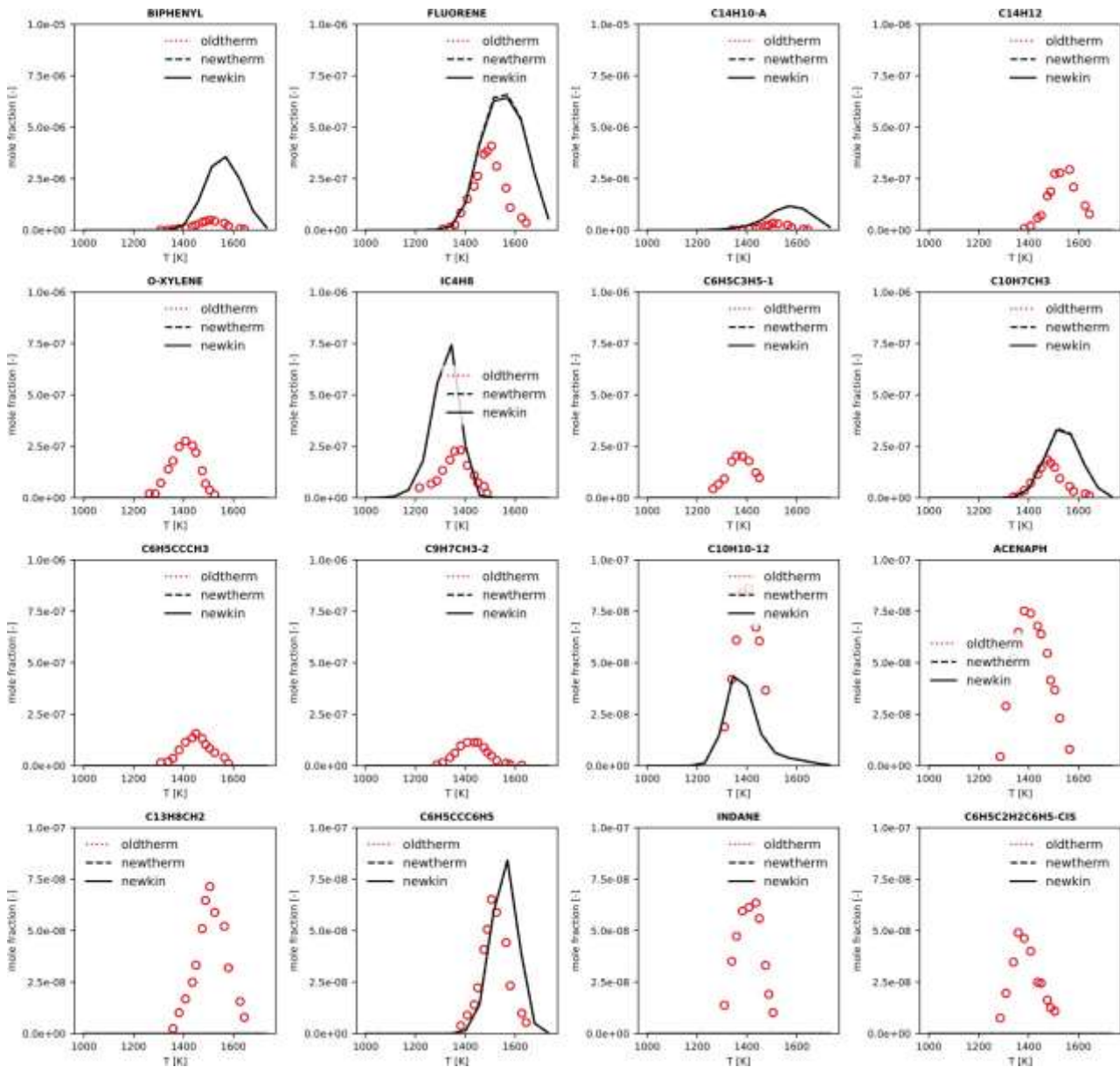
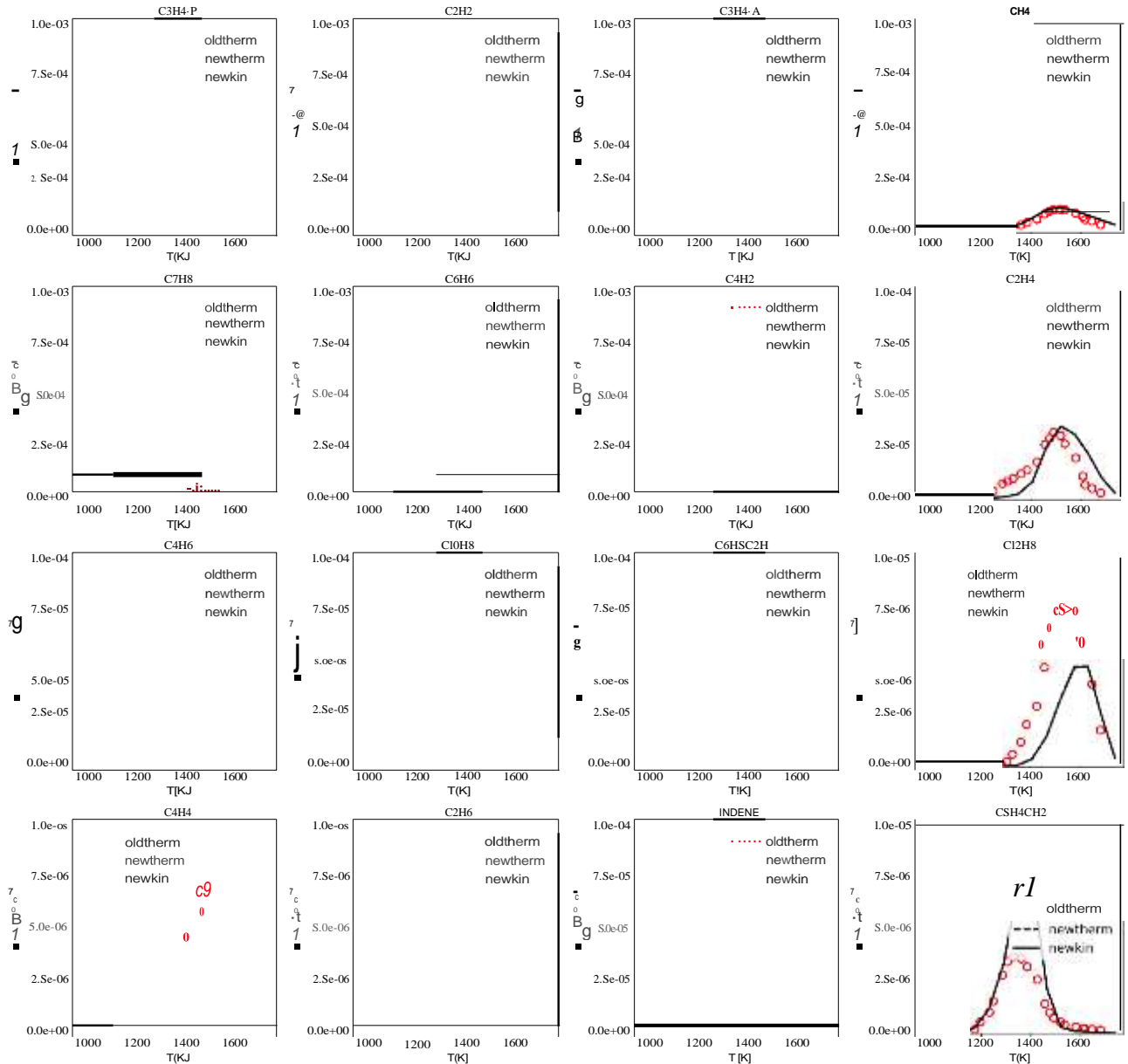
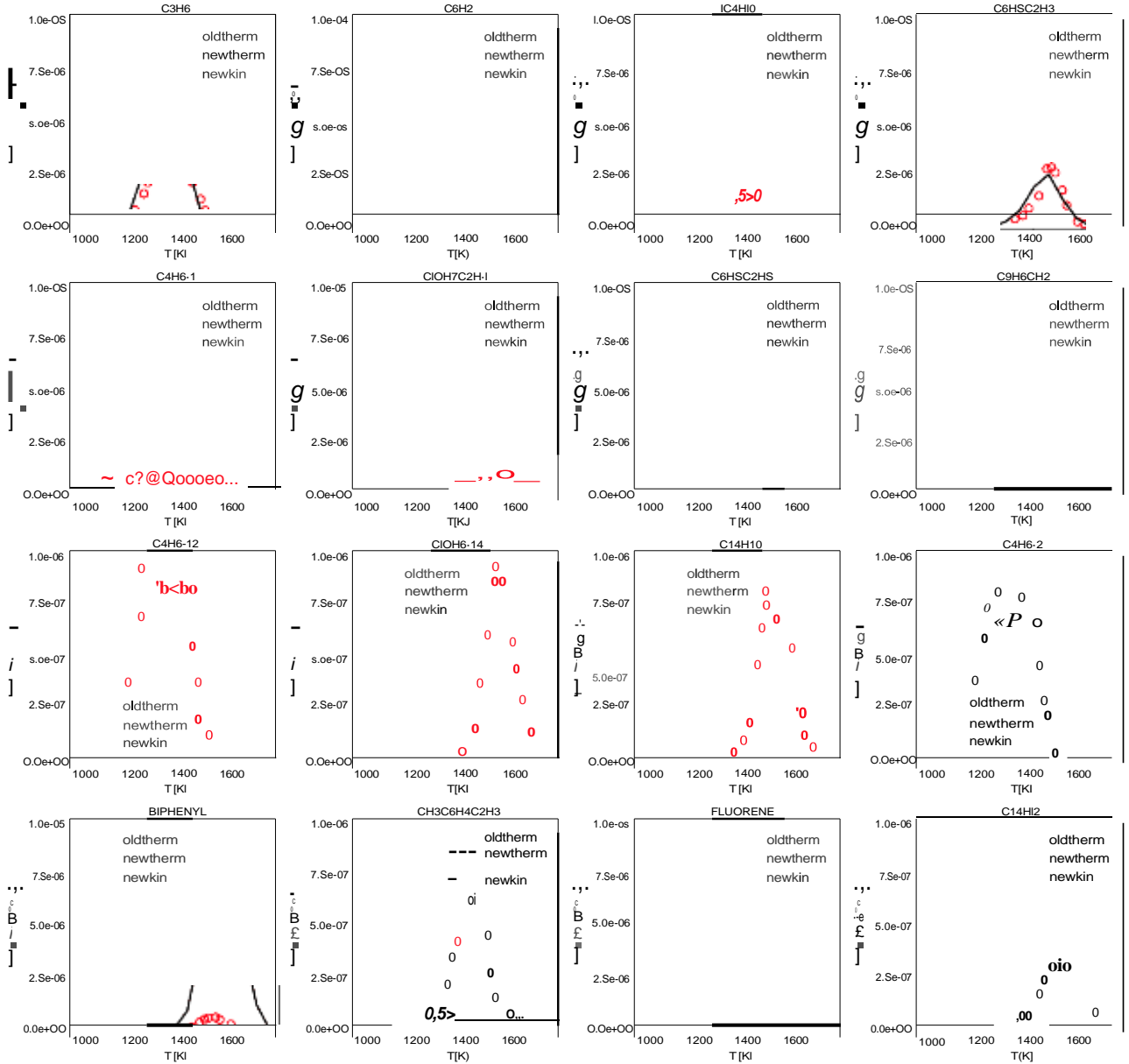


Figure S9: Experimental (points) and simulated (lines) mole fraction profiles of relevant detected products in the propene-doped toluene pyrolysis experiments of Sun et al.⁶ Dotted red lines: starting model (oldtherm), dashed black lines: updated thermochemistry (newtherm), solid black lines: final model with updated kinetics (newkin). *plot generated automatically with SciExpeM post-processing tools.





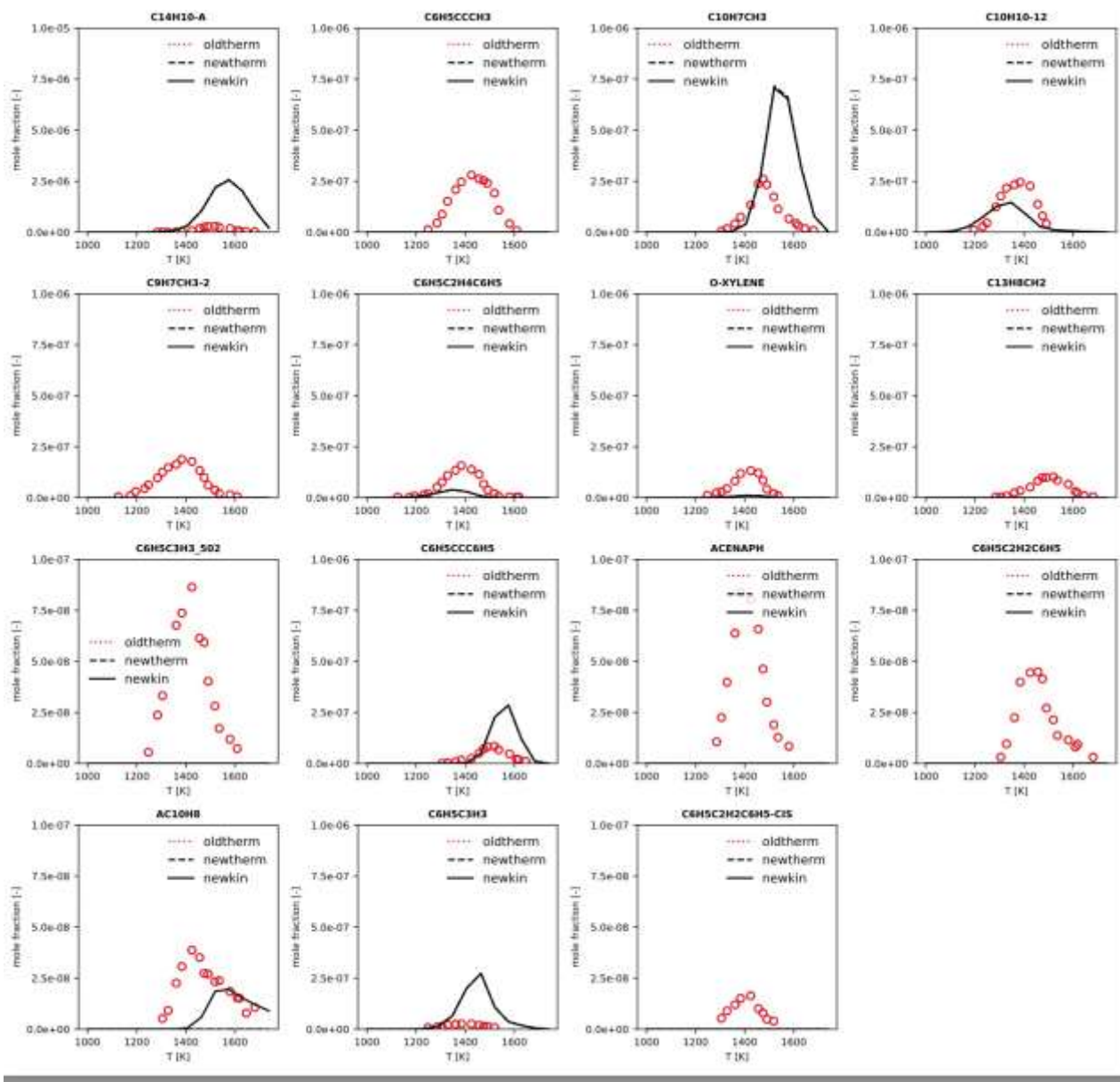
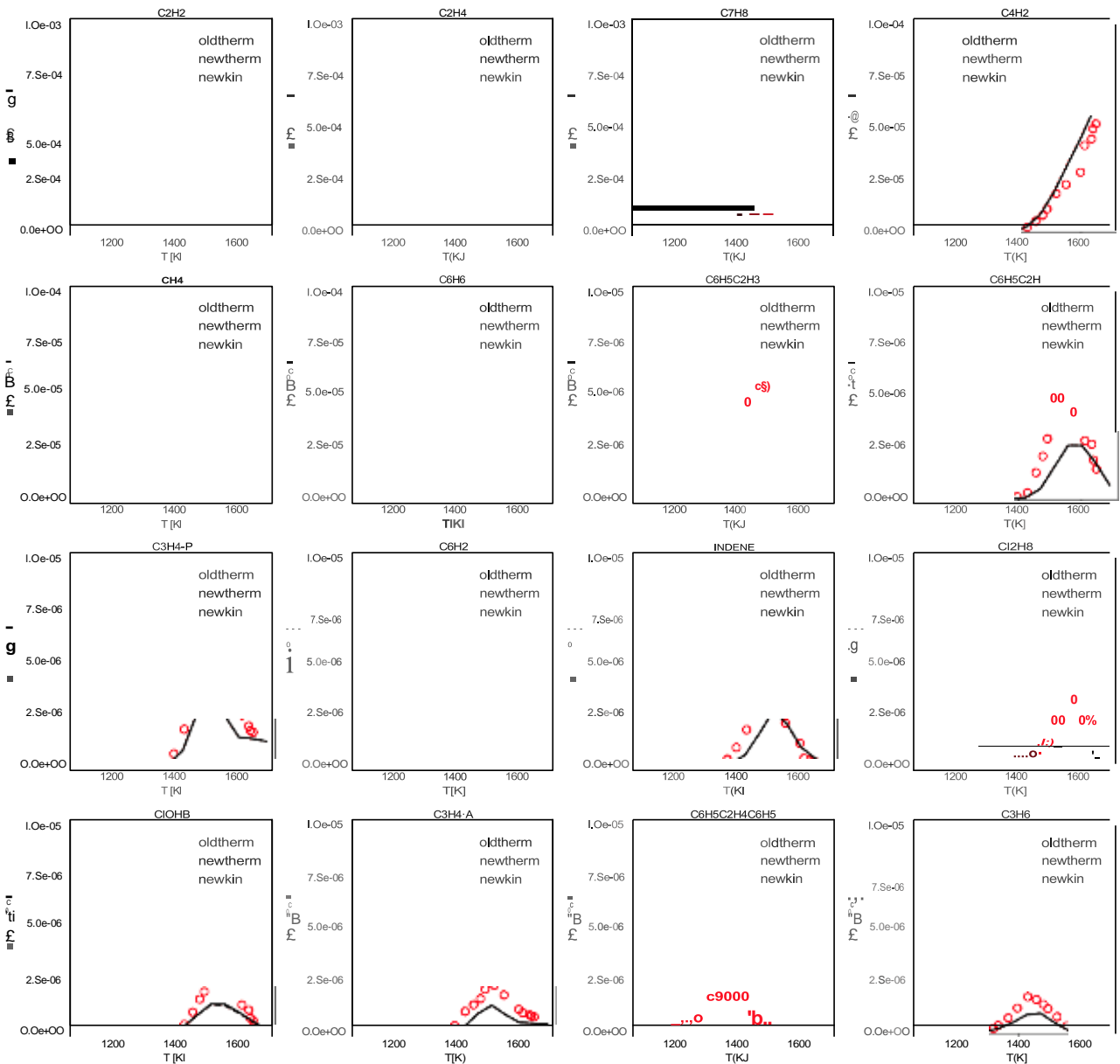
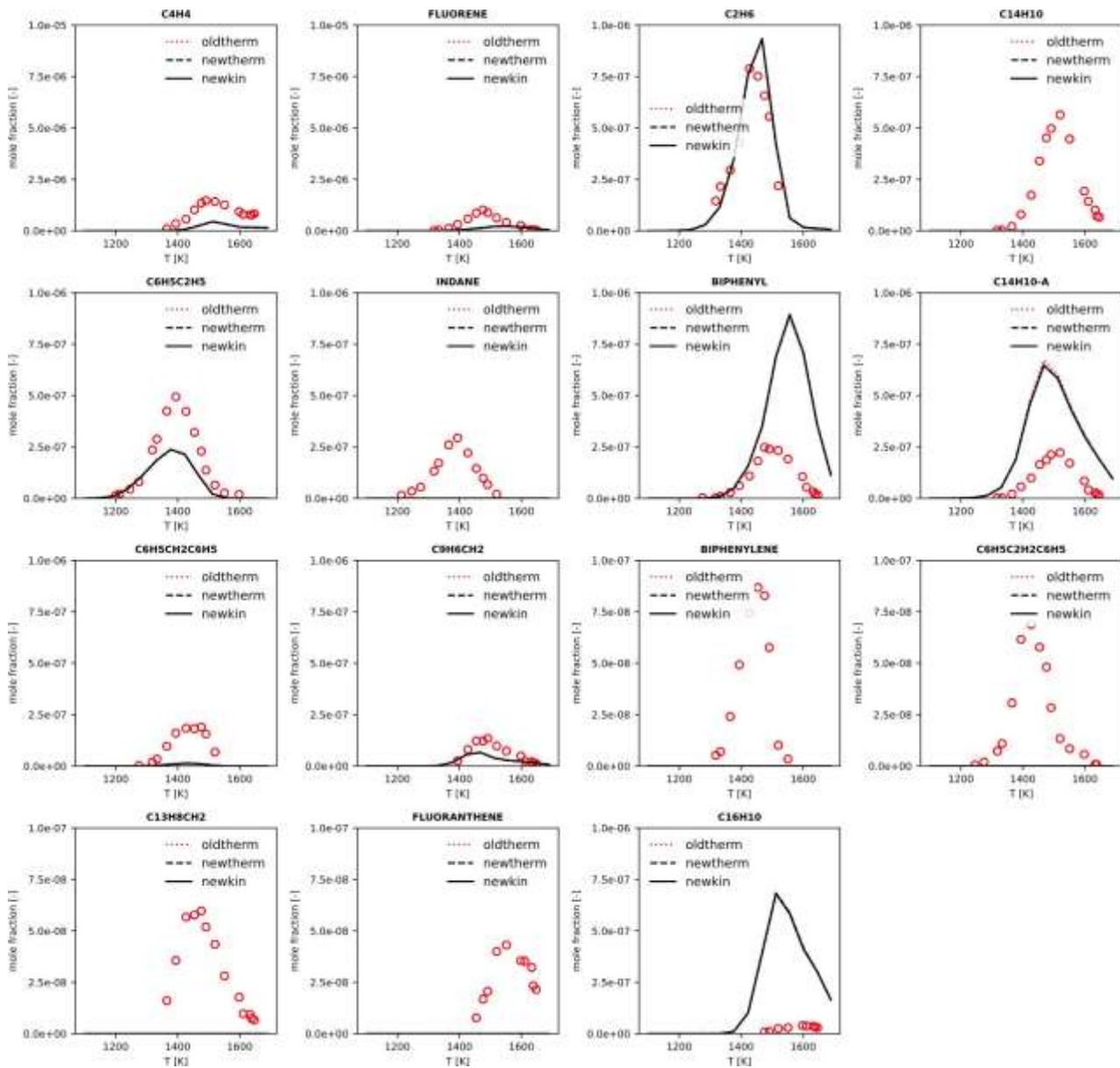


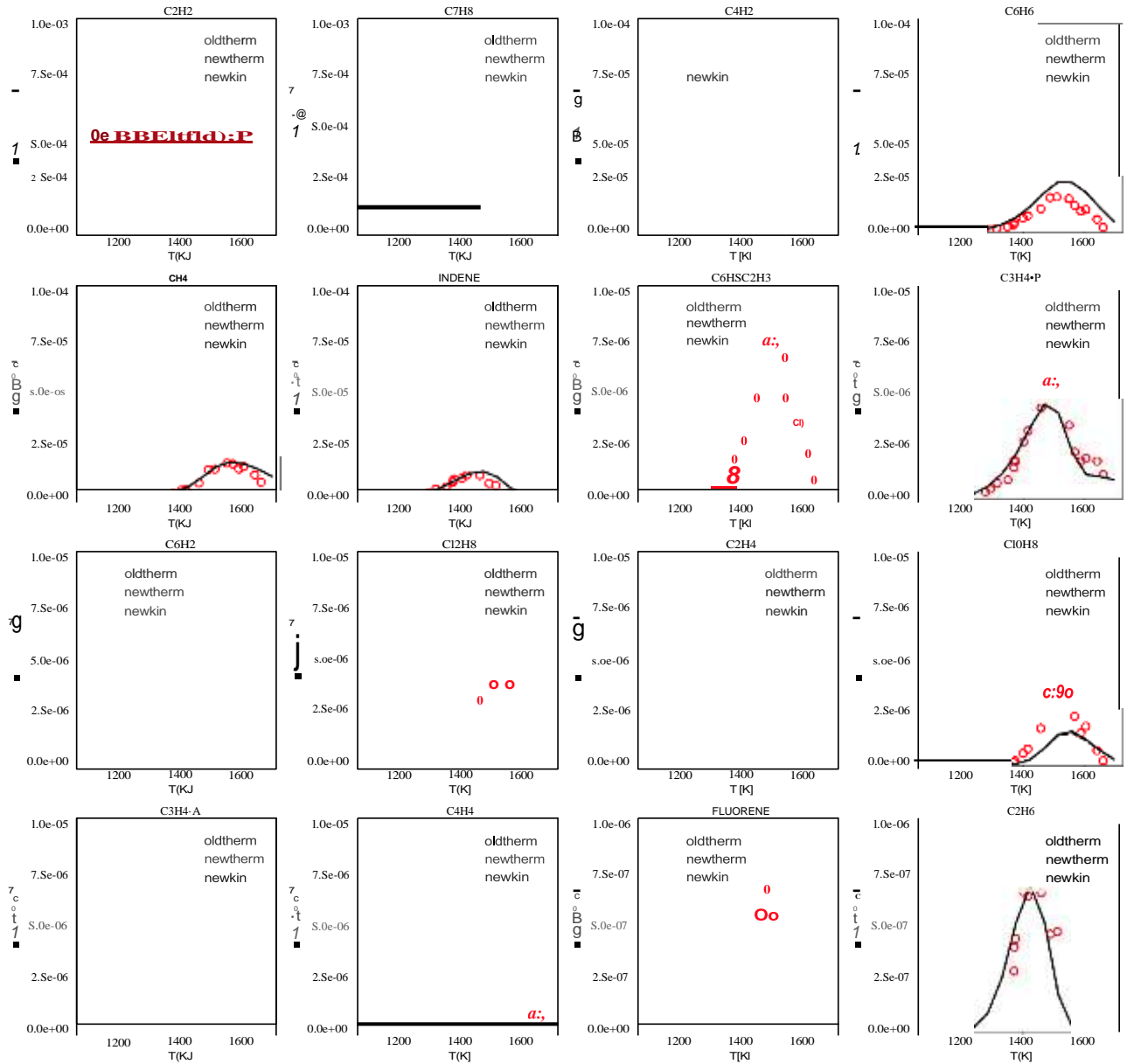
Figure S10: Experimental (points) and simulated (lines) mole fraction profiles of relevant detected products in the propyne-doped toluene pyrolysis experiments of Sun et al.⁶. Dotted red lines: starting model (oldtherm), dashed black lines: updated thermochemistry (newtherm), solid black lines: final model with updated kinetics (newkin). *plot generated automatically with SciExpeM post-processing tools.

C7H8/C2H2 C7H8/C2H4	ST	1100-1700	20	Inf	Sun et al. ⁷
------------------------	----	-----------	----	-----	-------------------------





*Figure S11: Experimental (points) and simulated (lines) mole fraction profiles of relevant detected products in the ethylene-doped toluene pyrolysis experiments of Sun et al.⁷ Dotted red lines: starting model (oldtherm), dashed black lines: updated thermochemistry (newtherm), solid black lines: final model with updated kinetics (newkin). *plot generated automatically with SciExpeM post-processing tools.*



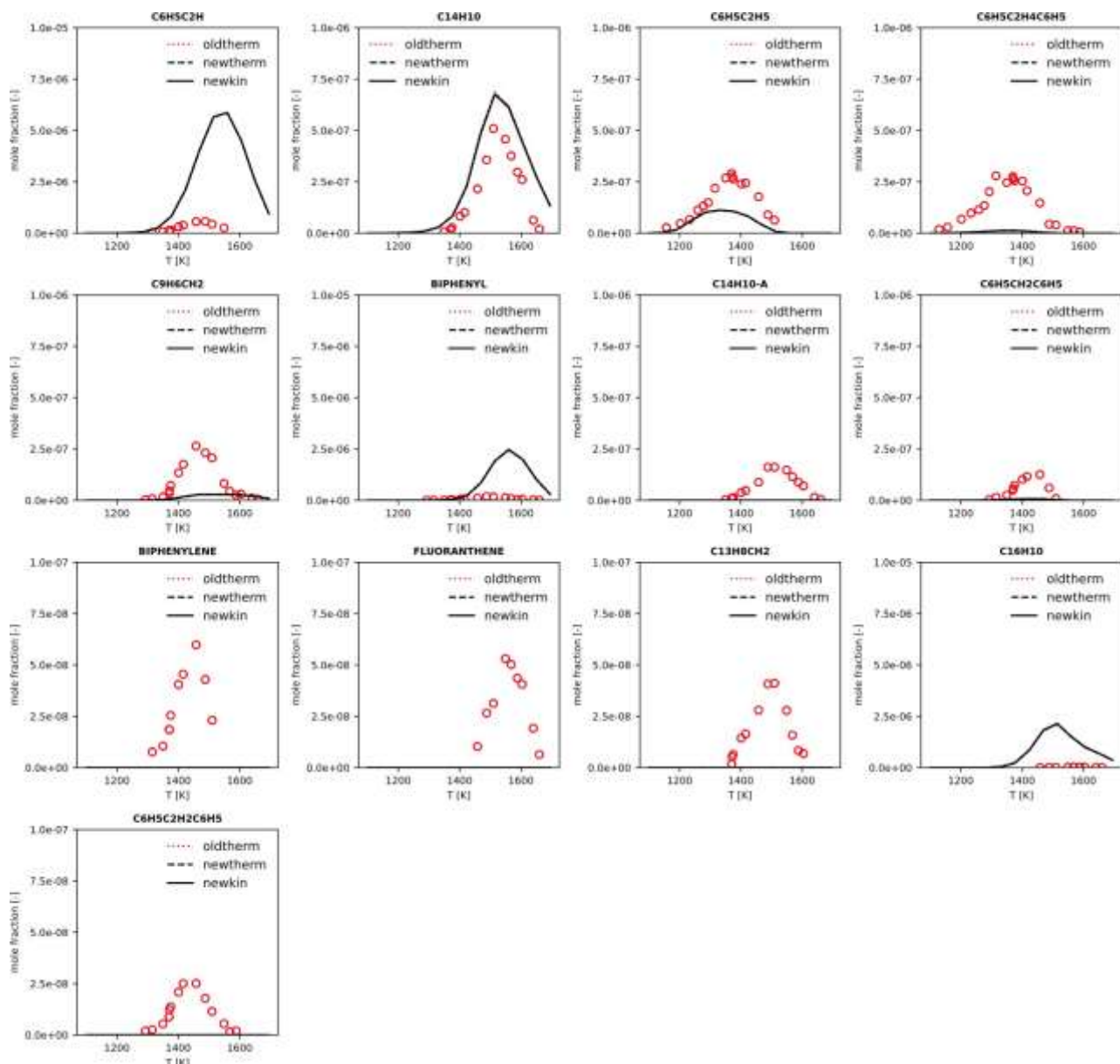


Figure S12: Experimental (points) and simulated (lines) mole fraction profiles of relevant detected products in the acetylene-doped toluene pyrolysis experiments of Sun et al.⁷. Dotted red lines: starting model (oldtherm), dashed black lines: updated thermochemistry (newtherm), solid black lines: final model with updated kinetics (newkin). *plot generated automatically with SciExpeM post-processing tools.

C7H8/Ar	PFR	1100-1800	0.26, 0.11, 0.04	inf	Yuan et al. ⁸
---------	-----	-----------	------------------	-----	--------------------------

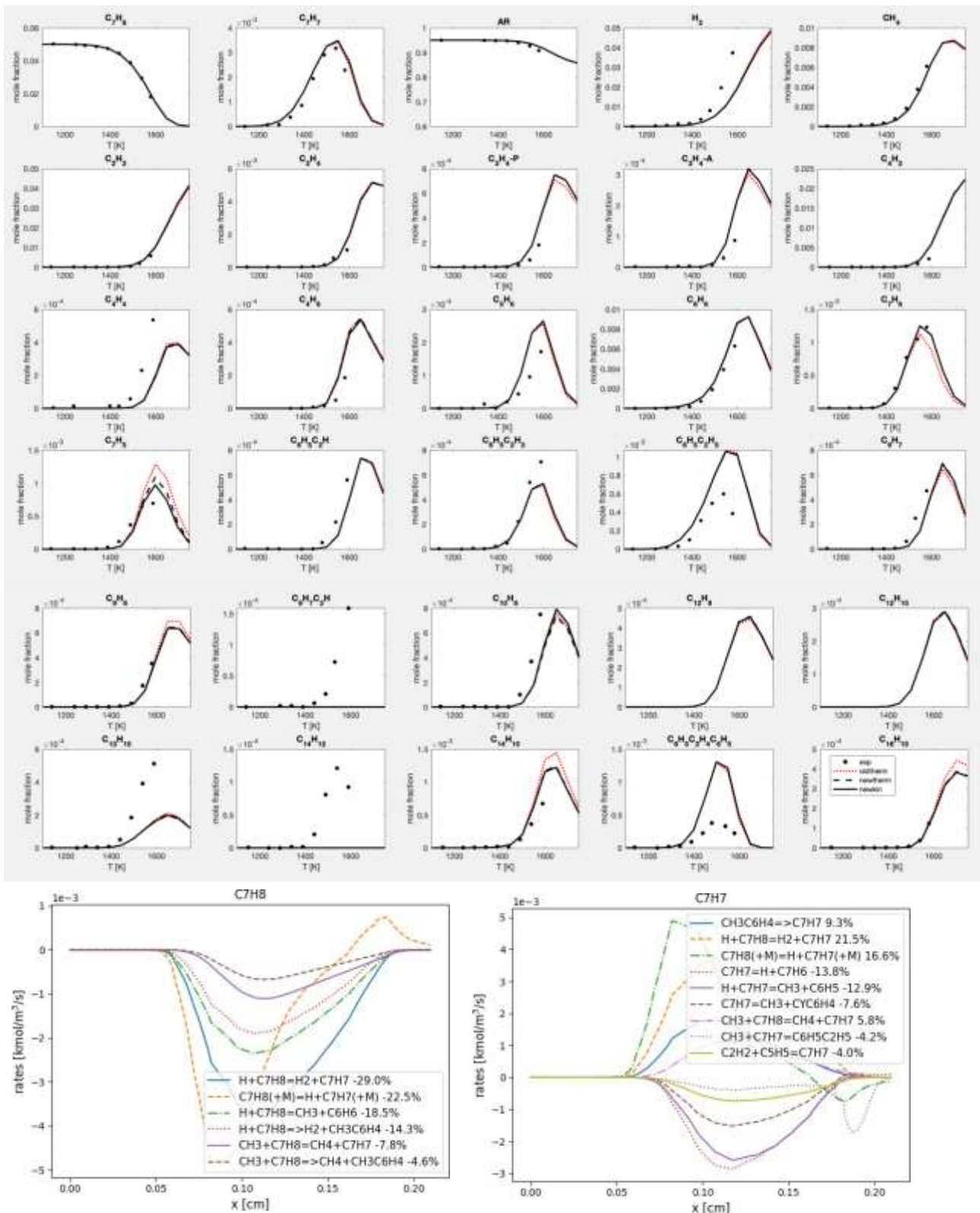


Figure S13: Experimental (points) and simulated (lines) mole fraction profiles of relevant detected products in the toluene pyrolysis experiments in the flow reactor of Yuan et al.⁸ ($p=30$ Torr). Dotted red lines: starting model (oldtherm), dashed black lines: updated thermochemistry (newtherm), solid black lines: final model with updated kinetics (newkin)

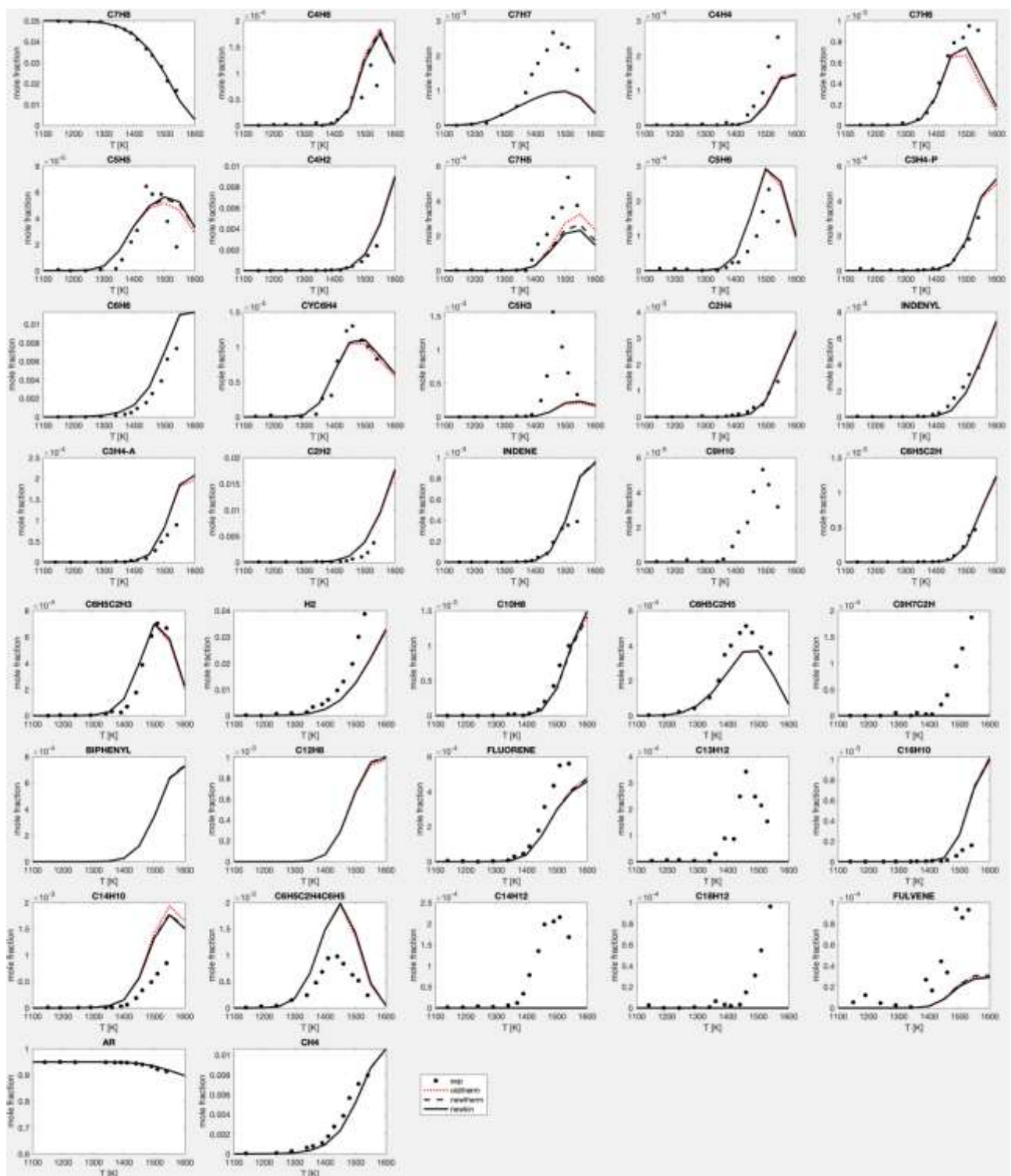


Figure S14: Experimental (points) and simulated (lines) mole fraction profiles of relevant detected products in the toluene pyrolysis experiments in the flow reactor of Yuan et al.⁸ ($p=80$ Torr). Dotted red lines: starting model (oldtherm), dashed black lines: updated thermochemistry (newtherm), solid black lines: final model with updated kinetics (newkin)

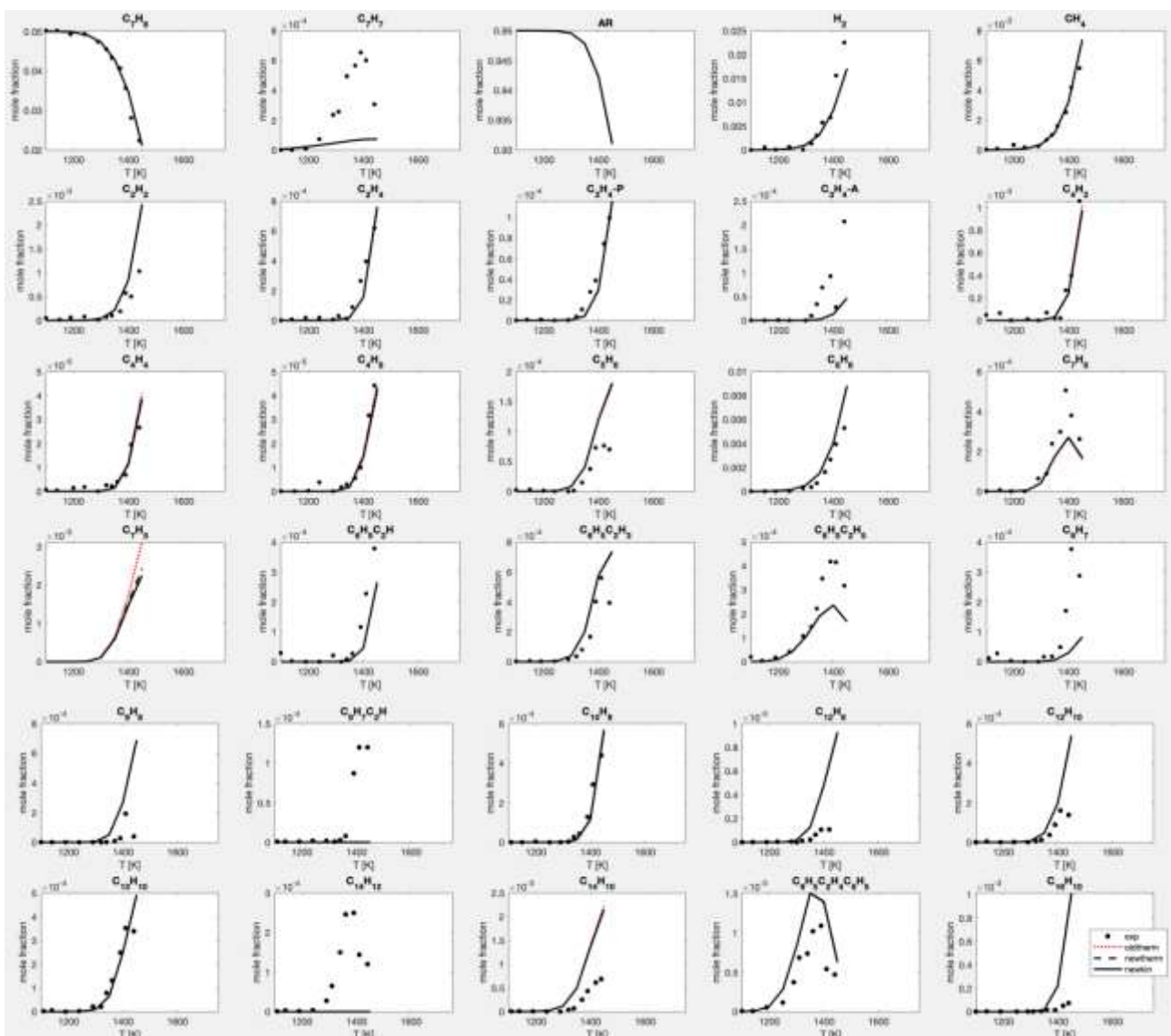


Figure S15: Experimental (points) and simulated (lines) mole fraction profiles of relevant detected products in the toluene pyrolysis experiments in the flow reactor of Yuan et al.⁸ ($p=200$ Torr). Dotted red lines: starting model (oldtherm), dashed black lines: updated thermochemistry (newtherm), solid black lines: final model with updated kinetics (newkin).

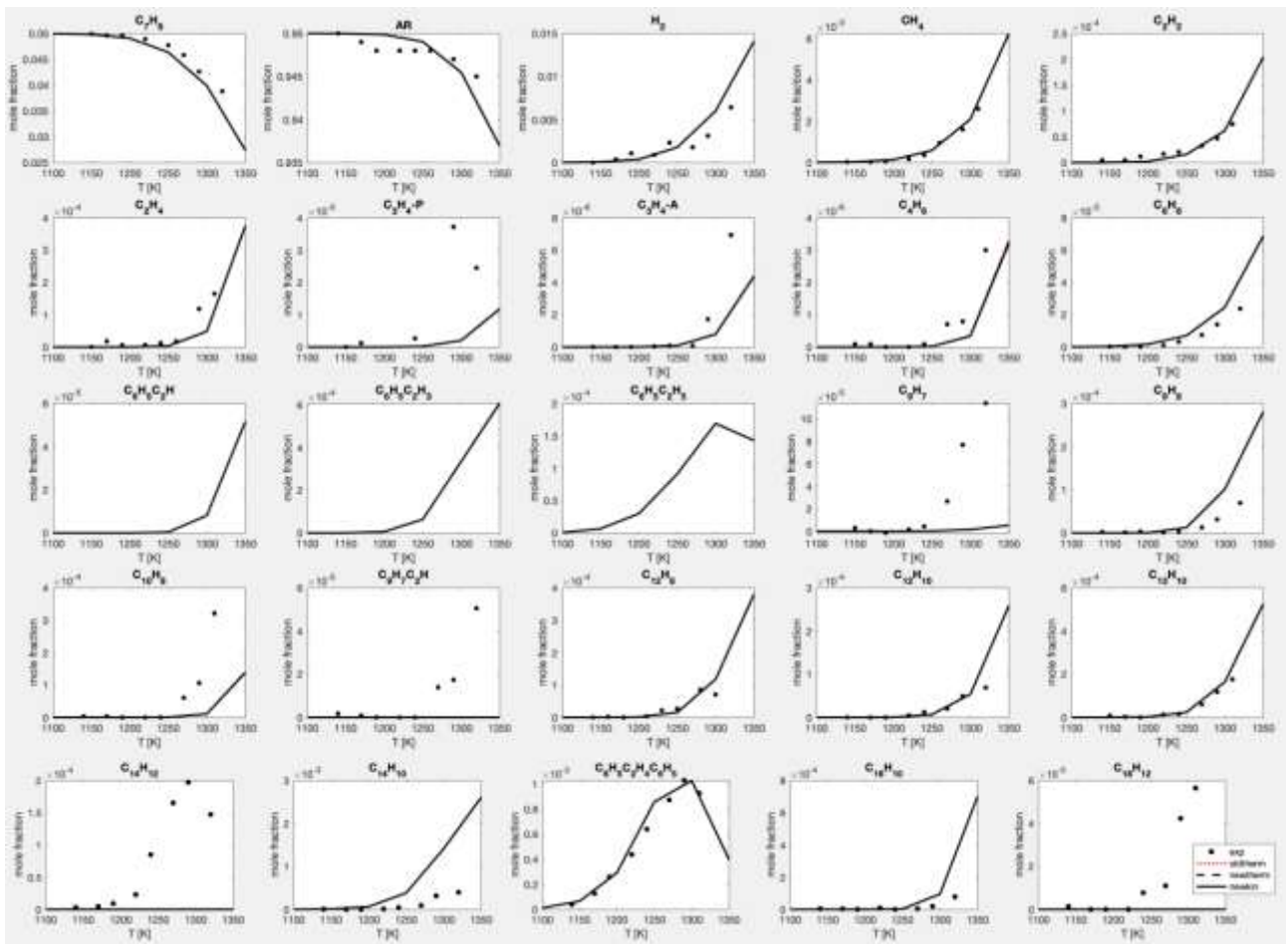
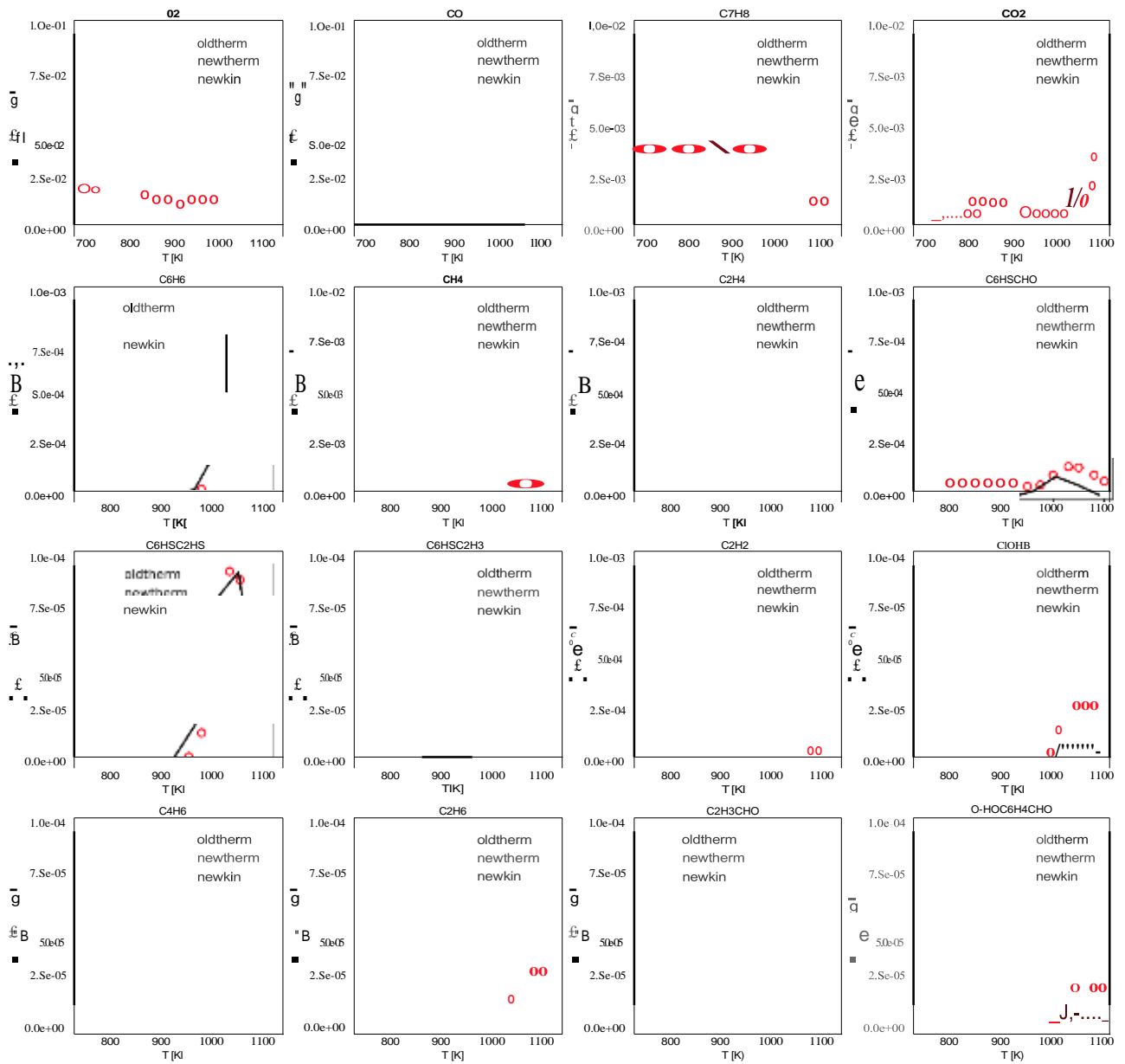


Figure S16: Experimental (points) and simulated (lines) mole fraction profiles of relevant detected products in the toluene pyrolysis experiments in the flow reactor of Yuan et al.⁸ ($p=200$ Torr). Dotted red lines: starting model (oldtherm), dashed black lines: updated thermochemistry (newtherm), solid black lines: final model with updated kinetics (newkin)

C7H8/O2	JSR	600-1000	1	2.0, 1.0, 0.5	Meziane et al. ⁹
---------	-----	----------	---	---------------	-----------------------------



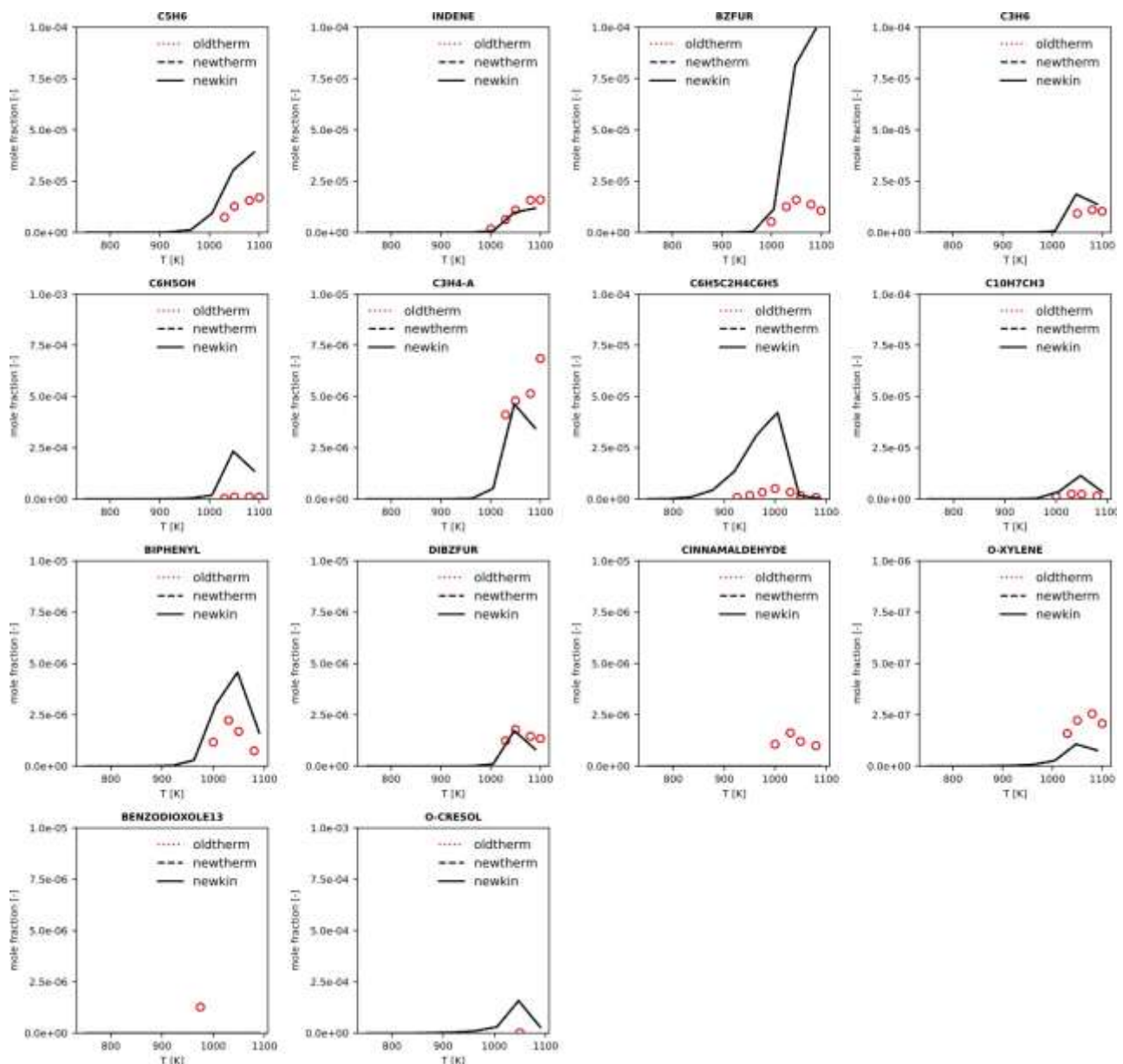
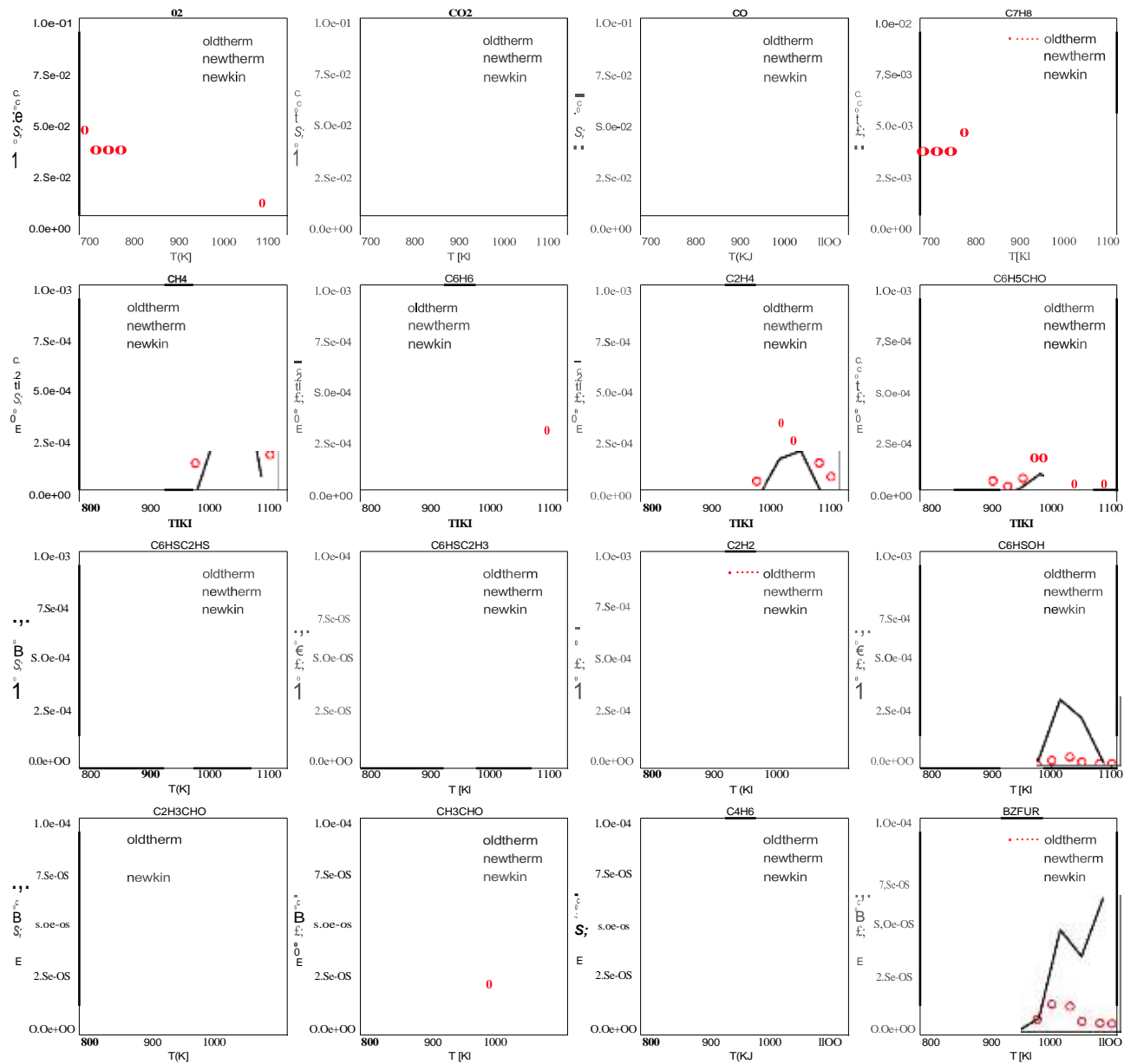


Figure S17: Experimental (points) and simulated (lines) mole fraction profiles of relevant detected products in the toluene oxidation experiments in the jet stirred reactor of Meziane et al.⁹ ($\phi = 2$). Dotted red lines: starting model (oldtherm), dashed black lines: updated thermochemistry (newtherm), solid black lines: final model with updated kinetics (newkin). *Plot generated automatically with SciExpeM post-processing tools.



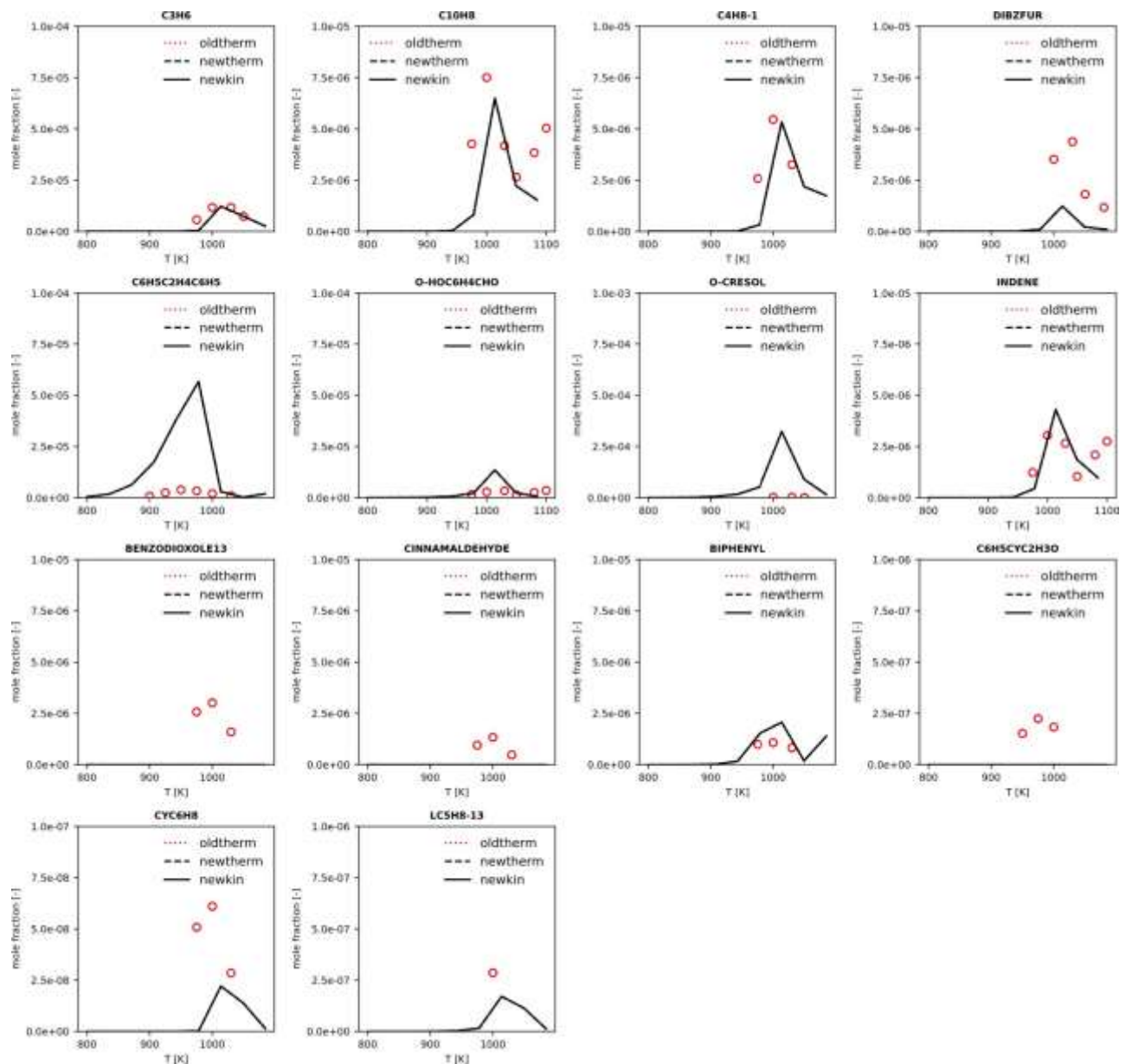
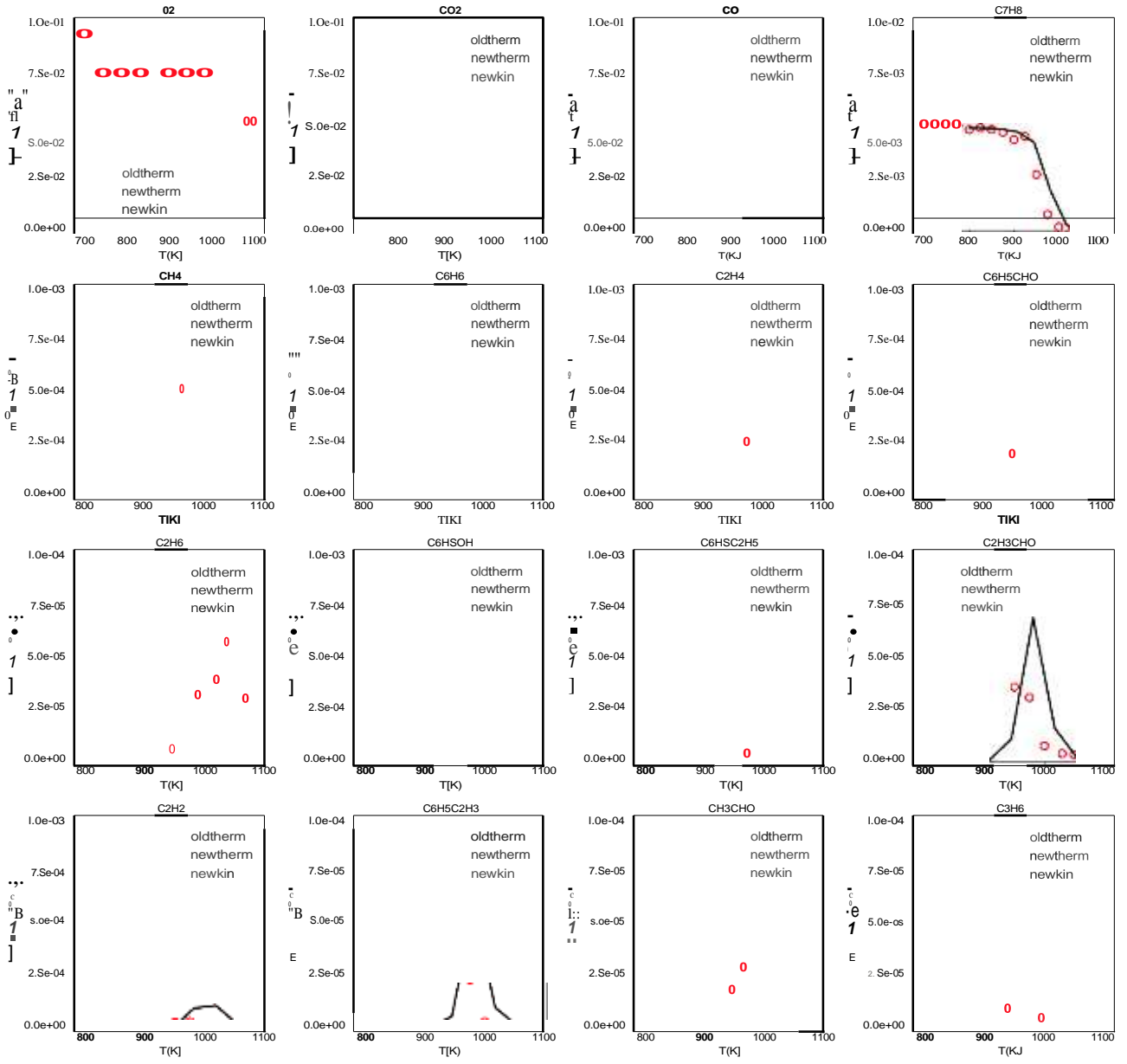


Figure S18: Experimental (points) and simulated (lines) mole fraction profiles of relevant detected products in the toluene oxidation experiments in the jet stirred reactor of Meziane et al.⁹ ($\phi = 1$). Dotted red lines: starting model (oldtherm), dashed black lines: updated thermochemistry (newtherm), solid black lines: final model with updated kinetics (newkin.) *Plot generated automatically with SciExpeM post-processing tools.



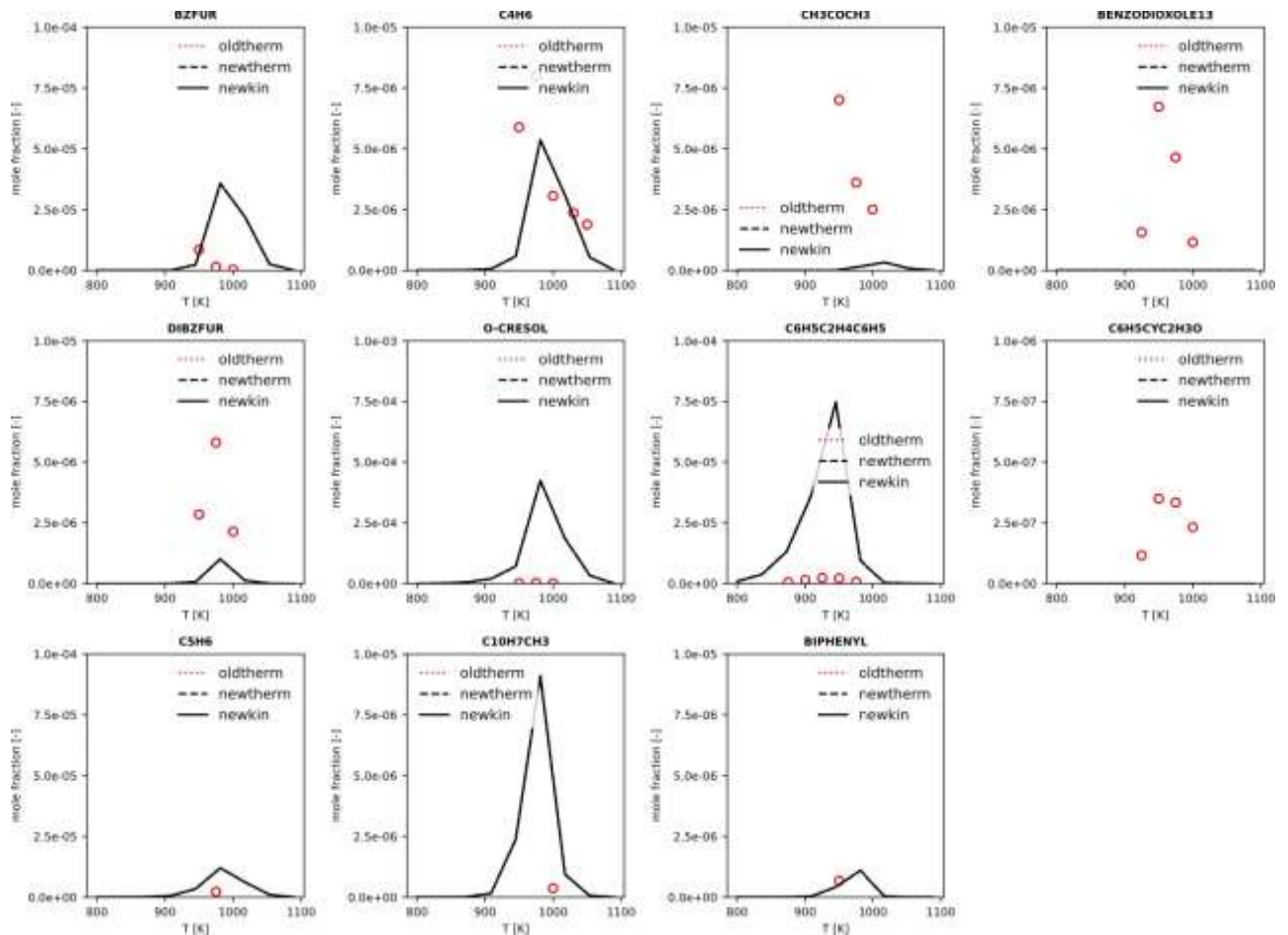
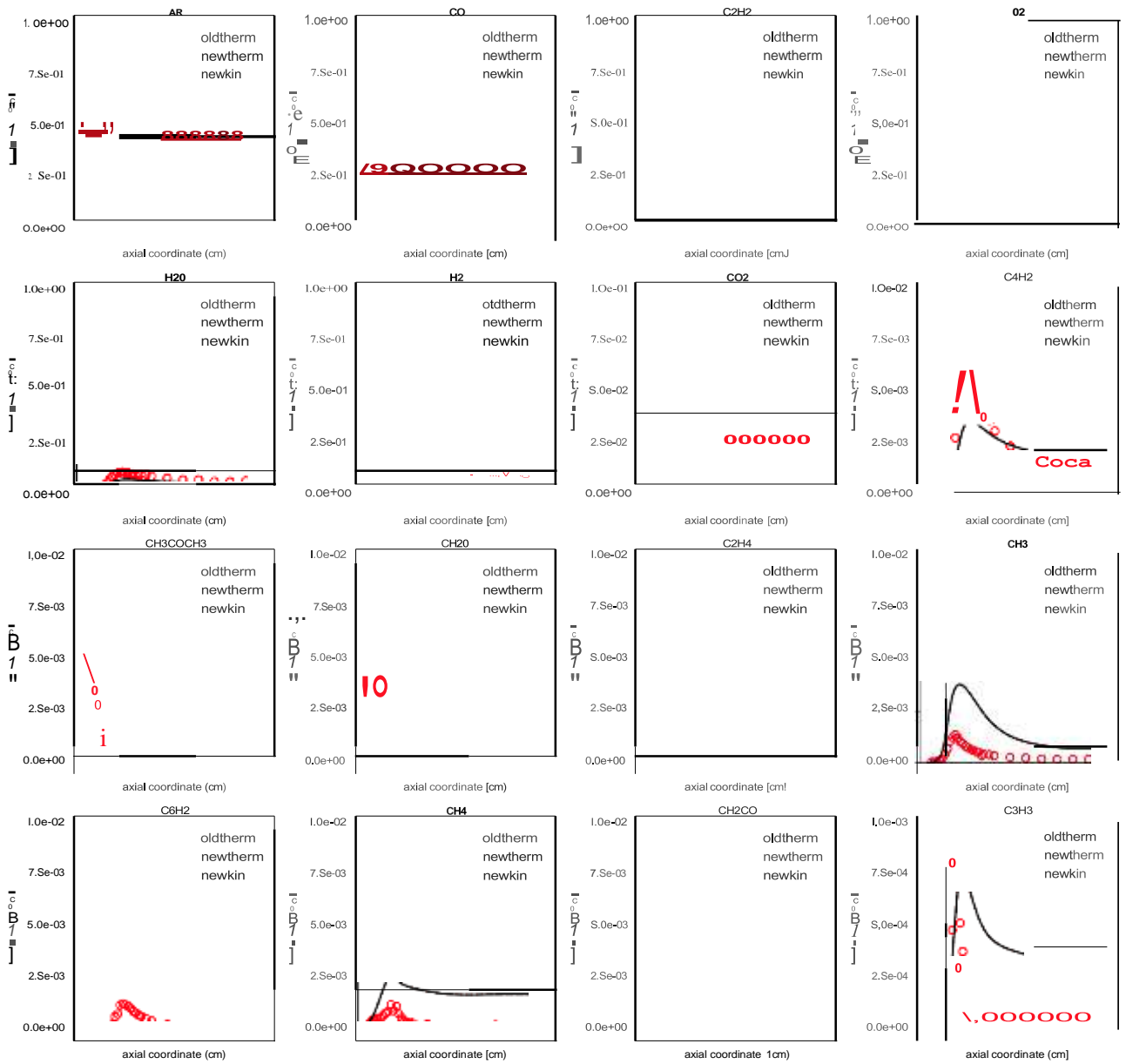


Figure S19: Experimental (points) and simulated (lines) mole fraction profiles of relevant detected products in the toluene oxidation experiments in the jet stirred reactor of Meziane et al.⁹ ($\phi = 0.5$). Dotted red lines: starting model (oldtherm), dashed black lines: updated thermochemistry (newtherm), solid black lines: final model with updated kinetics (newkin). *Plot generated automatically with SciExpeM post-processing tools.

C2H2/O2	PF	500-1990	0.04	2.4	Bierkandt et al. ¹⁰
---------	----	----------	------	-----	--------------------------------



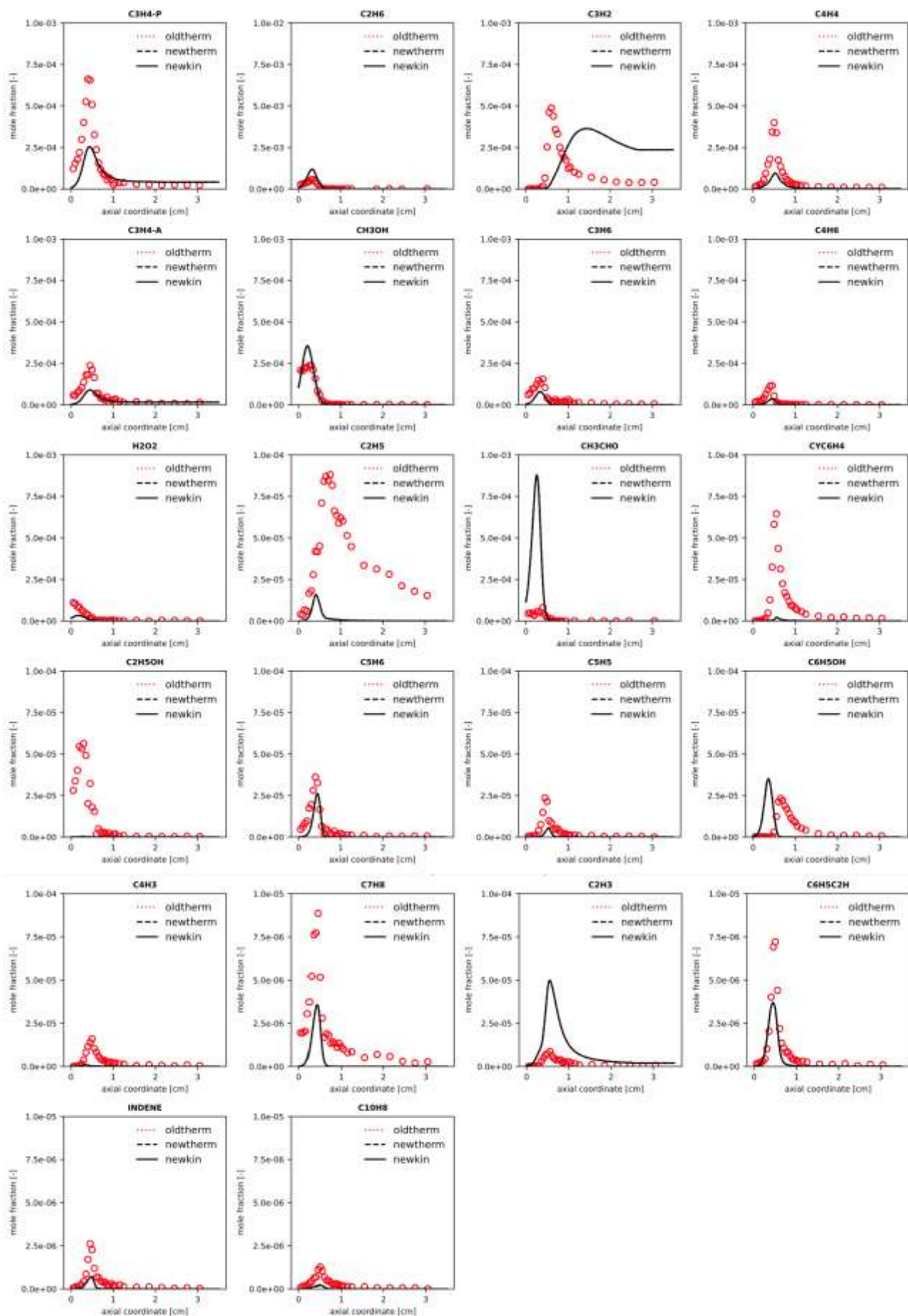


Figure S20: Experimental (points) and simulated (lines) mole fraction profiles of relevant detected products in the acetylene oxidation experiments in the premixed flame of Bierkandt et al.¹⁰. Dotted red lines: starting model (oldtherm), dashed black lines: updated thermochemistry (newtherm), solid black lines: final model with updated kinetics (newkin). *Plot generated automatically with SciExpeM post-processing tools.

C2H2/O2	CF	300-1900	1	-	Baroncelli et al. ¹¹
---------	----	----------	---	---	---------------------------------

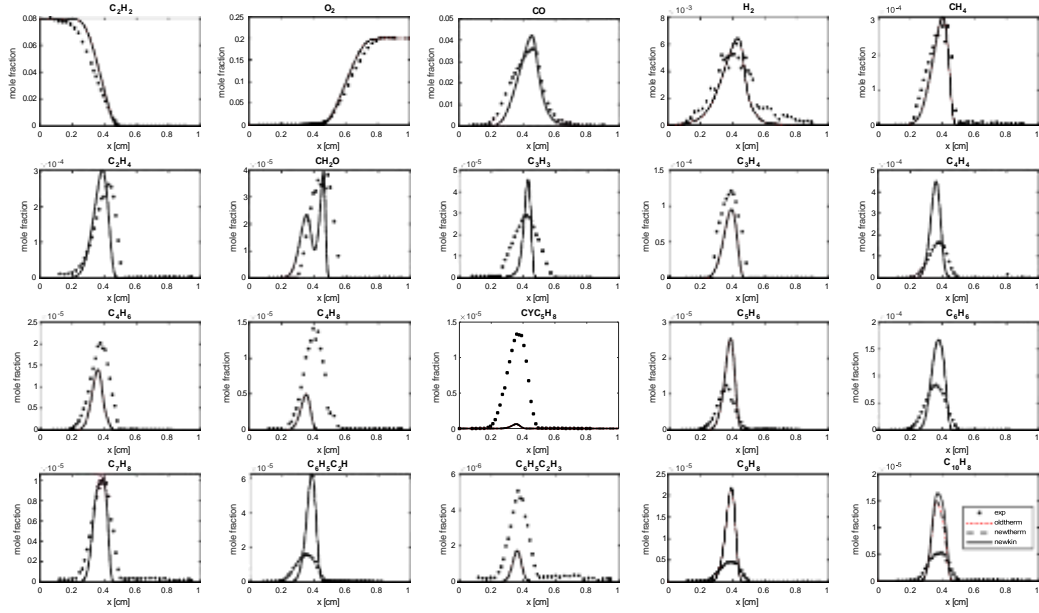
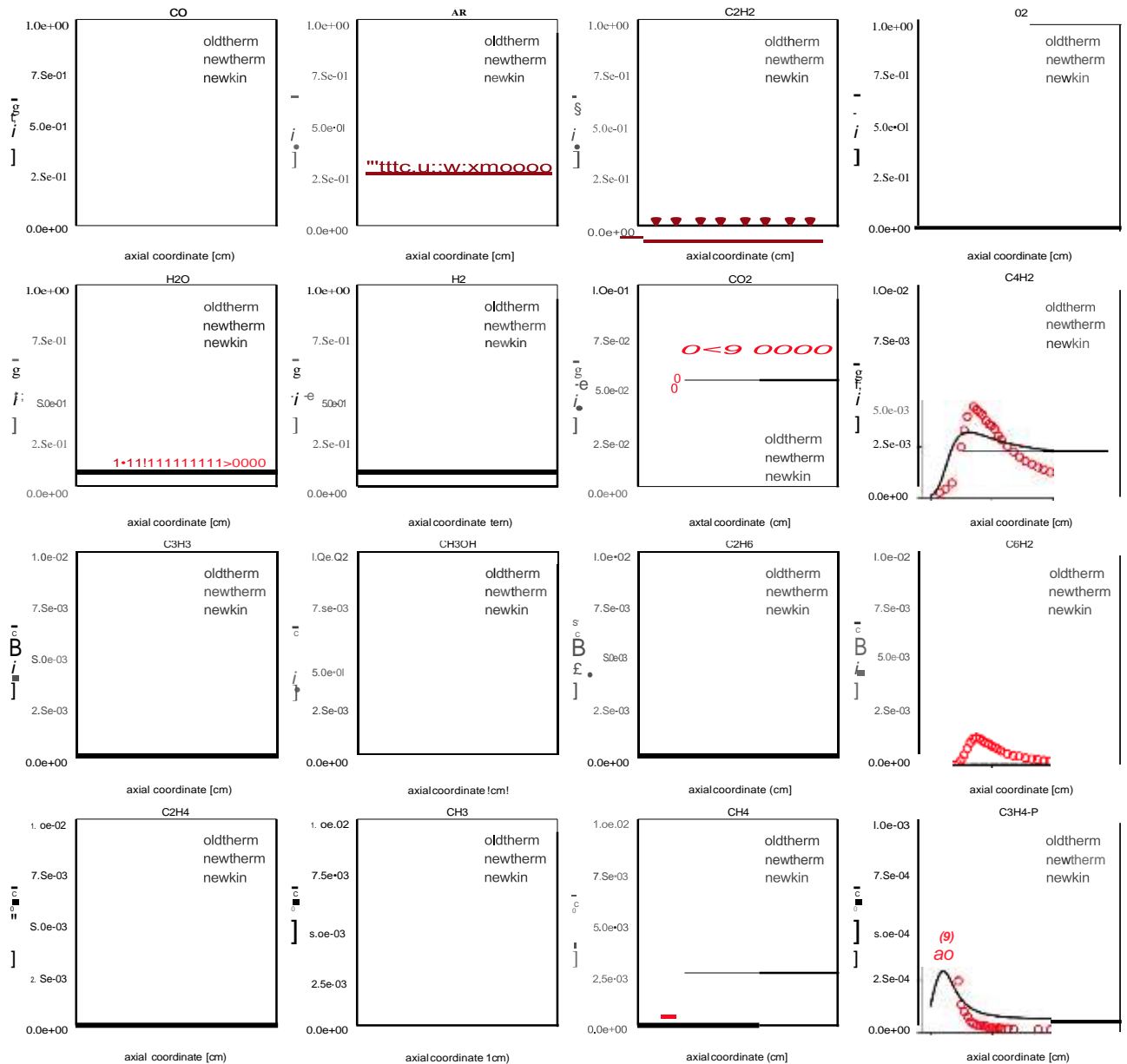


Figure S21: Experimental (points) and simulated (lines) mole fraction profiles of relevant detected products in the counterflow diffusion flame experiments of acetylene oxidation of Baroncelli et al.¹¹. Dotted red lines: starting model (oldtherm), dashed black lines: updated thermochemistry (newtherm), solid black lines: final model with updated kinetics (newkin)

C2H2/O2/Ar	PF	450-1912	0.03	2.25	Li et al. ¹²
------------	----	----------	------	------	-------------------------



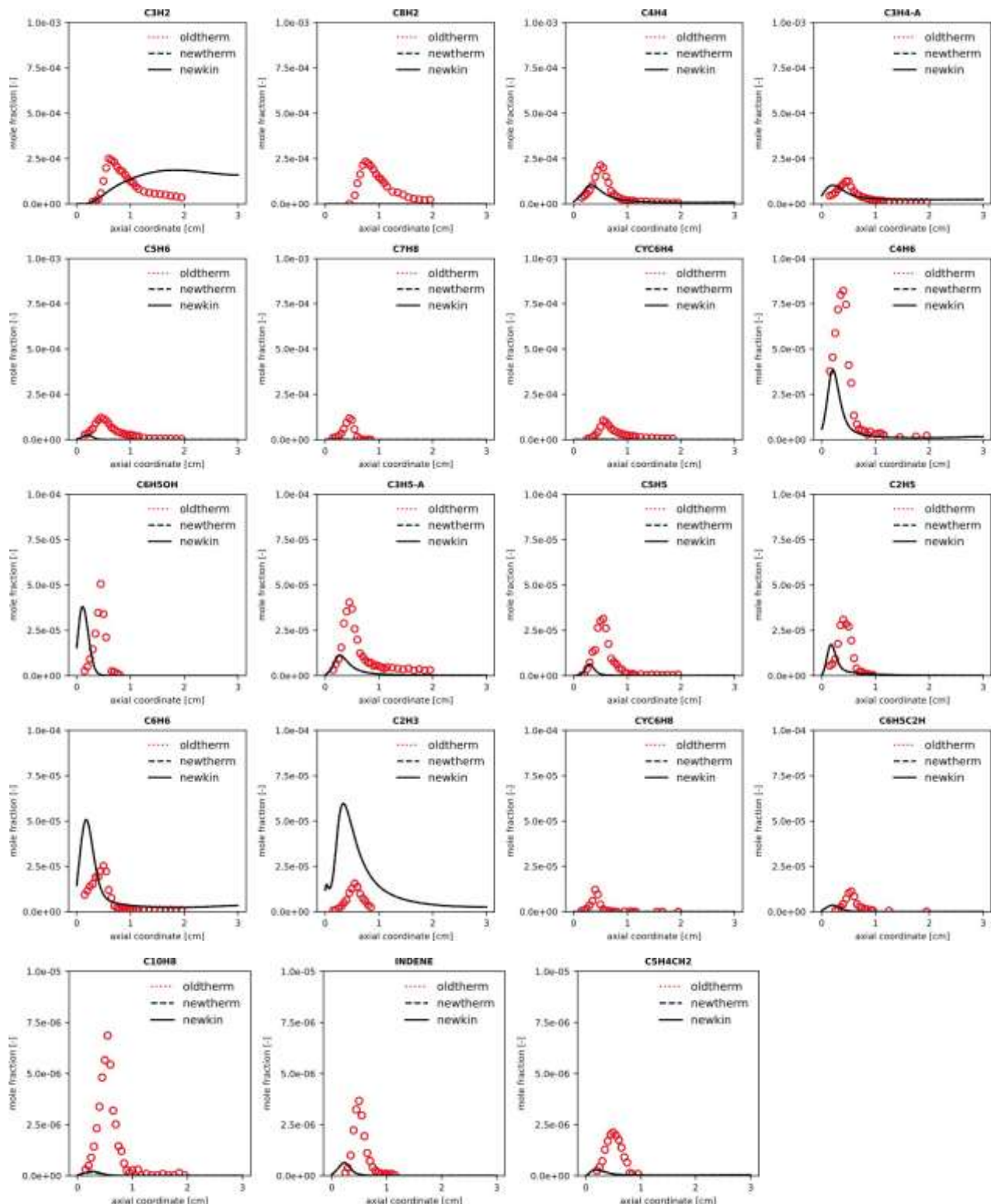
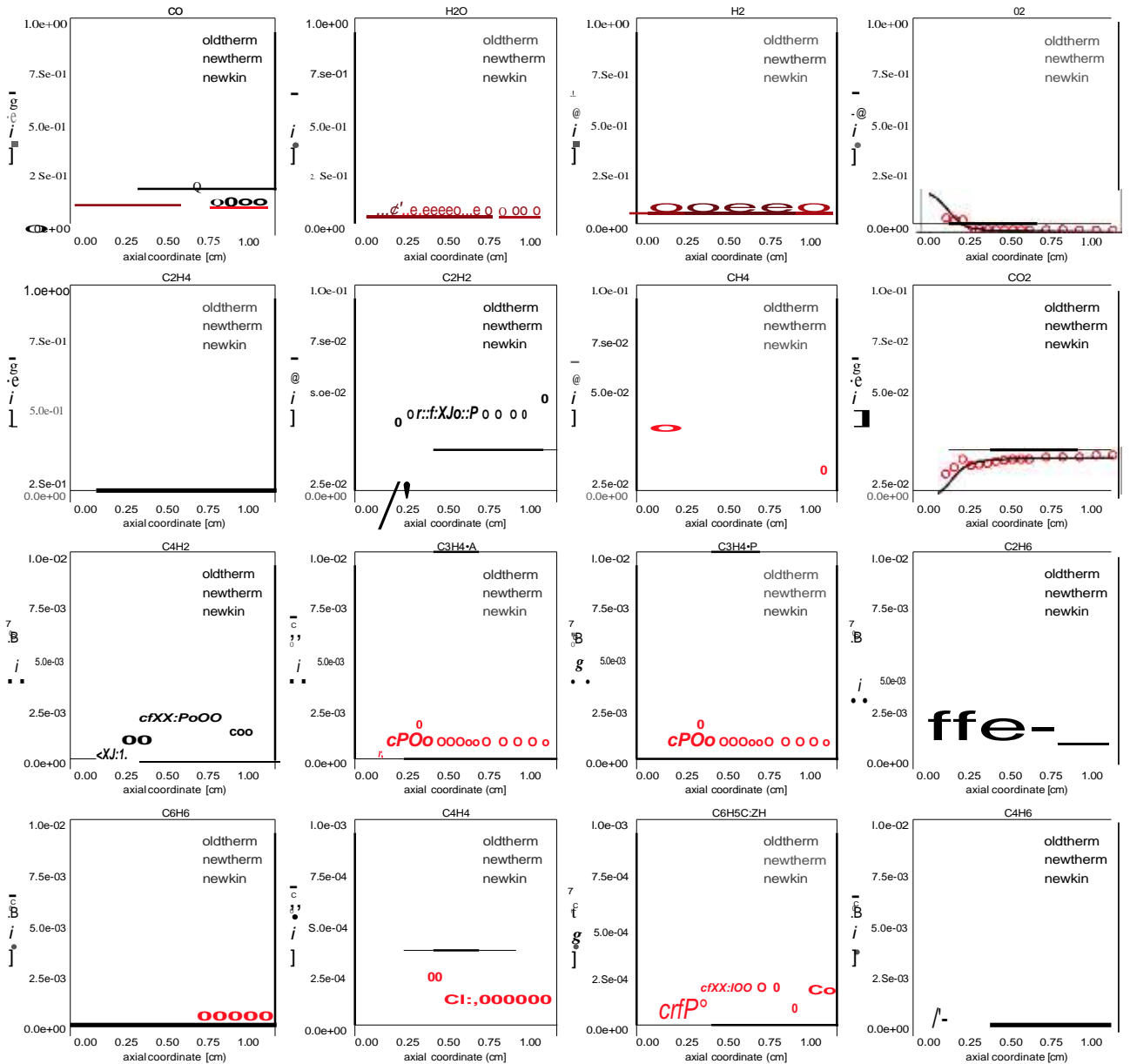


Figure S22: Experimental (points) and simulated (lines) mole fraction profiles of relevant detected products in the acetylene oxidation experiments in the premixed flame of Li et al.¹². Dotted red lines: starting model (oldtherm), dashed black lines: updated thermochemistry (newtherm), solid black lines: final model with updated kinetics (newkin). *Plot generated automatically with SciExpeM post-processing tools.

C2H4/O2/Ar	PF	300-1430	1	3.1	Castaldi et al. ¹³
------------	----	----------	---	-----	-------------------------------



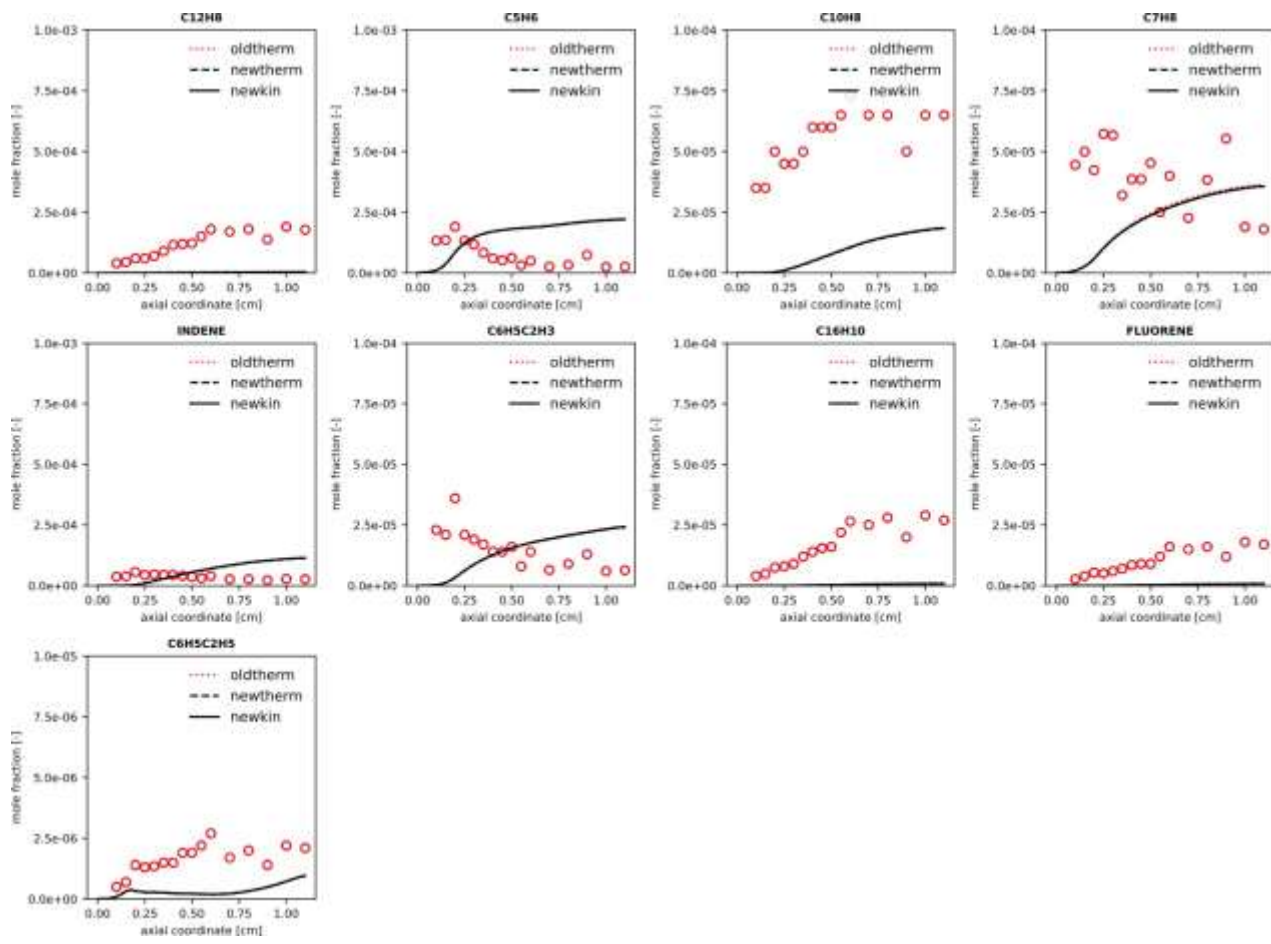


Figure S23: Experimental (points) and simulated (lines) mole fraction profiles of relevant detected products in the ethylene oxidation experiments in the premixed flame of Castaldi et al.¹³. Dotted red lines: starting model (oldtherm), dashed black lines: updated thermochemistry (newtherm), solid black lines: final model with updated kinetics (newkin). *Plot generated automatically with SciExpeM post-processing tools.

C2H4/O2/Ar	PF	300-1600	1	2.7	Harris et al. ¹⁴
------------	----	----------	---	-----	-----------------------------

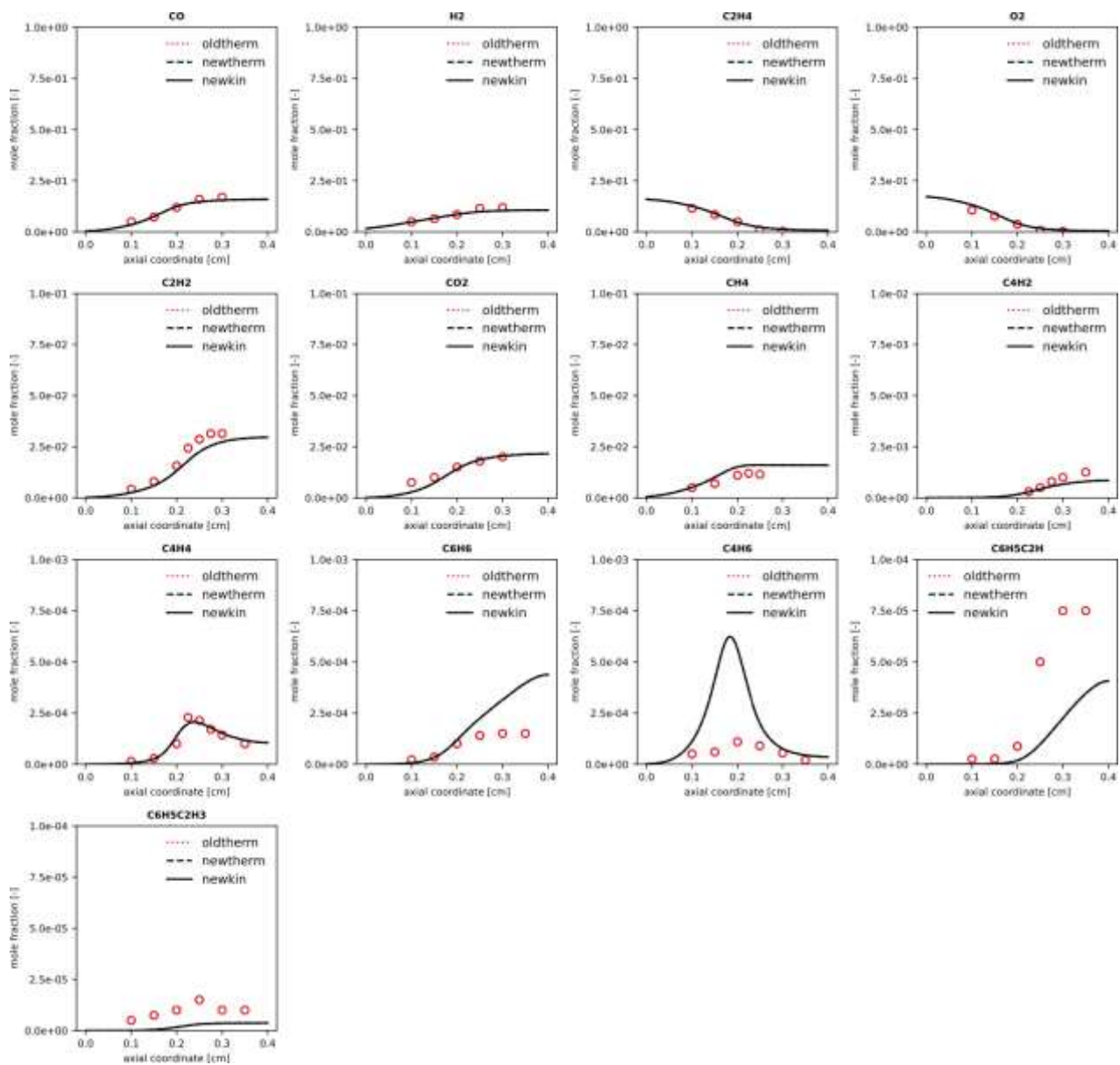
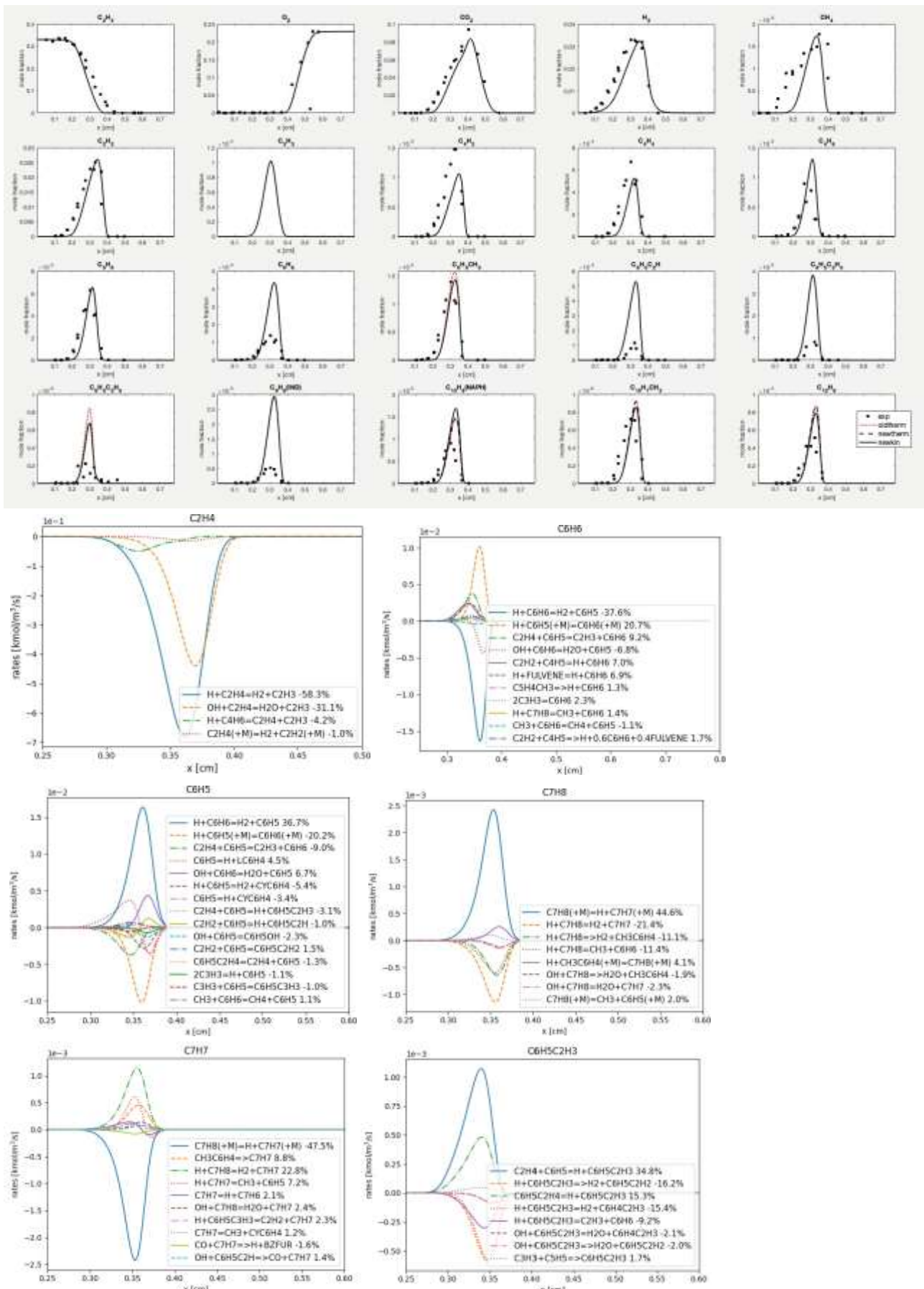


Figure S24: Experimental (points) and simulated (lines) mole fraction profiles of relevant detected products in the ethylene oxidation experiments in the premixed flame of Harris et al.¹⁴. Dotted red lines: starting model (oldtherm), dashed black lines: updated thermochemistry (newtherm), solid black lines: final model with updated kinetics (newkin). *Plot generated automatically with SciExpeM post-processing tools.

C2H4/O ₂	CF		1	-	Carbone et al. ¹⁵
---------------------	----	--	---	---	------------------------------



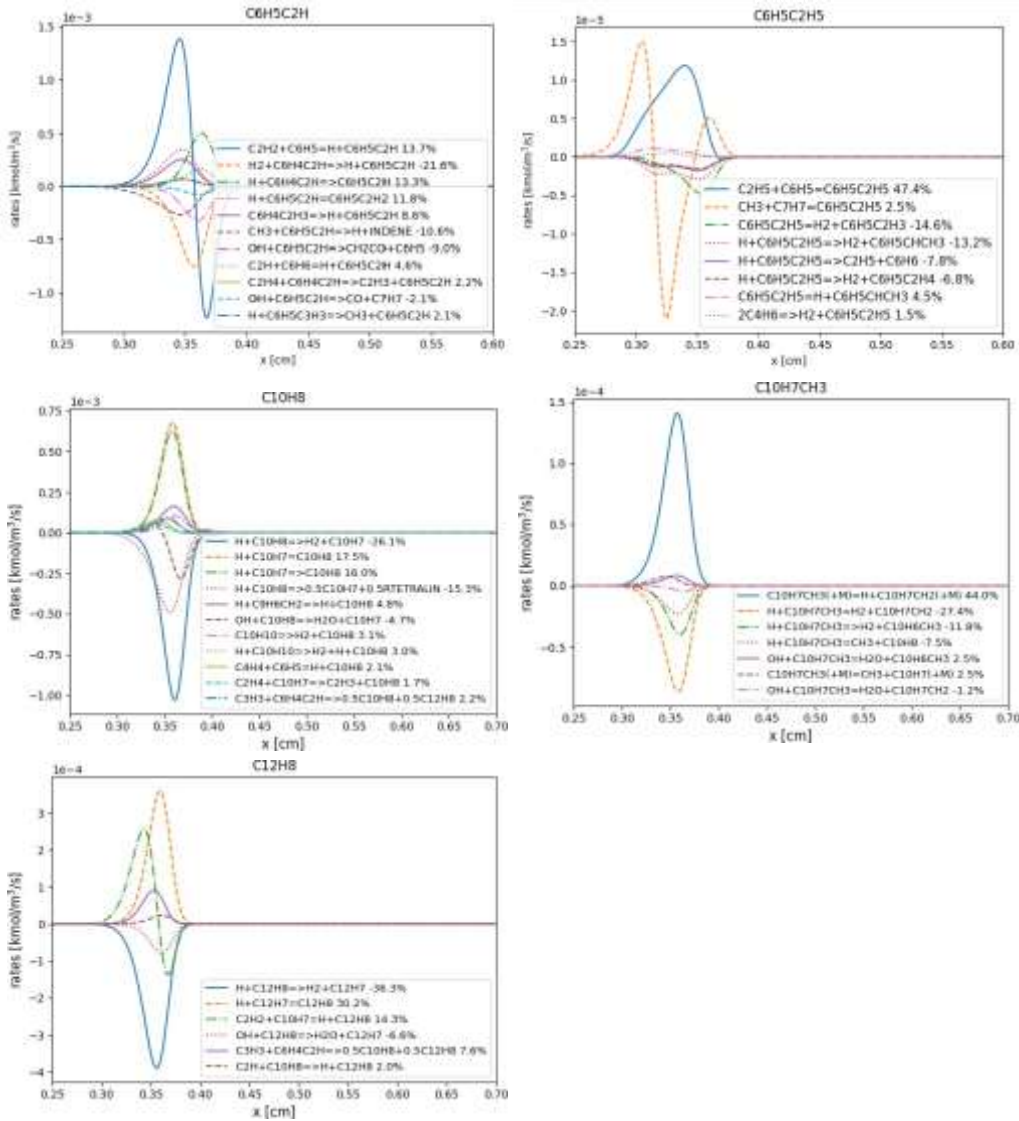
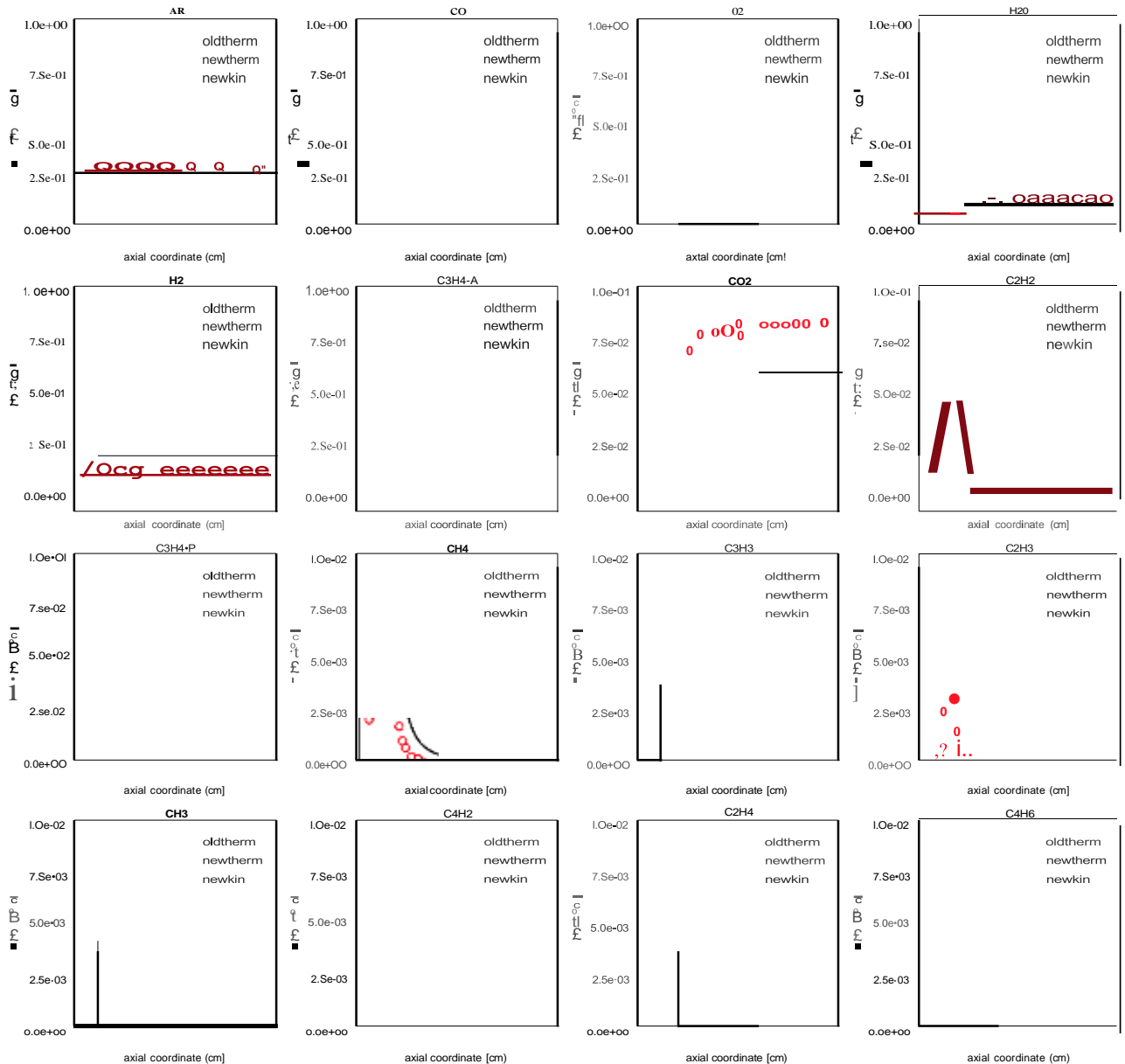


Figure S25: Experimental (points) and simulated (lines) mole fraction profiles of relevant detected products in the counterflow diffusion flame experiments of ethylene oxidation of Carbone et al.¹⁵. Dotted red lines: starting model (oldtherm), dashed black lines: updated thermochemistry (newtherm), solid black lines: final model with updated kinetics (newkin). Bottom: reaction rate analysis for some relevant species in addition to that presented in the main text.

In the kinetic simulations presented, it is observed that the CRECK model generally overestimates benzene, monosubstituted aromatics with the exception of toluene, and naphthalene. However, the smaller species are generally well predicted by the model. The discrepancy in terms of benzene can be analyzed with the reaction rate analysis in the figure above. The main reaction pathways involving H-abstractions from benzene and H recombination with phenyl are well known in the literature. The main formation pathway of benzene is $\text{C}_2\text{H}_2 + \text{C}_4\text{H}_5$. It is noted that in the CRECK model C_4H_5 is lumped and the main form considered is n- C_4H_5 . The reactivity of the latter is faster than that of i- C_4H_5 , such that it is possible that the rate constants of this reaction should be decreased in the model to account for the averaging with the reactivity of i- C_4H_5 . In addition, it is noted that the model overestimates slightly the concentration of 1,3-butadiene, suggesting that the large production of benzene might also be associated with this overprediction. Another reaction whose rate constant

might need improvement is that of $C_6H_5 + C_2H_4 = C_6H_6 + C_2H_3$, which was taken from a relatively old literature work. Concerning phenyl reactivity, the most uncertain reactions that appear in the reaction rate analysis are those of its unimolecular decomposition. From the rate analysis, the overpredictions of phenylacetylene and styrene can be directly attributed to that of benzene, which is their main precursor. Ethylbenzene formation instead is equally due to benzene and toluene, hence is overestimation is not as strong as in the case of phenylacetylene and styrene. Naphthalene formation is dominated by reaction pathways involving $C_6 + C_4$, the HACA mechanism, or phenyl-like radicals + C_3H_3 reactions. Therefore, the overestimation of naphthalene with respect to the experimental data is associated with that of benzene. The same applies to acenaphthylene, which comes primarily from naphthyl radical. Conversely, toluene and methylnaphthalene are well predicted by the model. The rate analyses show that abstraction and recombination reactions from the respective radicals dominate their formation and consumption. However, these species ultimately trace back to methyl recombinations with phenyl and naphthyl, respectively.

C3H4-A/O2 C3H4-P/O2	PF	298-2260	0.03	1.8	Hansen et al. ¹⁶
------------------------	----	----------	------	-----	-----------------------------



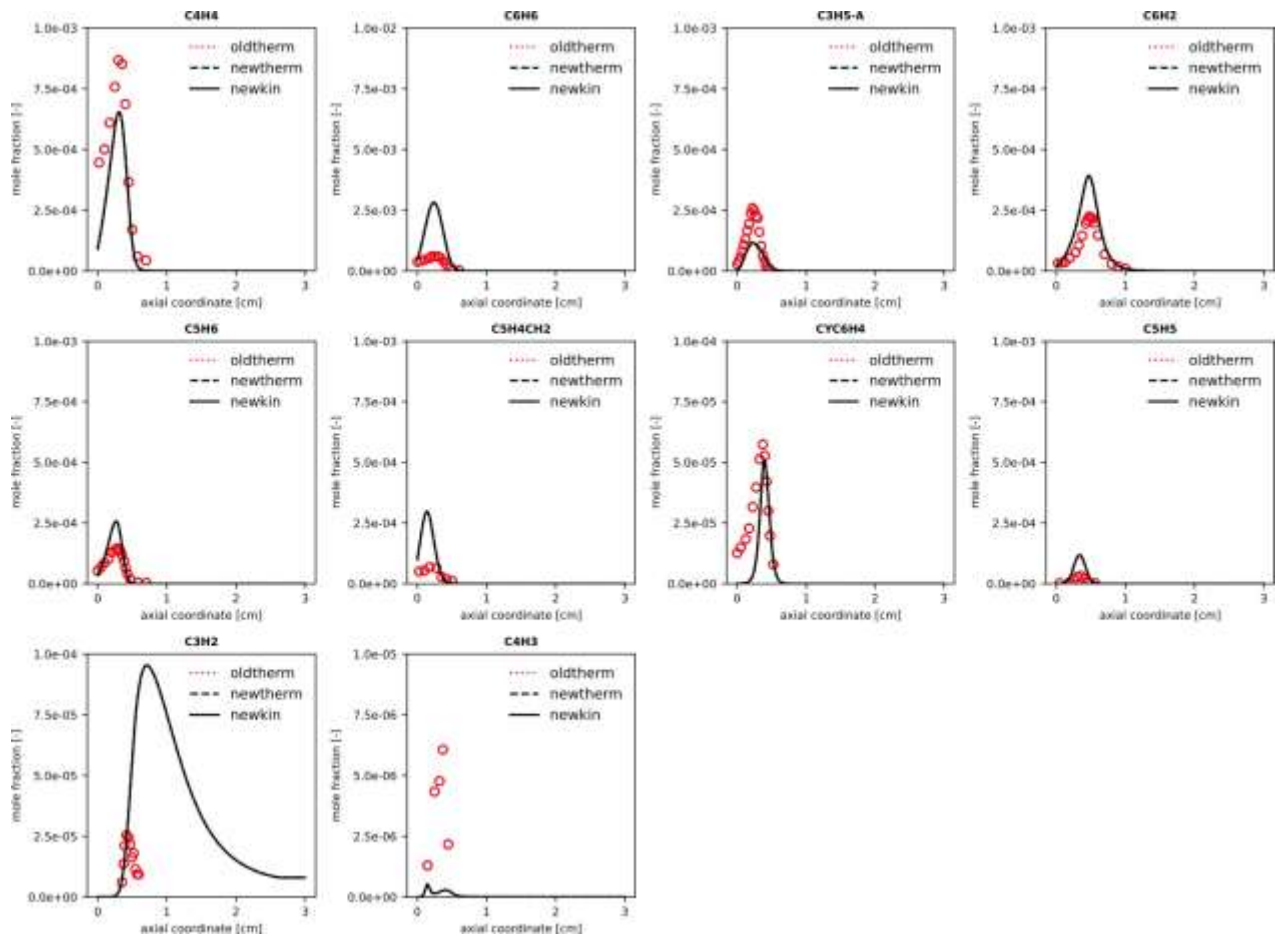
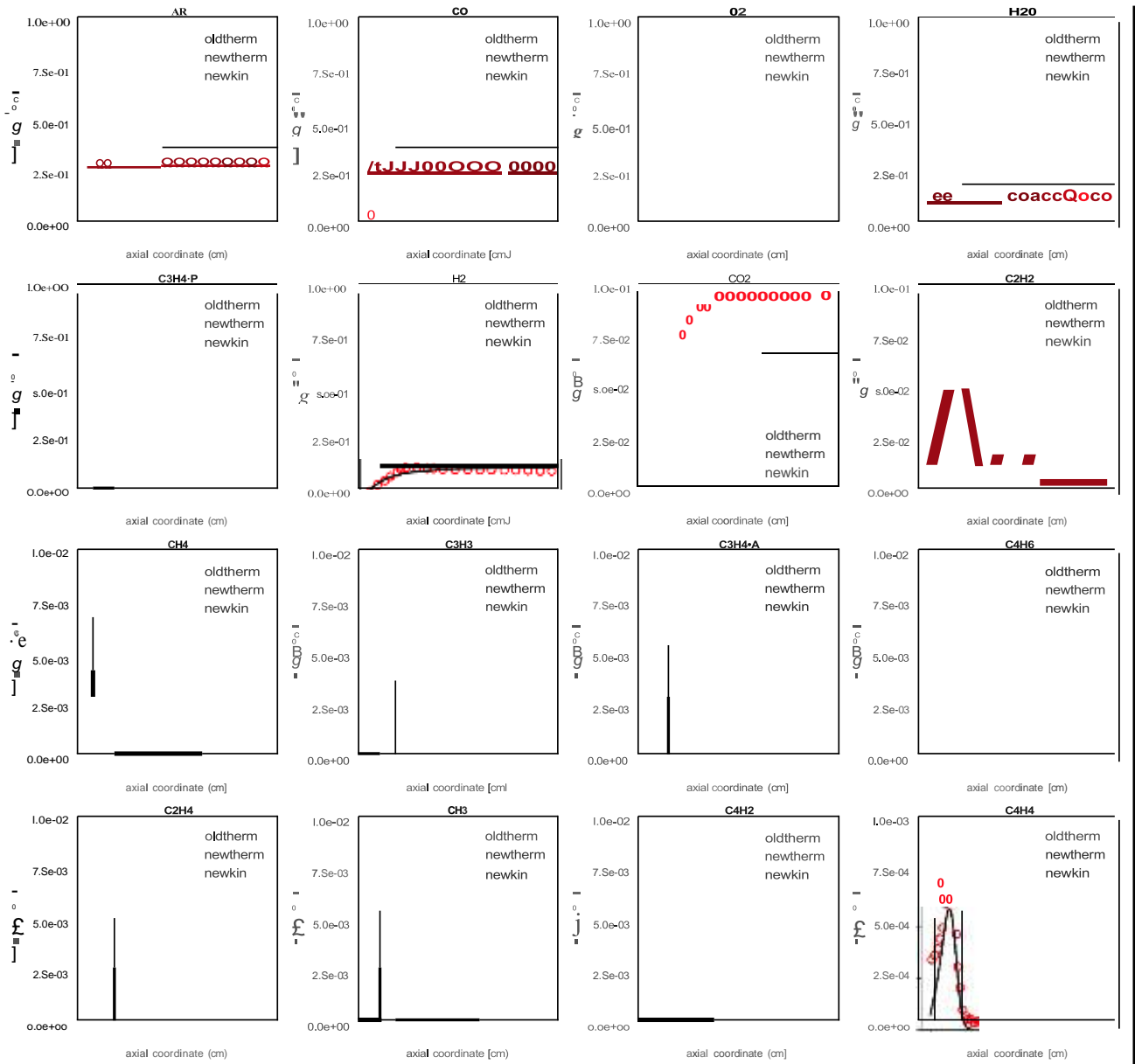
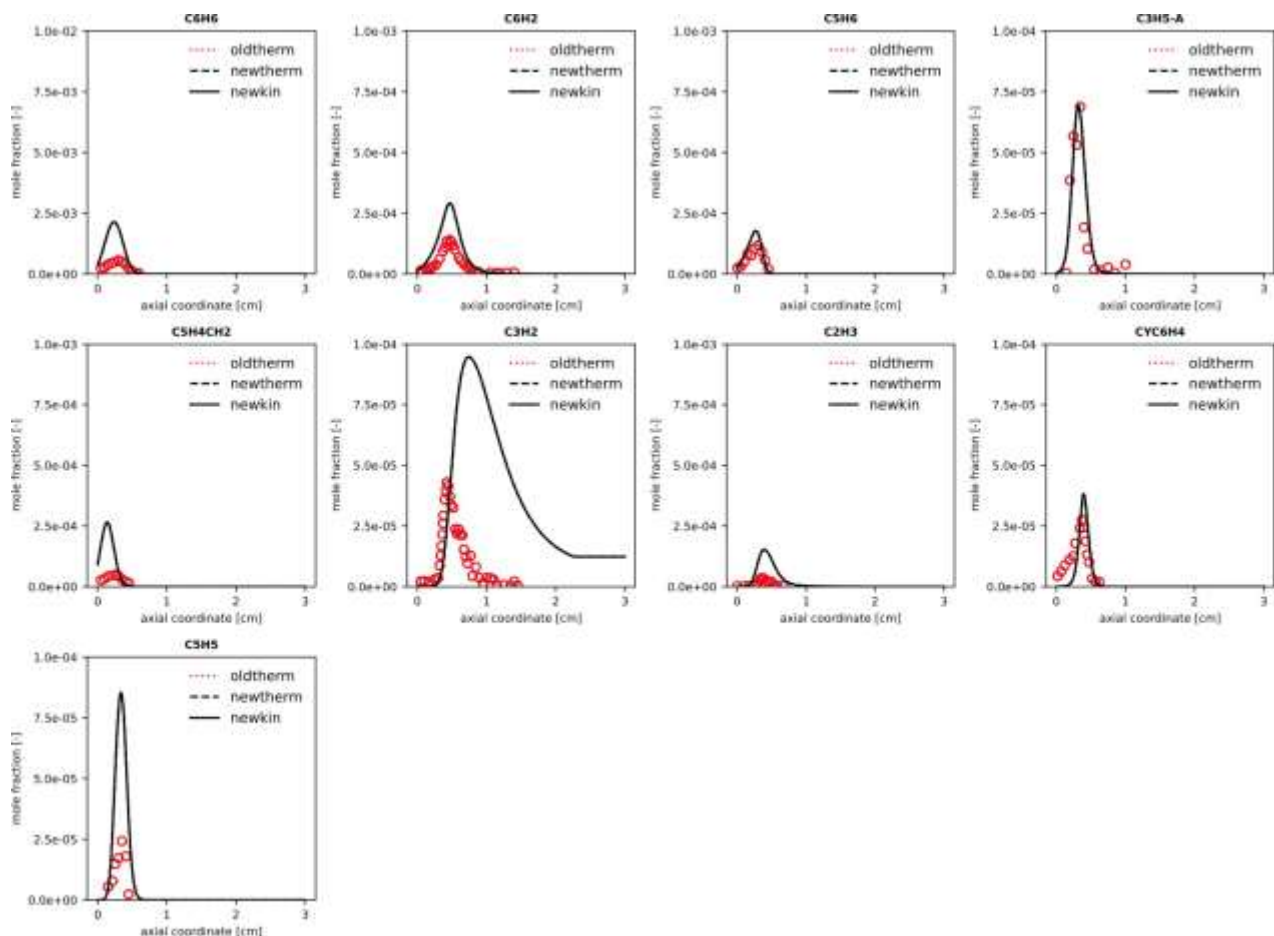


Figure S26: Experimental (points) and simulated (lines) mole fraction profiles of relevant detected products in the allene oxidation experiments in the premixed flame of Hansen et al.¹⁶. Dotted red lines: starting model (oldtherm), dashed black lines: updated thermochemistry (newtherm), solid black lines: final model with updated kinetics (newkin). *Plot generated automatically with SciExpeM post-processing tools.





*Figure S27: Experimental (points) and simulated (lines) mole fraction profiles of relevant detected products in the propyne oxidation experiments in the premixed flame of Hansen et al.¹⁶. Dotted red lines: starting model (oldtherm), dashed black lines: updated thermochemistry (newtherm), solid black lines: final model with updated kinetics (newkin). *Plot generated automatically with SciExpeM post-processing tools.*

C3H4-A/O ₂	CF	300-1870	0.9	-	Kukkadapu et al. ¹⁷
C3H4-P/O ₂					

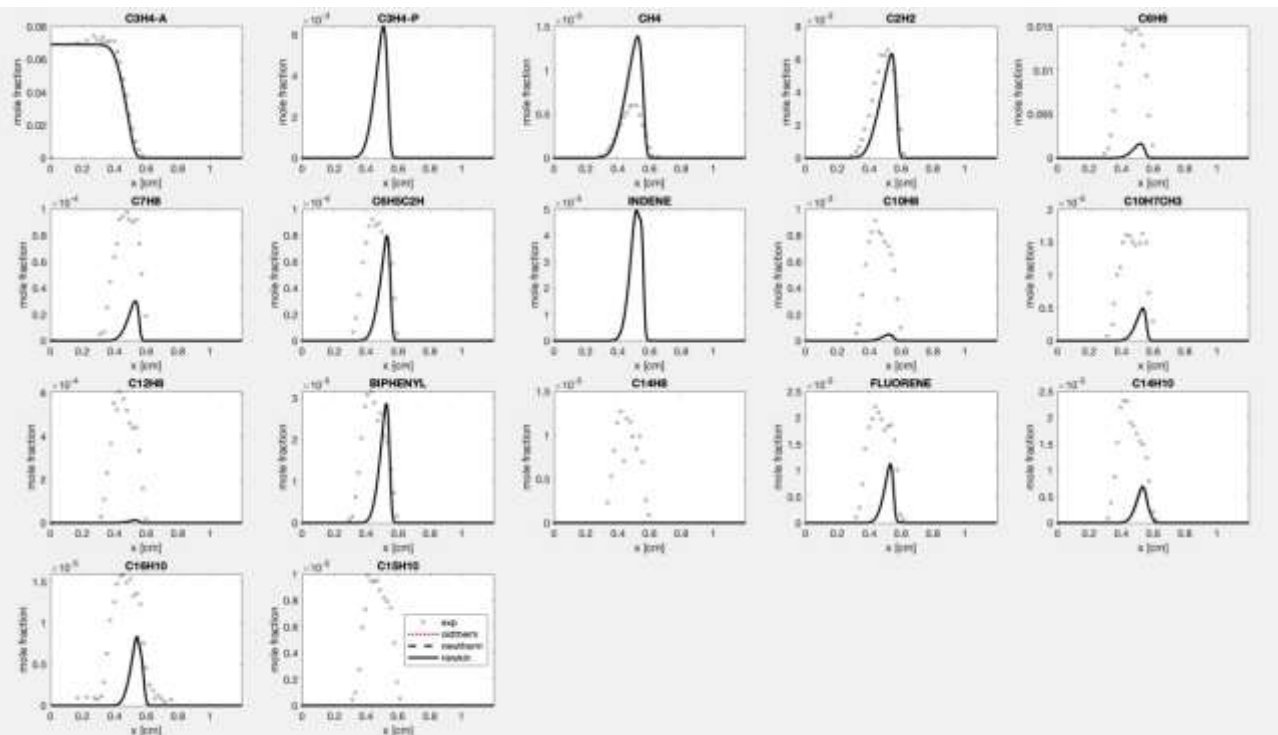


Figure S28: Experimental (points) and simulated (lines) mole fraction profiles of relevant detected products in the counterflow diffusion flame experiments of allene oxidation of Kukkadapu et al.¹⁷. Dotted red lines: starting model (oldtherm), dashed black lines: updated thermochemistry (newtherm), solid black lines: final model with updated kinetics (newkin)

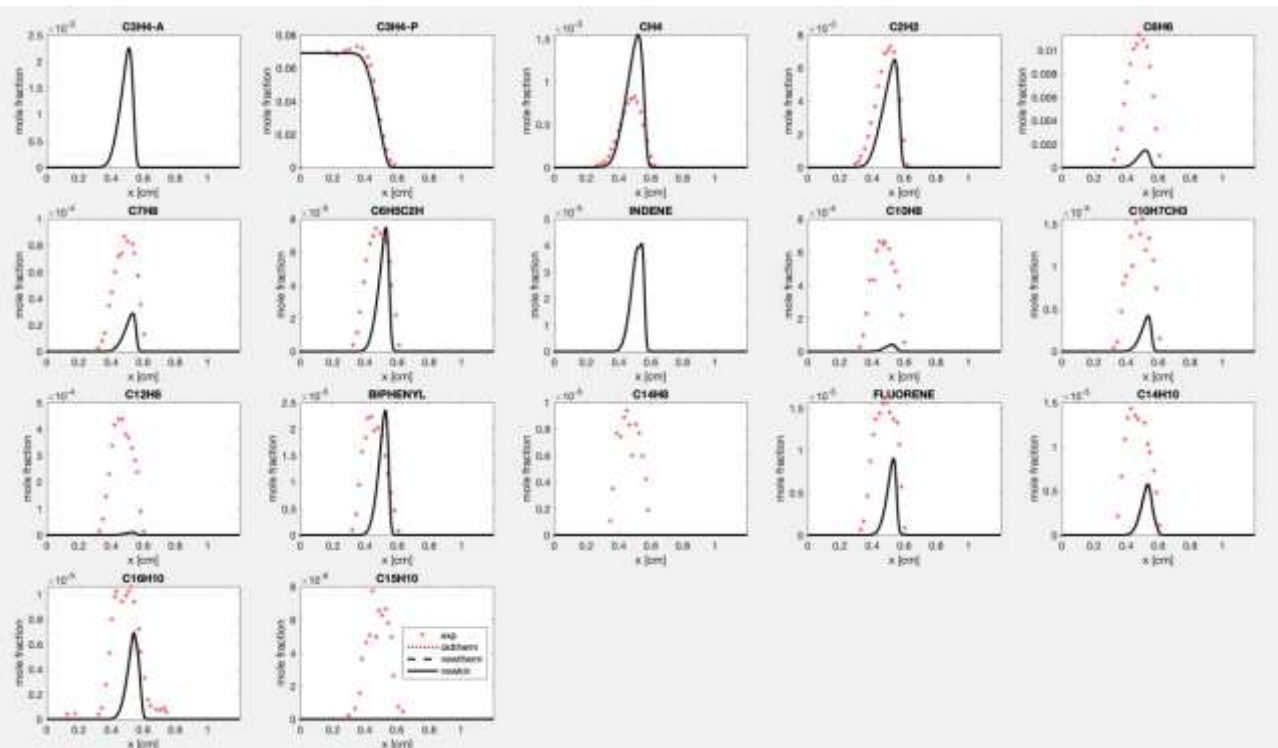
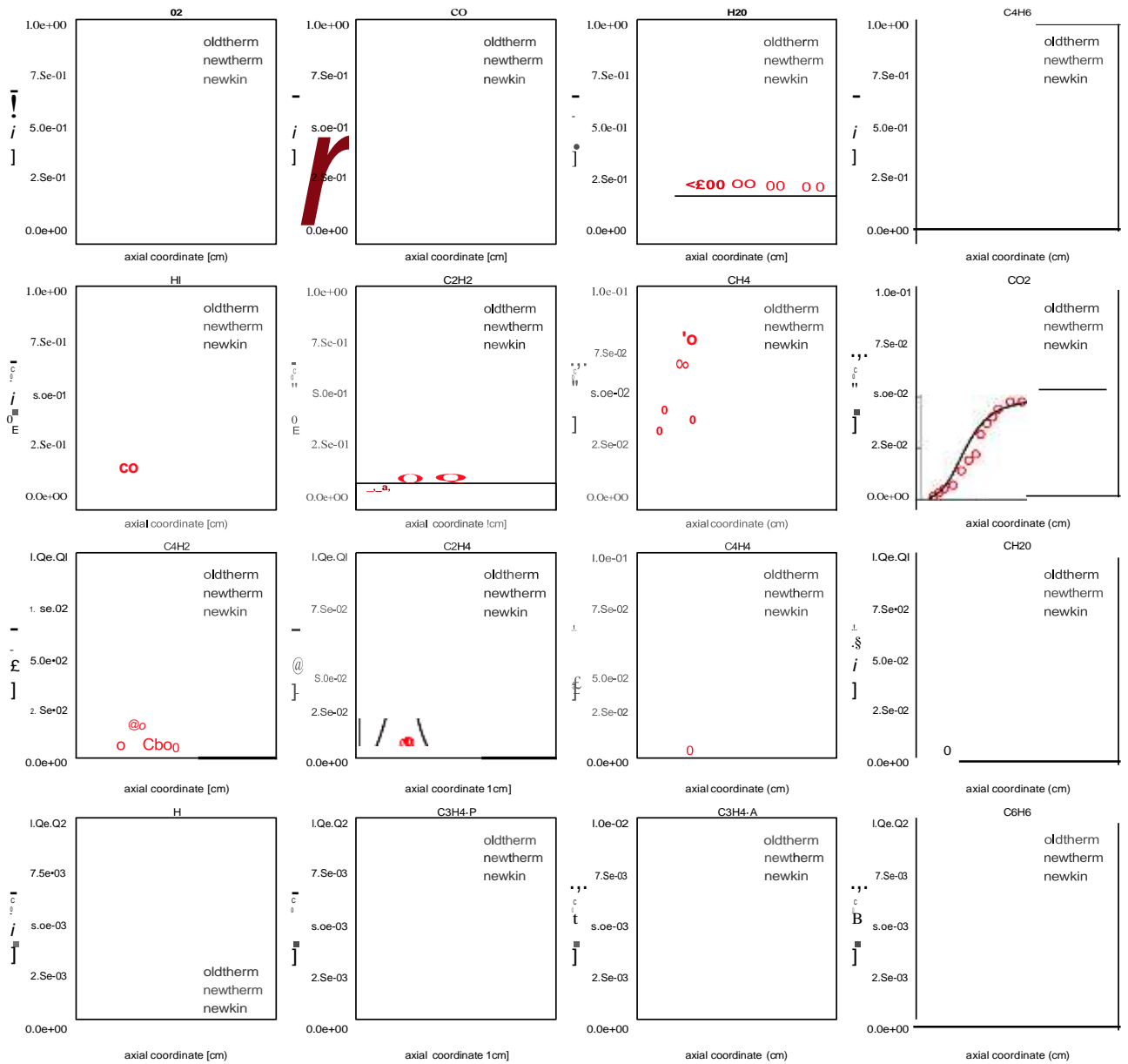


Figure S29: Experimental (points) and simulated (lines) mole fraction profiles of relevant detected products in the counterflow diffusion flame experiments of propyne oxidation of Kukkadapu et al.¹⁷. Dotted red lines: starting model (oldtherm), dashed black lines: updated thermochemistry (newtherm), solid black lines: final model with updated kinetics (newkin)

C4H6	PF	300-2050	0.026	2.4	Cole et al. ¹⁸
------	----	----------	-------	-----	---------------------------



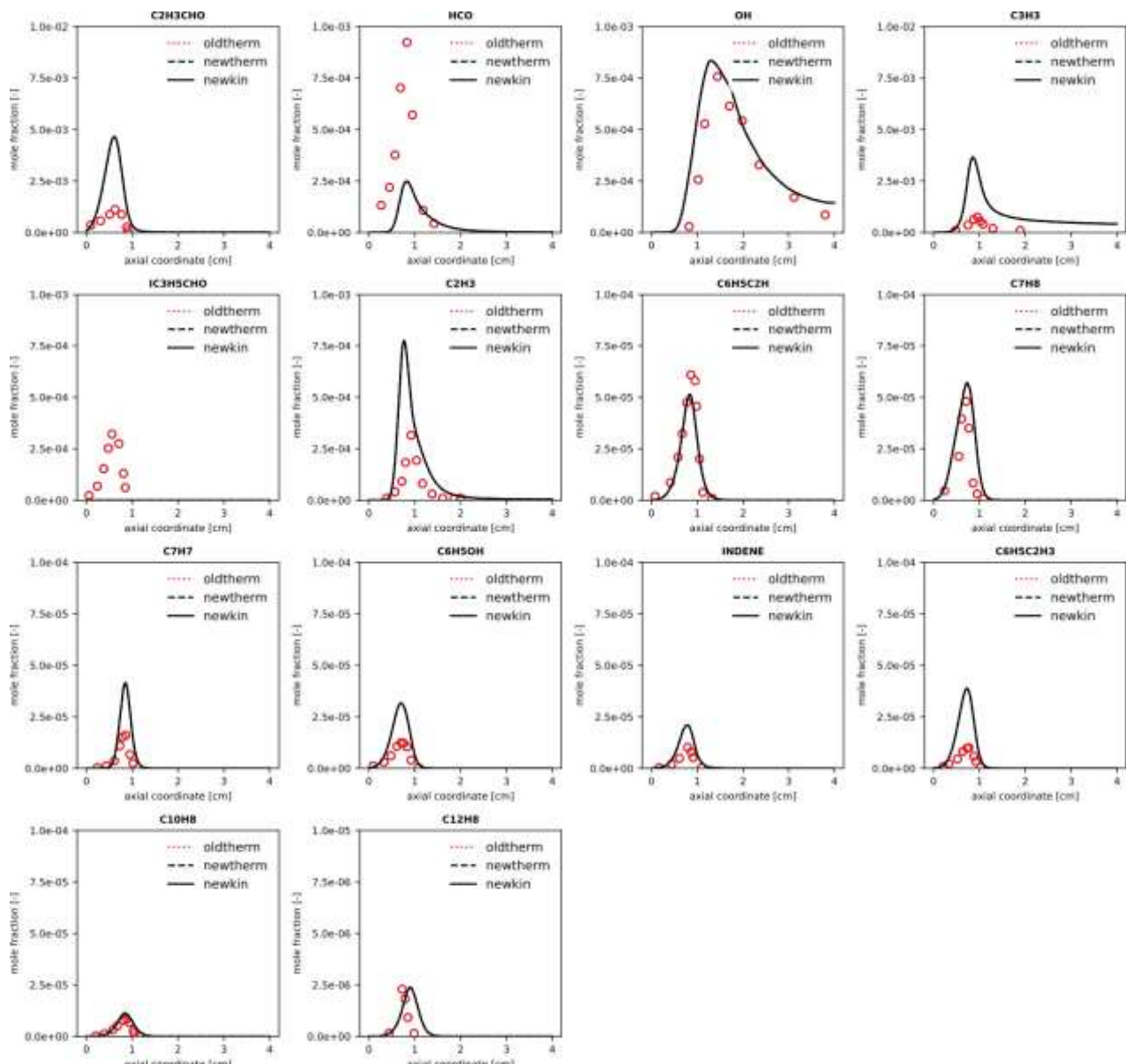
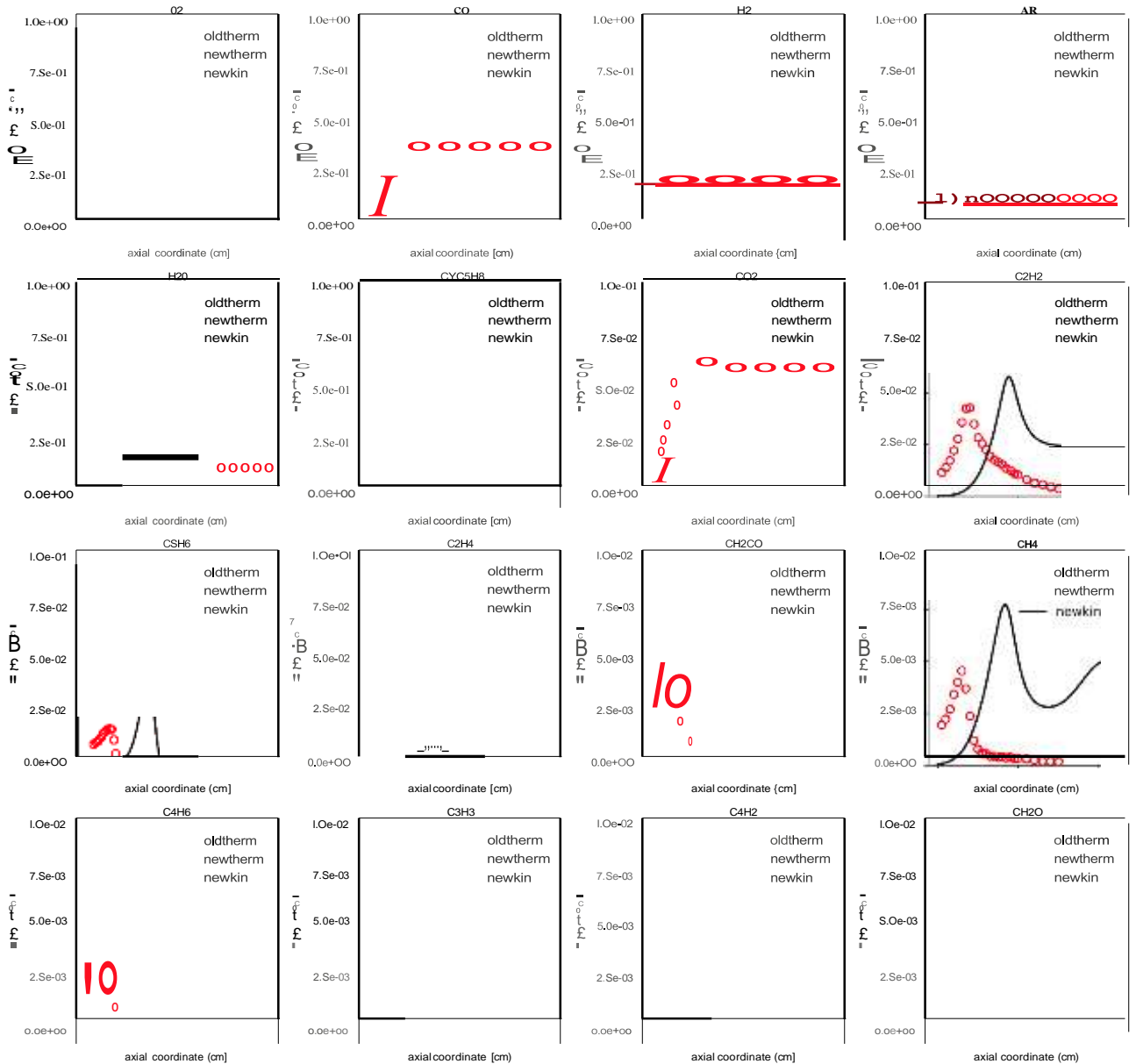
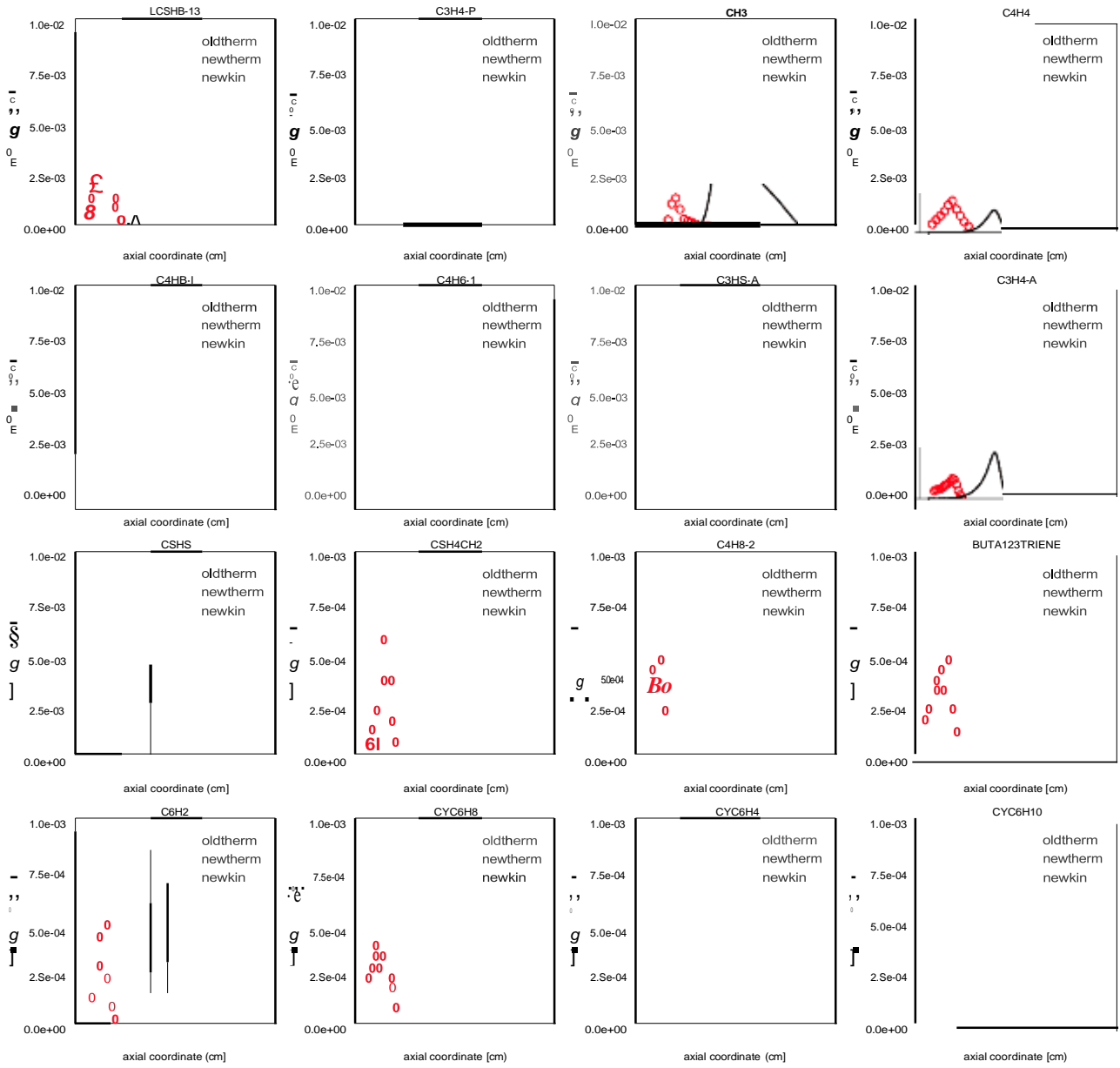


Figure S30: Experimental (points) and simulated (lines) mole fraction profiles of relevant detected products in the 1,3-butadiene oxidation experiments in the premixed flame of Cole et al.¹⁸. Dotted red lines: starting model (oldtherm), dashed black lines: updated thermochemistry (newtherm), solid black lines: final model with updated kinetics (newkin). *Plot generated automatically with SciExpeM post-processing tools.

CYC5H8	PF	350-2200	0.05	2	Hansen et al. ¹⁹
--------	----	----------	------	---	-----------------------------





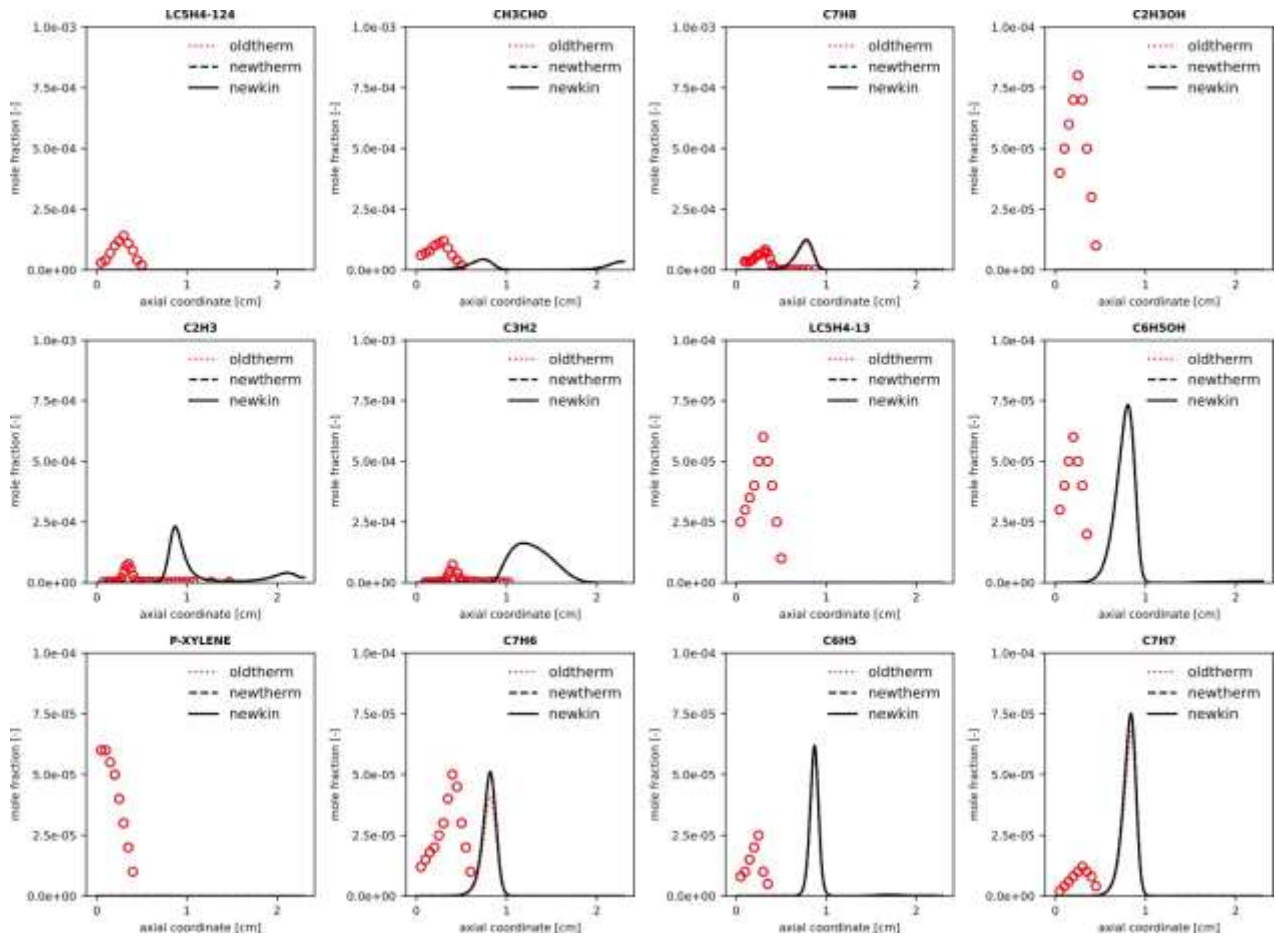


Figure S31: Experimental (points) and simulated (lines) mole fraction profiles of relevant detected products in the 1,3-butadiene oxidation experiments in the premixed flame of Hansen et al.¹⁹. Dotted red lines: starting model (oldtherm), dashed black lines: updated thermochemistry (newtherm), solid black lines: final model with updated kinetics (newkin). *Plot generated automatically with SciExpeM post-processing tools. Simulated lines should be shifted by 0.5 cm to account for facility effects.

CYC5H8/CH4/O2	CF	300-2100	0.08	-	Baroncelli et al. ²⁰
---------------	----	----------	------	---	---------------------------------

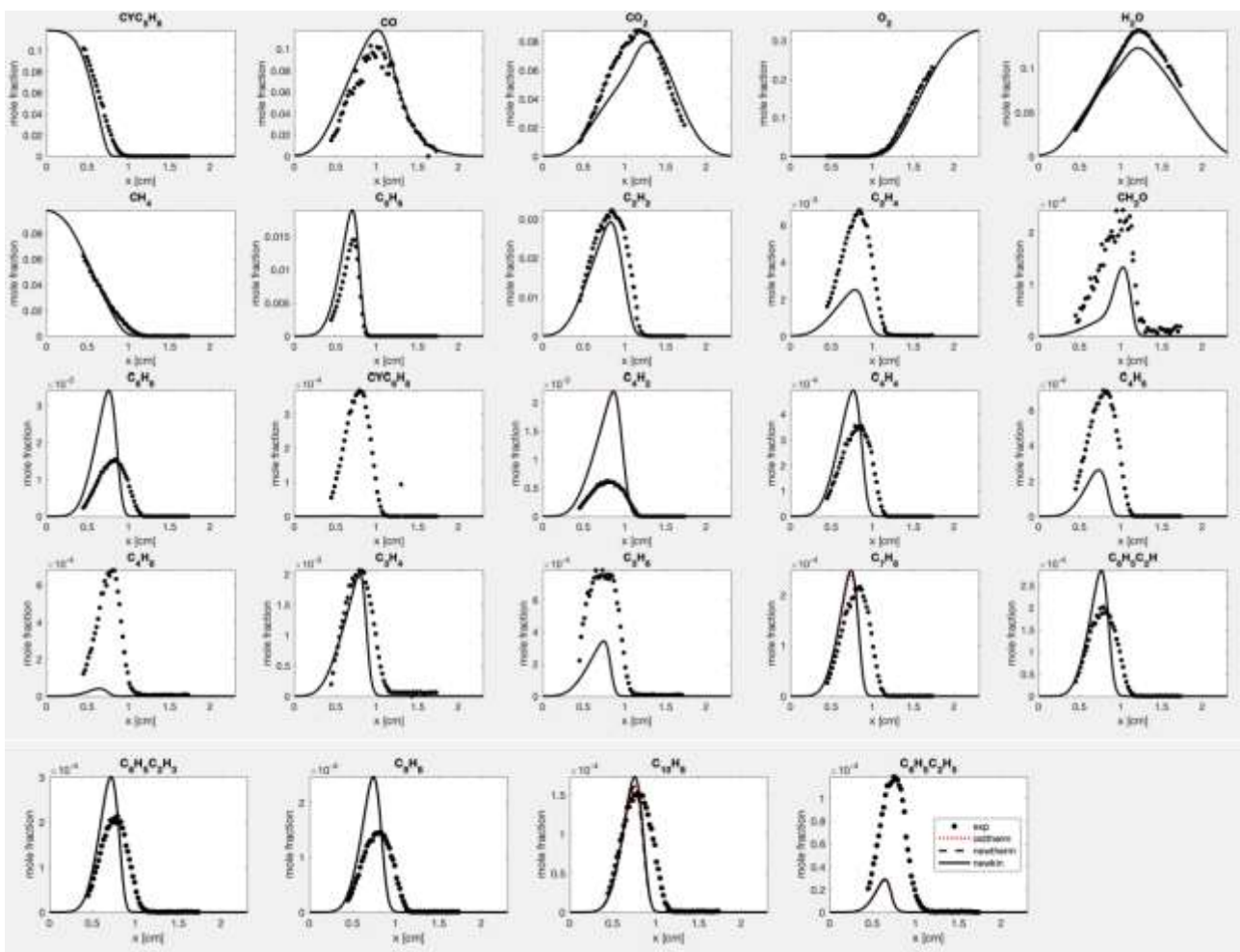


Figure S32: Experimental (points) and simulated (lines) mole fraction profiles of relevant detected products in the counterflow diffusion flame experiments of methane-doped cyclopentene oxidation of Baroncelli et al.²⁰. Dotted red lines: starting model (oldtherm), dashed black lines: updated thermochemistry (newtherm), solid black lines: final model with updated kinetics (newkin)

C7H8/O2/Ar	PF	426-2050	0.04	0.75, 1.0, 1.25, 1.75, 1.9	Li et al. ^{21,22}
------------	----	----------	------	-------------------------------	----------------------------

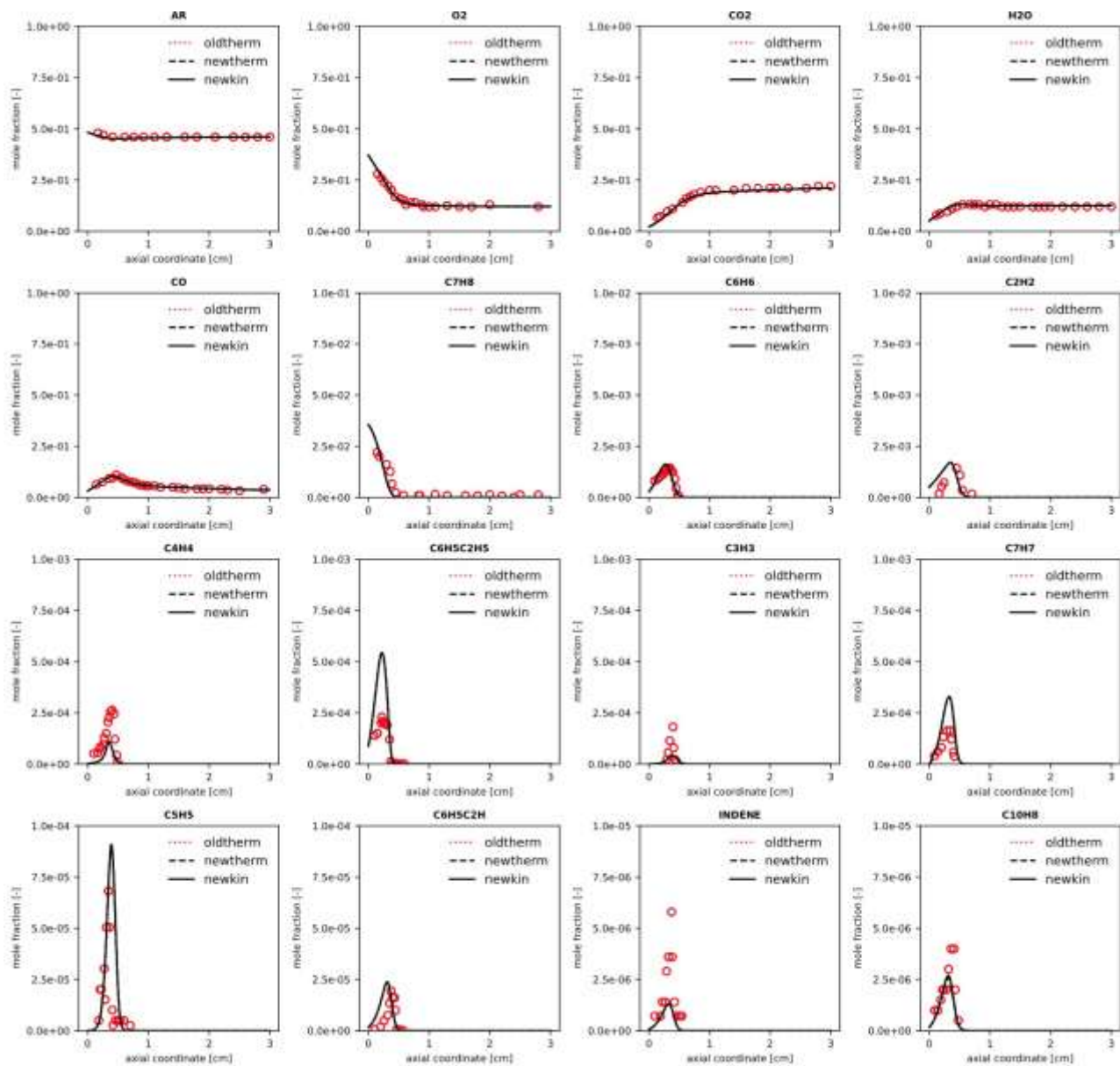


Figure S33: Experimental (points) and simulated (lines) mole fraction profiles of relevant detected products in the toluene oxidation experiments in the premixed flame of Li et al.²¹ ($\phi = 0.75$). Dotted red lines: starting model (oldtherm), dashed black lines: updated thermochemistry (newtherm), solid black lines: final model with updated kinetics (newkin). *Plot generated automatically with SciExpeM post-processing tools.

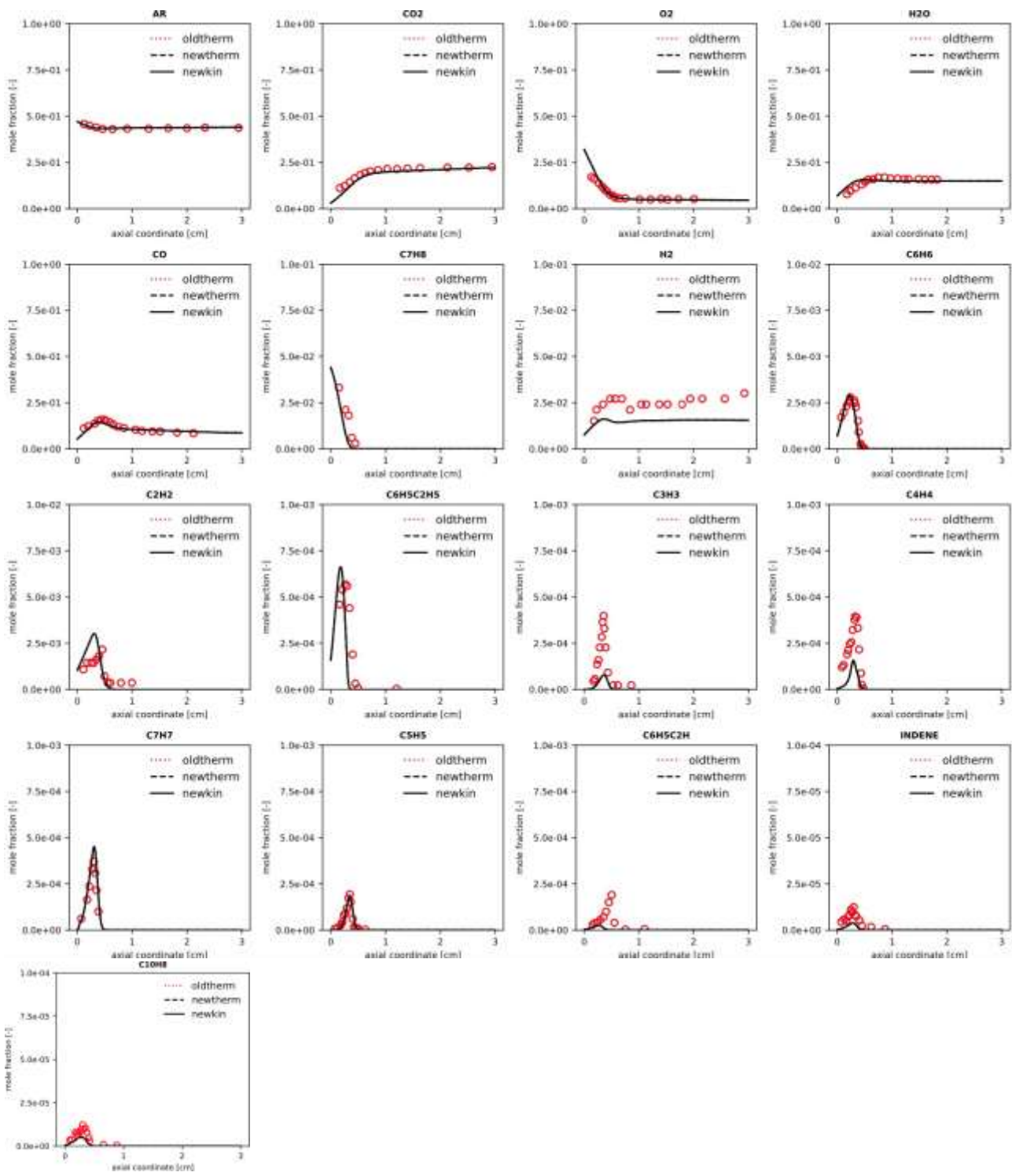


Figure S34: Experimental (points) and simulated (lines) mole fraction profiles of relevant detected products in the toluene oxidation experiments in the premixed flame of Li et al.²¹ ($\phi = 1.0$). Dotted red lines: starting model (oldtherm), dashed black lines: updated thermochemistry (newtherm), solid black lines: final model with updated kinetics (newkin). *Plot generated automatically with SciExpeM post-processing tools.

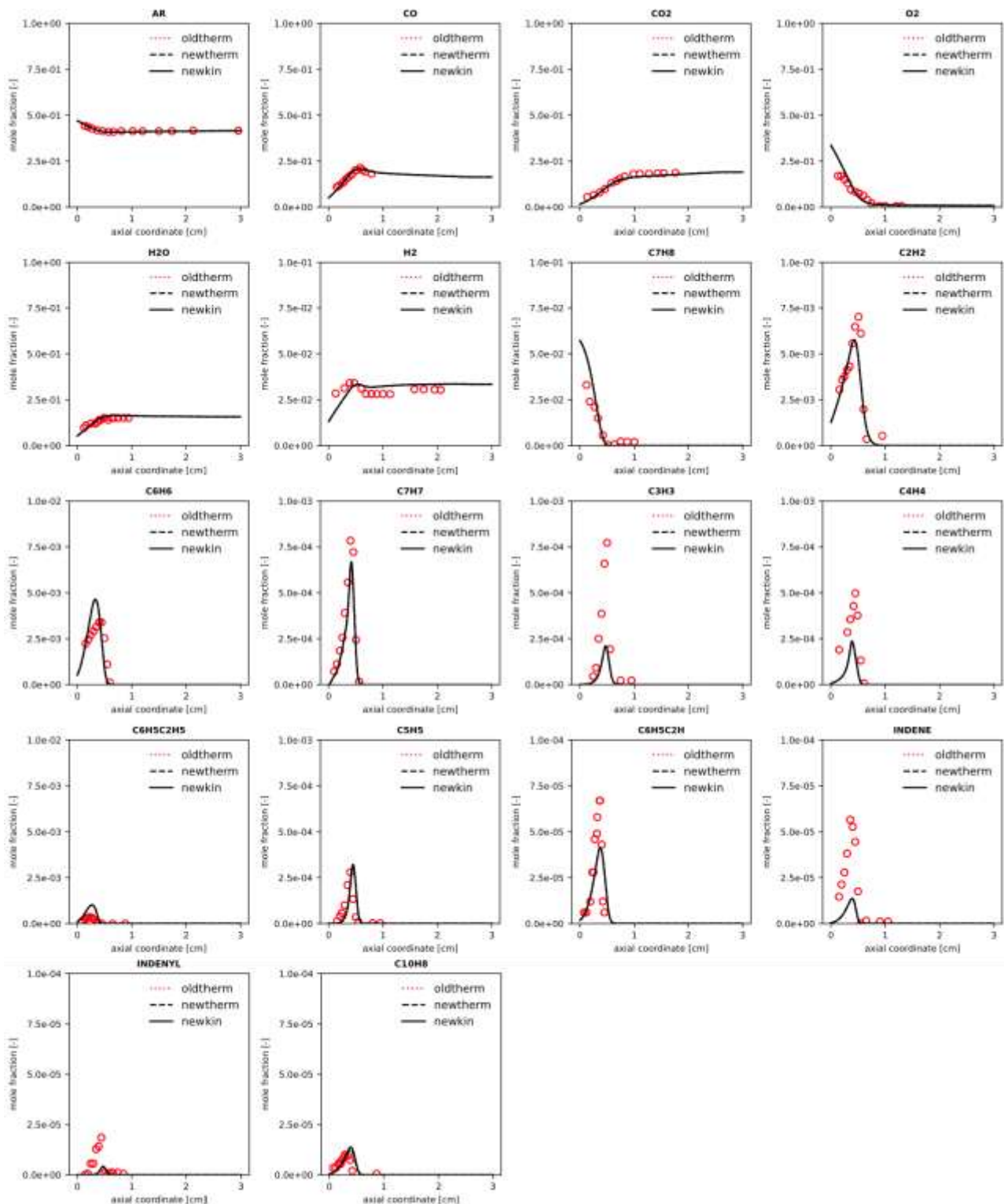


Figure S35: Experimental (points) and simulated (lines) mole fraction profiles of relevant detected products in the toluene oxidation experiments in the premixed flame of Li et al.²¹ ($\phi = 1.25$). Dotted red lines: starting model (oldtherm), dashed black lines: updated thermochemistry (newtherm), solid black lines: final model with updated kinetics (newkin). *Plot generated automatically with SciExpeM post-processing tools.

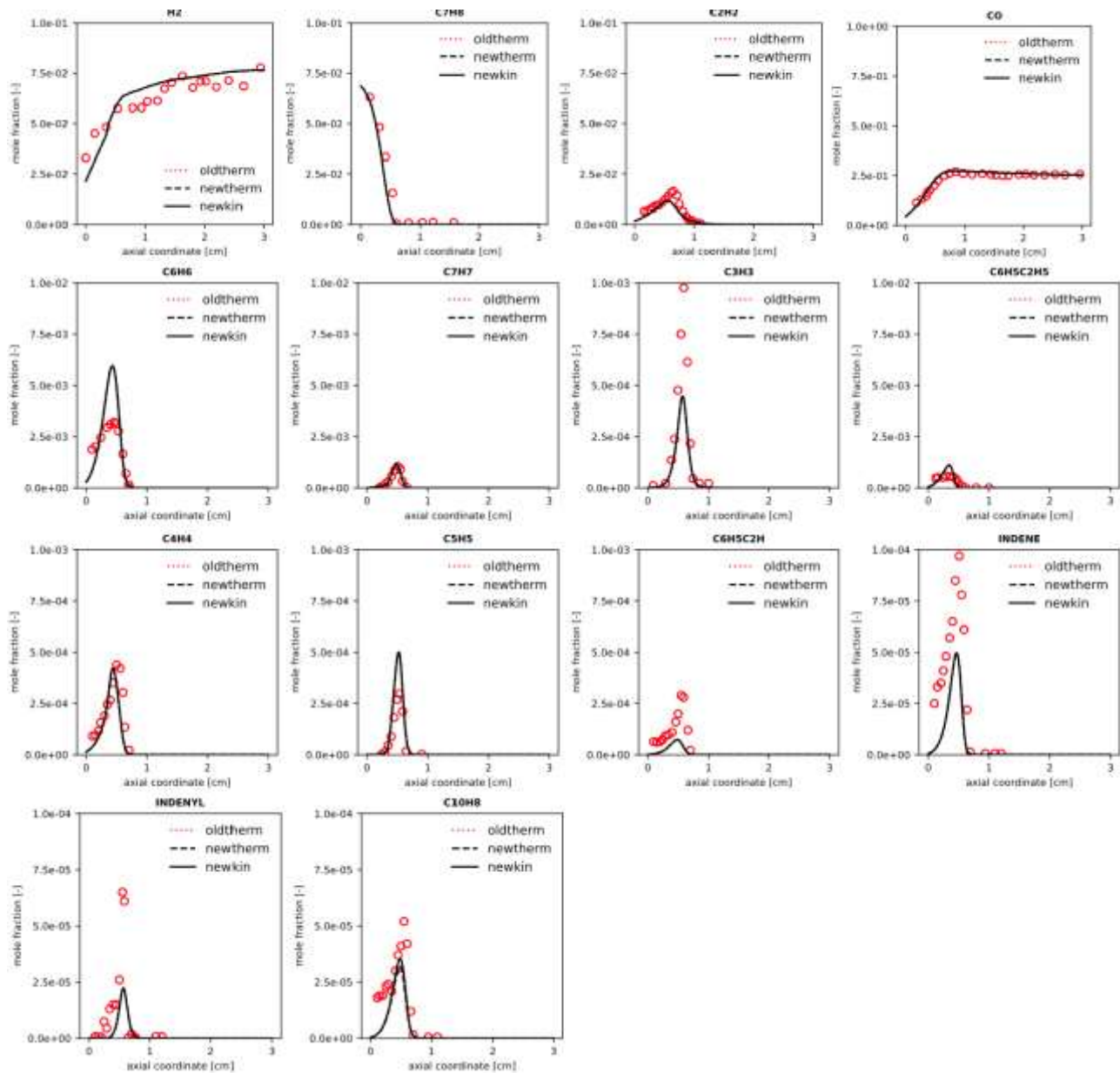


Figure S36: Experimental (points) and simulated (lines) mole fraction profiles of relevant detected products in the toluene oxidation experiments in the premixed flame of Li et al.²² ($\phi = 1.5$). Dotted red lines: starting model (oldtherm), dashed black lines: updated thermochemistry (newtherm), solid black lines: final model with updated kinetics (newkin). *Plot generated automatically with SciExpeM post-processing tools.

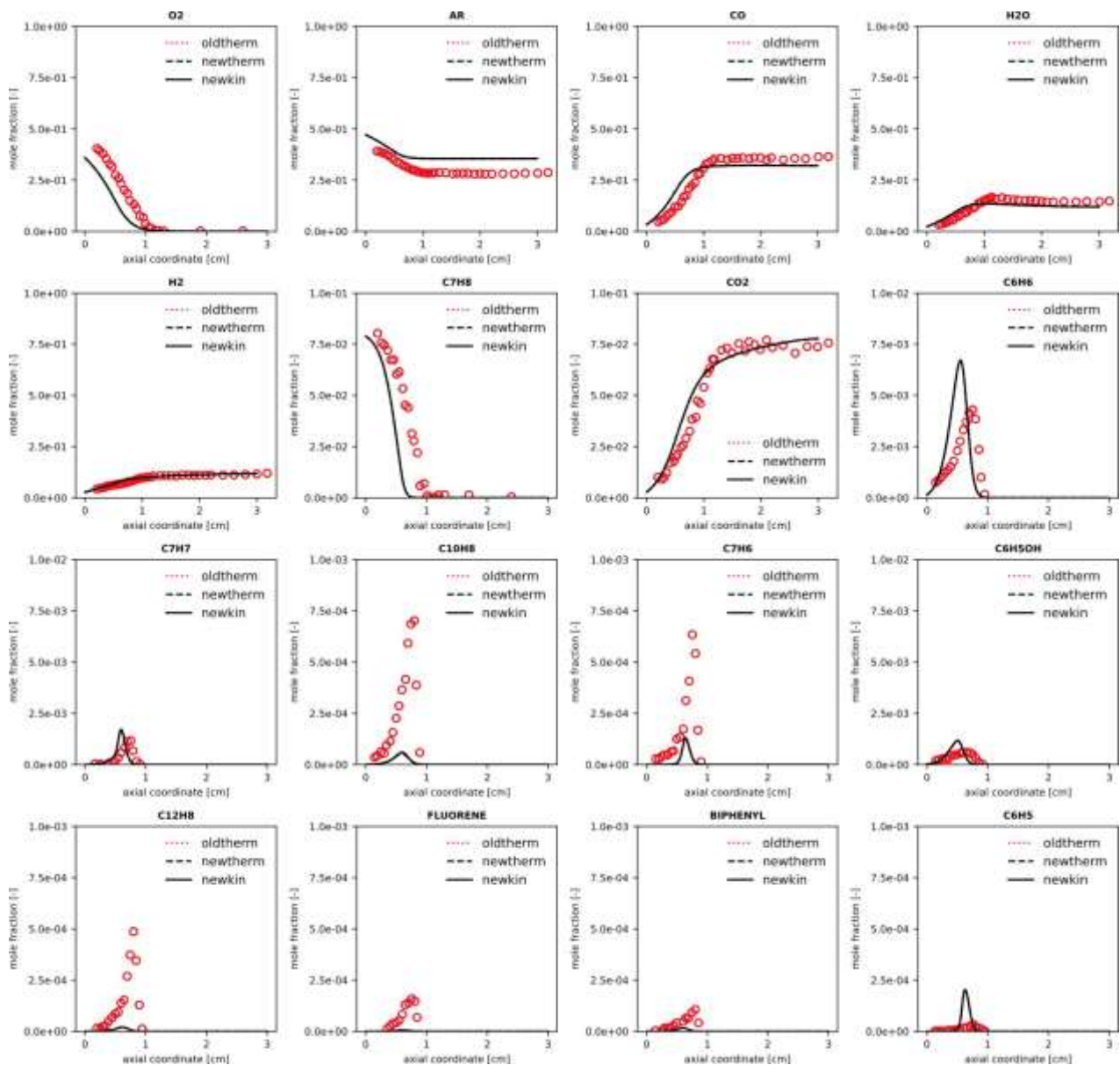
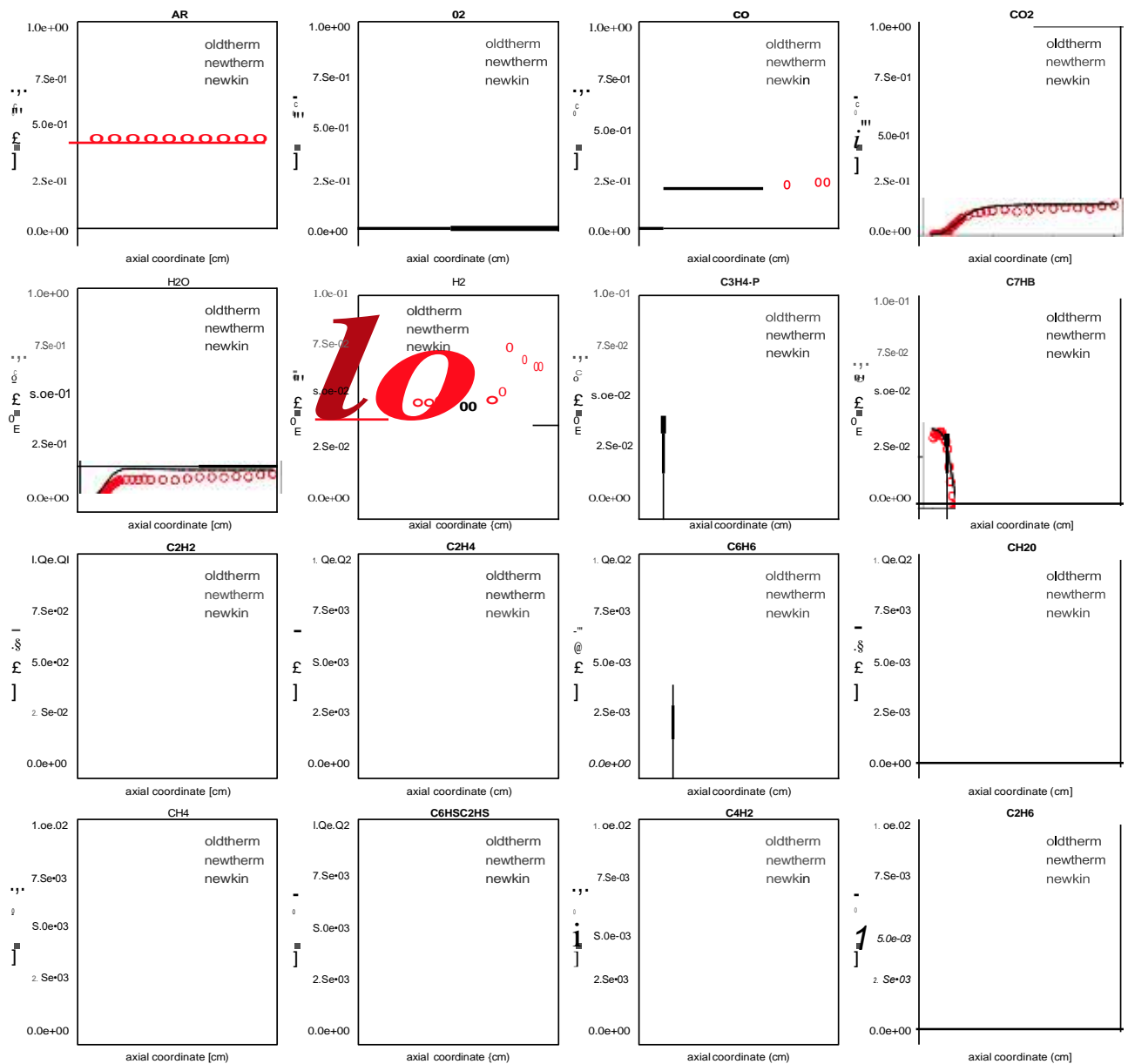
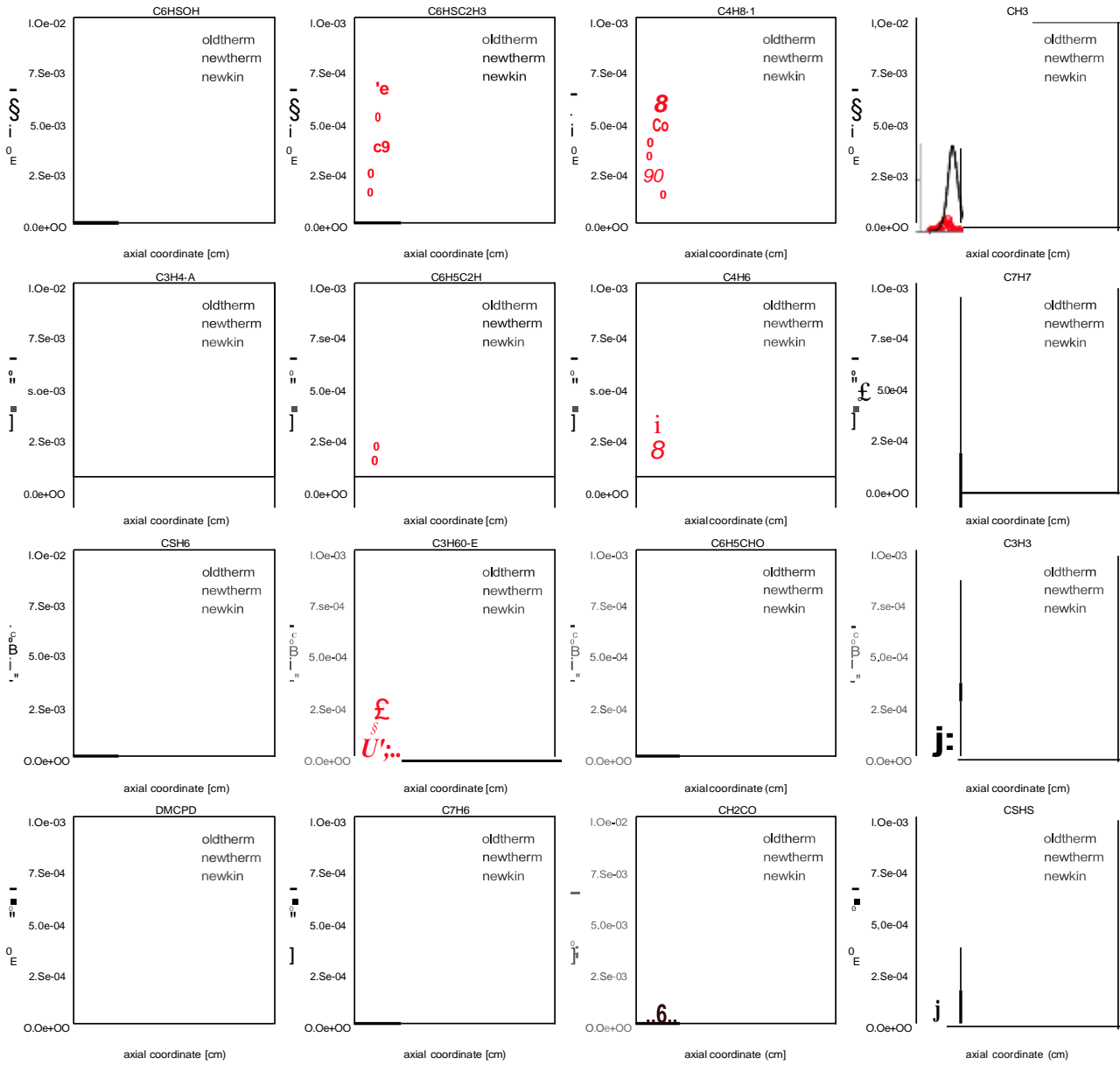
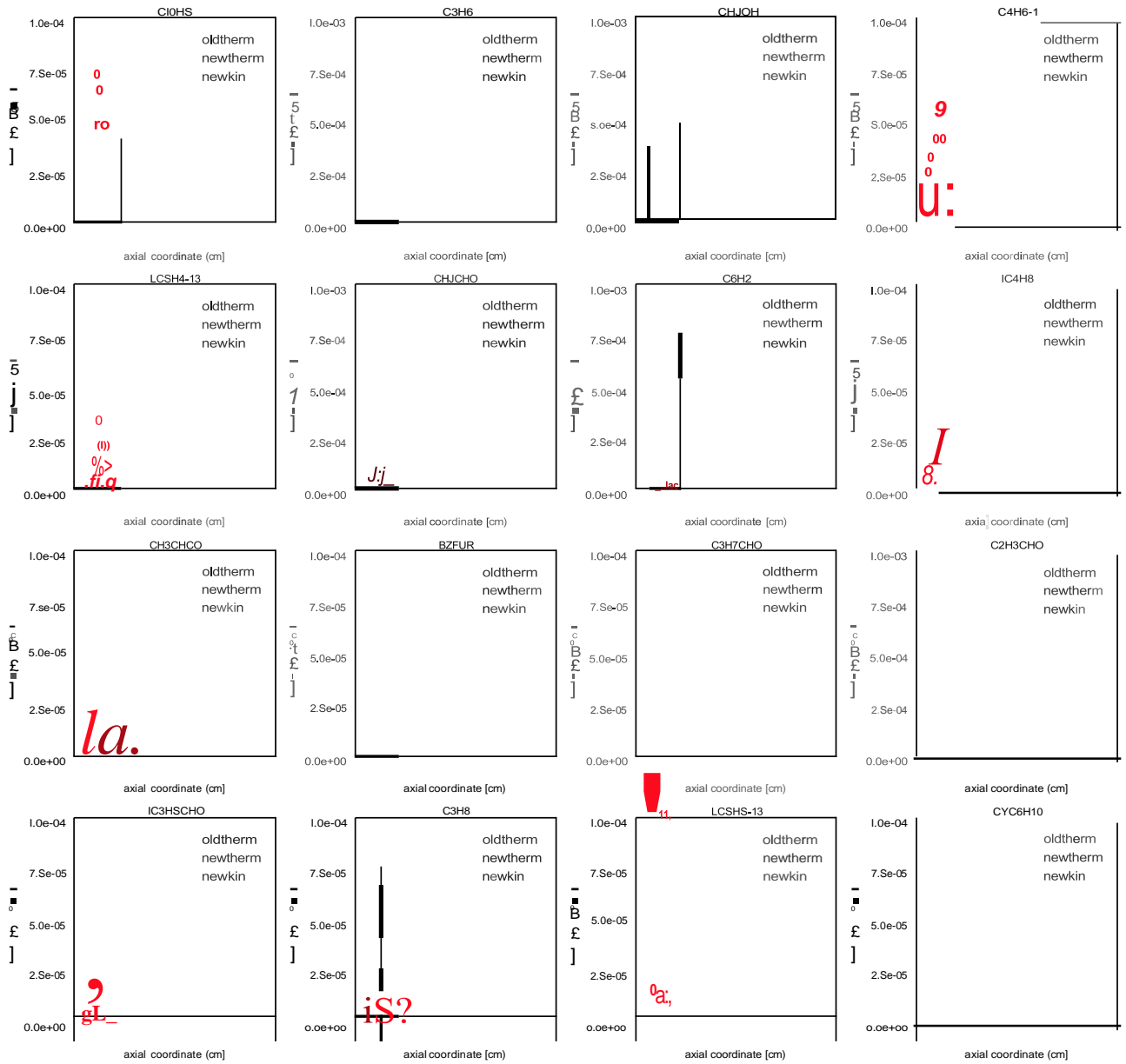


Figure S37: Experimental (points) and simulated (lines) mole fraction profiles of relevant detected products in the toluene oxidation experiments in the premixed flame of Li et al.²² ($\phi = 1.9$). Dotted red lines: starting model (oldtherm), dashed black lines: updated thermochemistry (newtherm), solid black lines: final model with updated kinetics (newkin). *Plot generated automatically with SciExpeM post-processing tools.

C7H8/C3H4-P	PF	500-2200	0.04	1.5	Hansen et al. ²³
-------------	----	----------	------	-----	-----------------------------







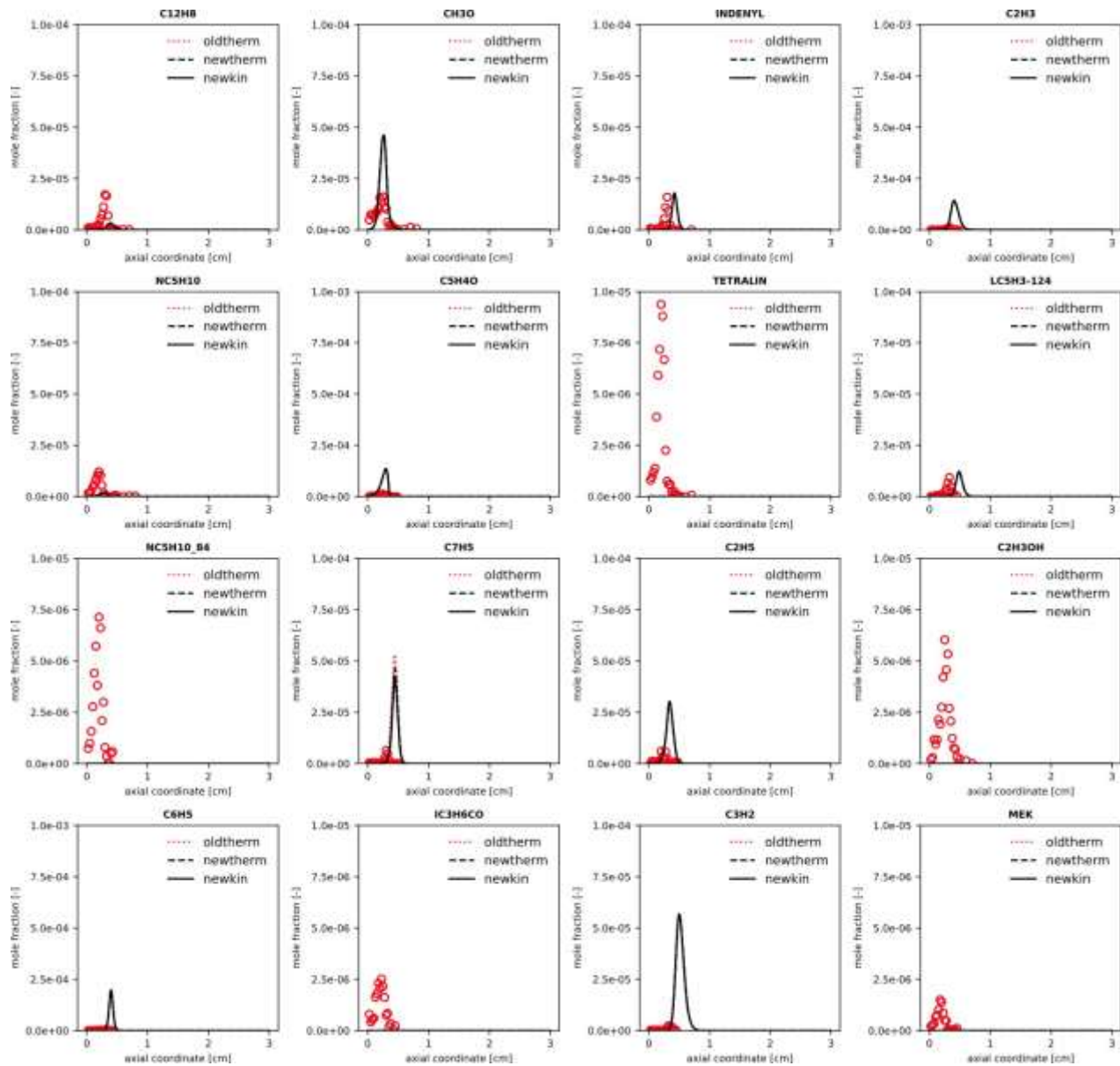
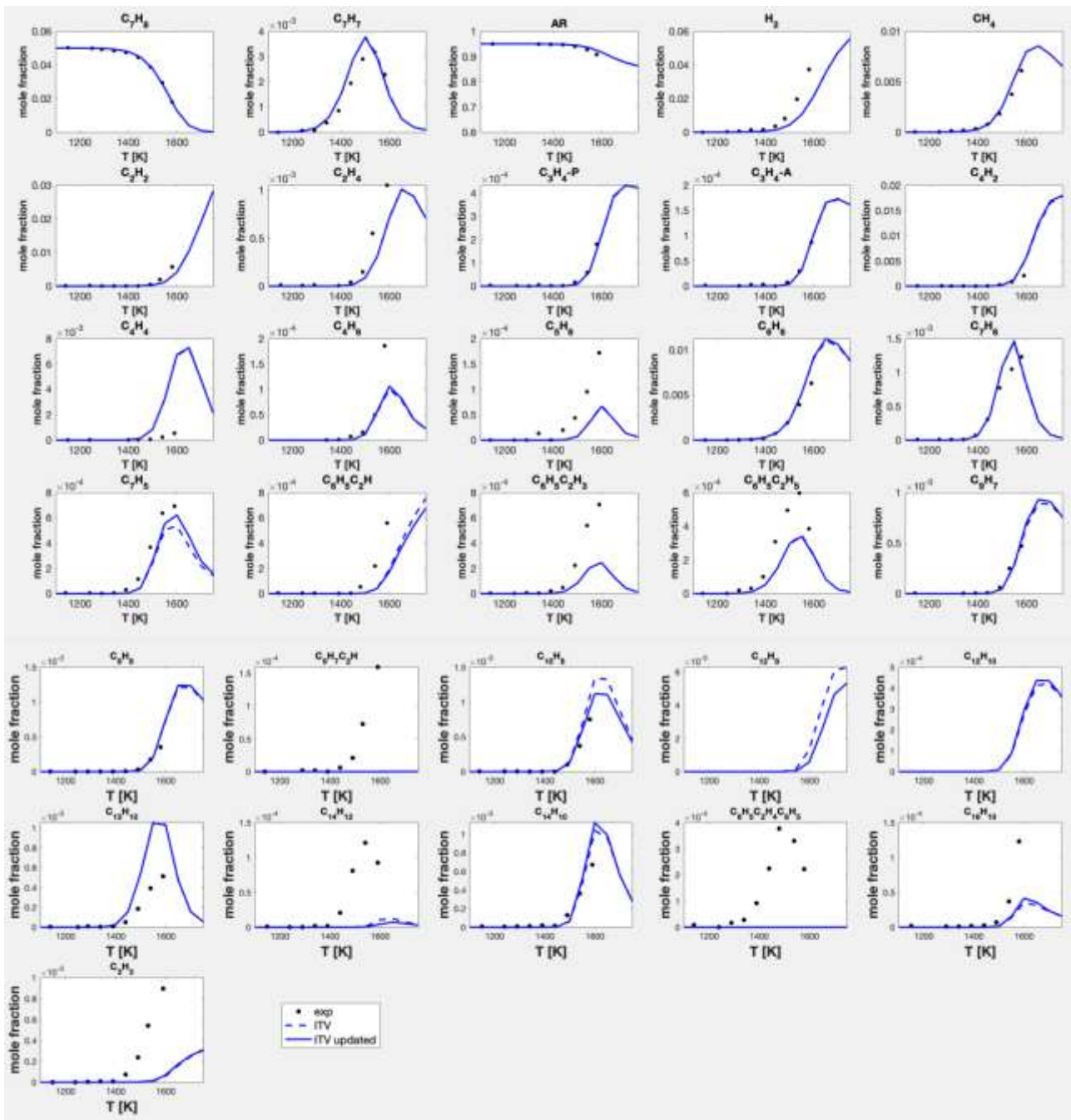


Figure S38: Experimental (points) and simulated (lines) mole fraction profiles of relevant detected products in the propyne-doped toluene oxidation experiments in the premixed flame of Hansen et al.²³. Dotted red lines: starting model (oldtherm), dashed black lines: updated thermochemistry (newtherm), solid black lines: final model with updated kinetics (newkin). *Plot generated automatically with SciExpeM post-processing tools.

Section S.3 Simulation cases using the ITV model



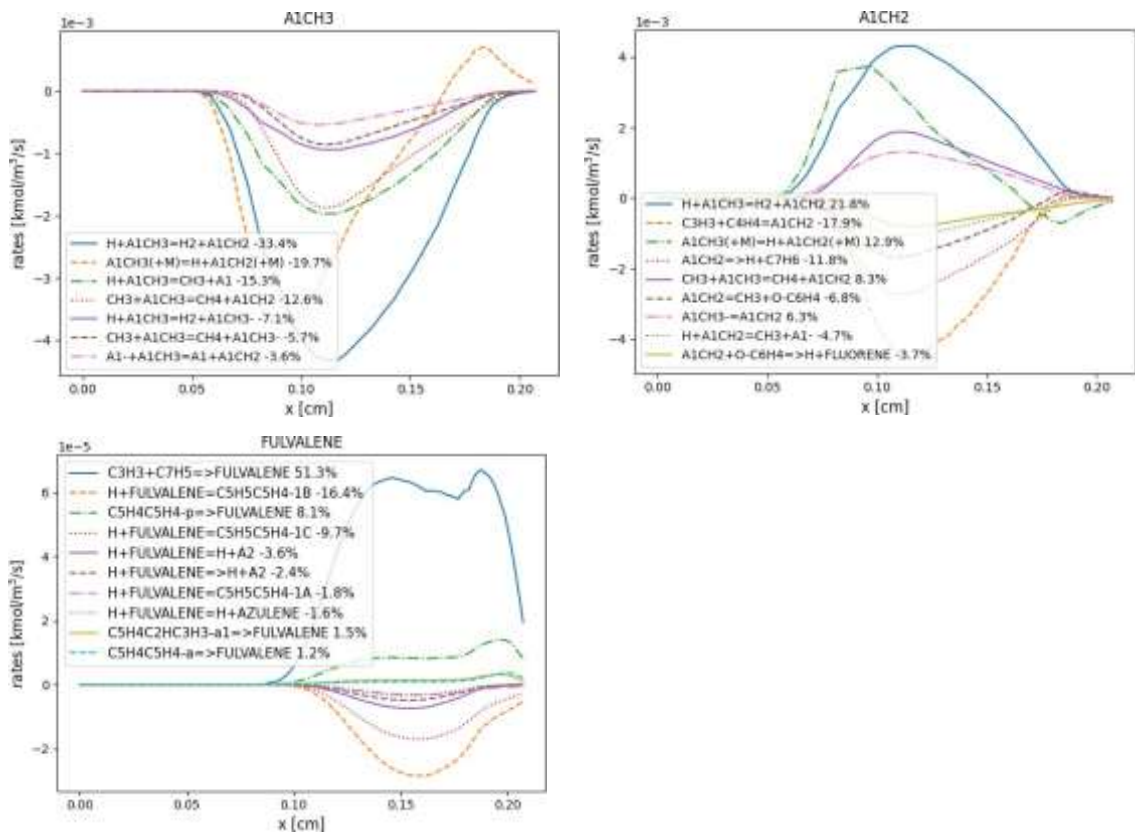
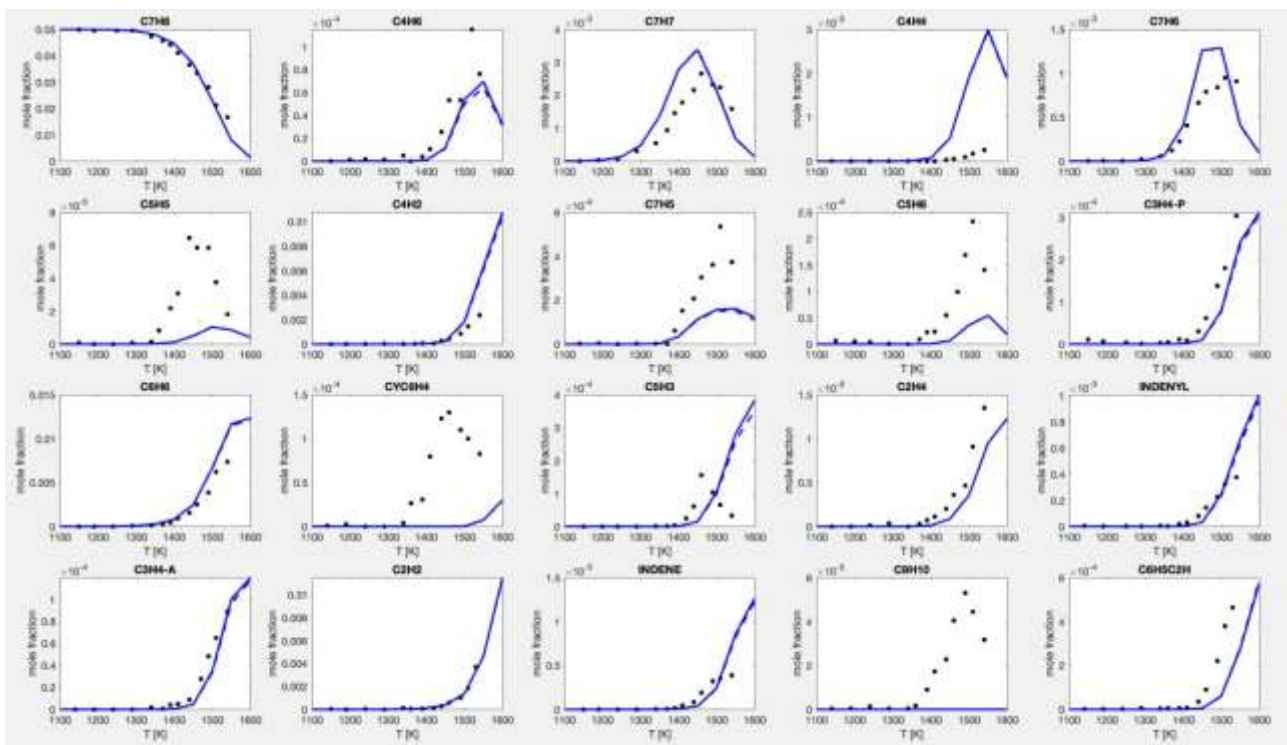


Figure S39: Experimental (points) and simulated (lines) mole fraction profiles of relevant detected products in the toluene pyrolysis experiments in the flow reactor of Yuan et al.⁸ ($p=30$ Torr). Dashed blue lines: starting model (ITV 2023), solid blue lines: final model with updated thermos and kinetics (ITV updated)



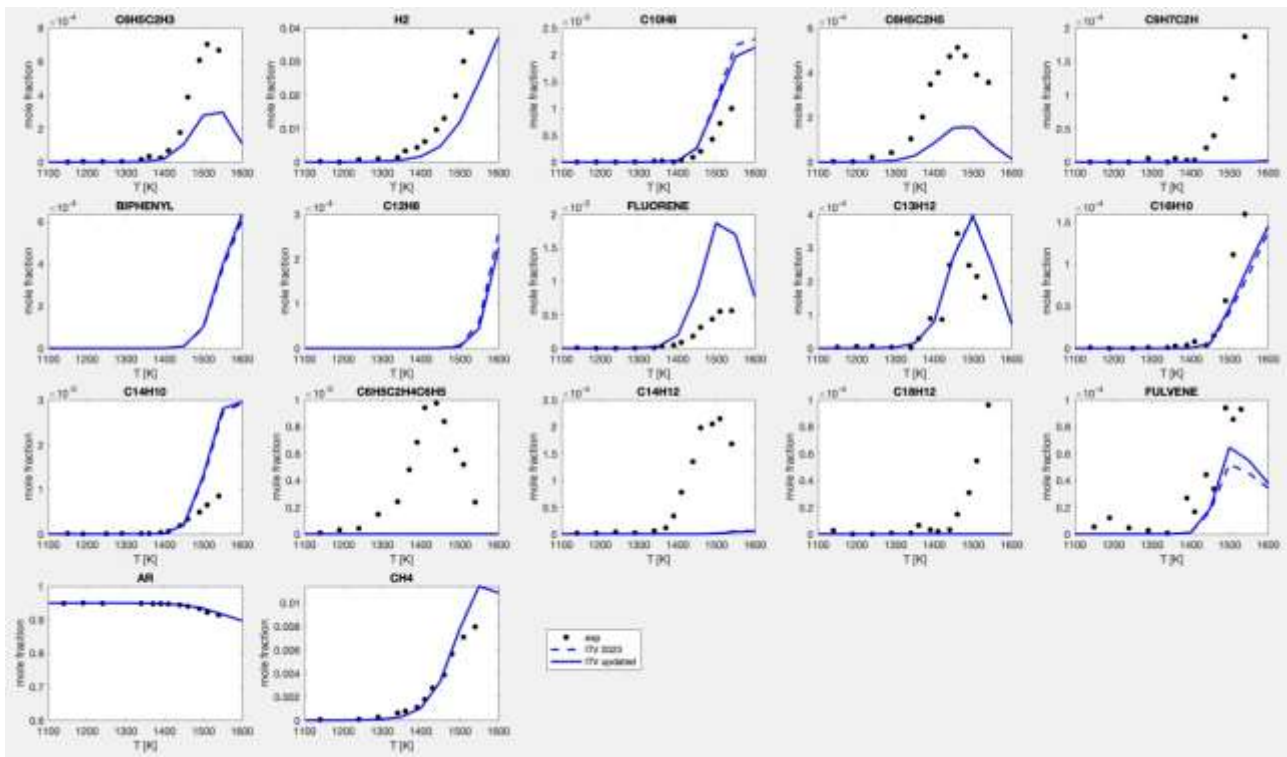
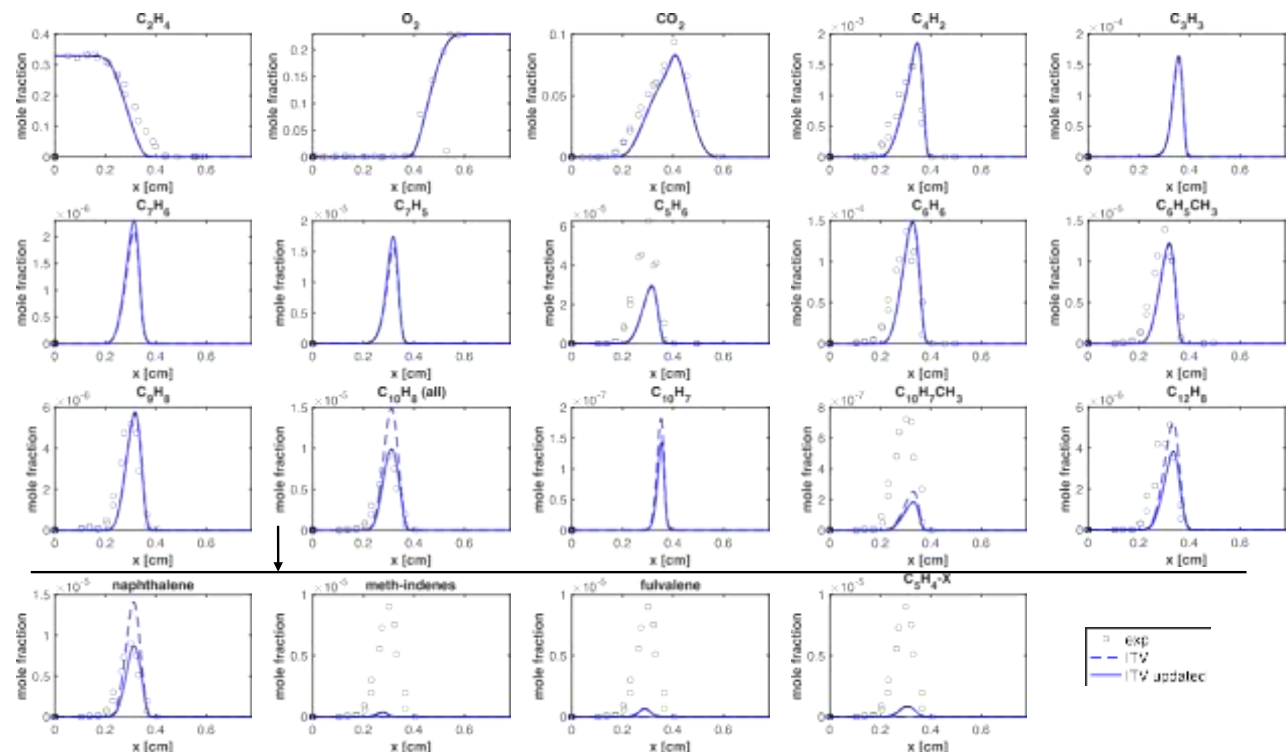


Figure S40: Experimental (points) and simulated (lines) mole fraction profiles of relevant detected products in the toluene pyrolysis experiments in the flow reactor of Yuan et al.⁸ ($p=80$ Torr). Dashed blue lines: starting model (ITV 2023), solid blue lines: final model with updated thermos and kinetics (ITV updated)



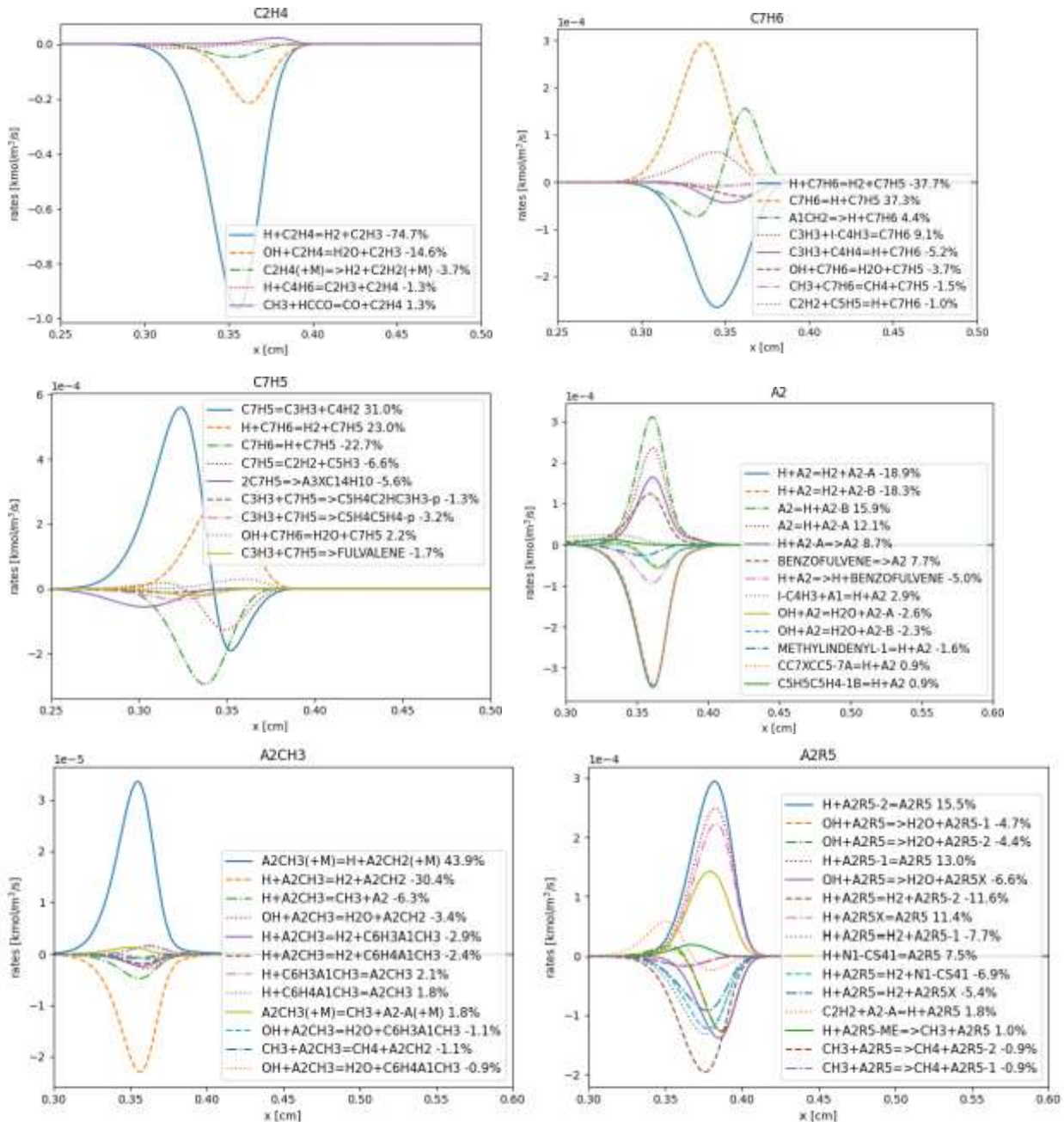


Figure S41: Experimental (points) and simulated (lines) mole fraction profiles of relevant detected products in the counterflow diffusion flame experiments of ethylene oxidation of Carbone et al.¹⁵. Dashed blue lines: starting model (ITV 2023), solid blue lines: final model with updated thermos and kinetics (ITV updated). Reaction rates for the production and consumption of ethylene, fulvenallene (C7H6), fulvenallenyl (C7H5), naphthalene (A2), methylnaphthalene (A2CH3) and acenaphthylene (A2R5) are shown at the bottom.

As for the toluene case presented in the main text, the updated kinetics results in a substantial decrease of naphthalene concentration also in ethylene counterflow flames, resulting in an improved agreement with experimental data. In the updated ITV model, methylene-indenes, fulvalene and C₅H₄-X accumulate, where the latter is even more abundant than fulvalene. However, in the ITV model fulvalene is largely consumed by H addition reactions that are instead missing for the C₅H₄-X pool. This suggests that if C₅H₄-X isomers are included in models, bimolecular reactions and in particular H-assisted isomerizations should also be considered. In addition to the accumulation of the

new isomers, the importance of the $C_7H_5 + C_3H_3$ reaction in the ITV model is supported by the large concentration of C_7H_6 and C_7H_5 species. Nevertheless, contrary to the toluene pyrolysis case, in the ITV model the fulvenallenyl radical concentration is about one order of magnitude larger than its molecular counterpart, suggesting the need to revise the main production and consumption pathways of this species. In fact, similar trends (i.e., C_7H_5 concentration being higher than C_7H_6 by factors of 2 – 10) are common to all simulated flames but they are in contrast with the only experimental measurement of both species in a flame (see Fig S38), as well as with the general ratios of molecule/radical equilibria.

The reaction rate analyses in Figure S41 shows reaction rates for the ethylene, fulvenallene and fulvenallenyl radical according to the updated ITV model. It is noted that both the core chemistry and several reaction pathways for MAH and PAH formation differ substantially in the CRECK (see main text and Figure S25) and ITV models. Even in terms of ethylene consumption, H-abstractions are the main consumption pathways in both models, however in the ITV model the abstraction by OH plays a less relevant role. The onset of fulvenallene but especially of fulvenallenyl production starts earlier than in the CRECK model. C_7H_6 formation and is dominated by the $C_7H_5 + H$ pathway. Additionally, consumption by H-atom abstraction reactions plays a major role on the fuel side, while recombination with H to produce benzyl is less relevant than in the CRECK model. Another relevant production pathway is the $C_3H_3 + C_4H_3$ reaction, which in the CRECK model only produces about 3% of fulvalene possibly due to the smaller concentration of the associated radical, as it can be inferred from the simulated profiles of the parent C_4H_2 molecule. Consistent with this observation, on the fuel side fulvenallenyl is mostly produced by $C_3H_3 + C_4H_2$ and $C_3H_3 + C_4H_3$ reactions and it is partially consumed by growth reactions. C_7H_5 self-recombination consumes about 5.5% of fulvenallenyl; as soon as propargyl radical becomes available, the updated reactions on $C_7H_5 + C_3H_3$ PES also activate, consuming about 6% of fulvenallenyl in total. It is noted that the channel to $C_5H_4C_5H_4-p$ activates first, as expected from the lower temperatures of the flame zone of interest, while towards the temperature peak of the flame the formation of $C_5H_4C_3HC_3H_3-p$ and fulvalene also play a role. The updated reactivity leads to a much lower naphthalene production compared to the original model, such that the added reaction pathways do not appear among the most important production reactions of naphthalene in the rate of production analysis (see Figure S41). Finally, similar to the CRECK model, the updated kinetics leads to a decrease in both methylnaphthalene and acenaphthylene. In this case, the fraction of toluene does not change in kinetic simulations. Therefore, the reduction in these two species can be attributed largely to the decrease in naphthalene and naphthyl radicals, which are also relevant precursors of these PAHs .

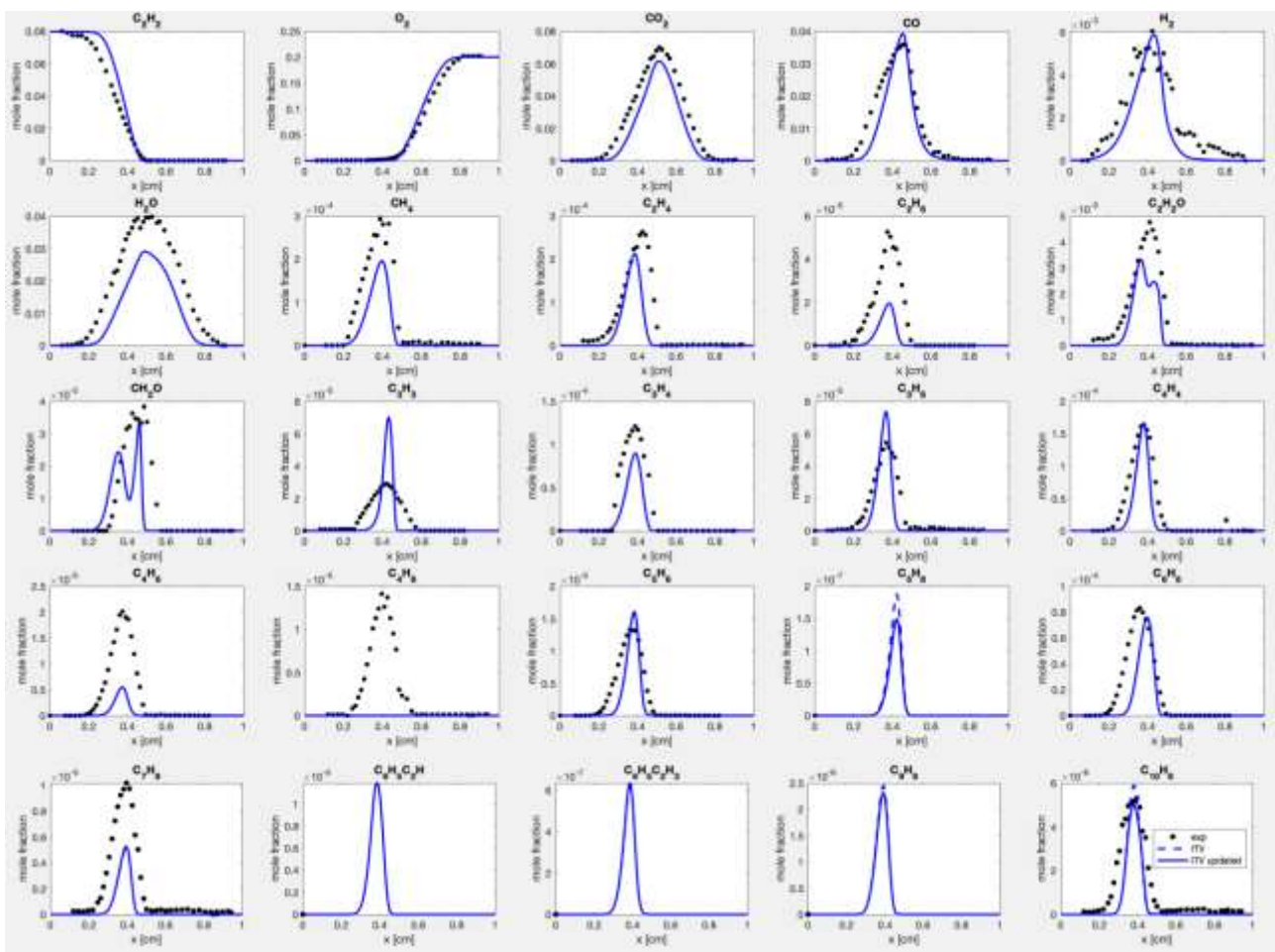


Figure S42: Experimental (points) and simulated (lines) mole fraction profiles of relevant detected products in the counterflow diffusion flame experiments of Baroncelli et al.¹¹. Dashed blue lines: starting model (ITV 2023), solid blue lines: final model with updated thermos and kinetics (ITV updated)

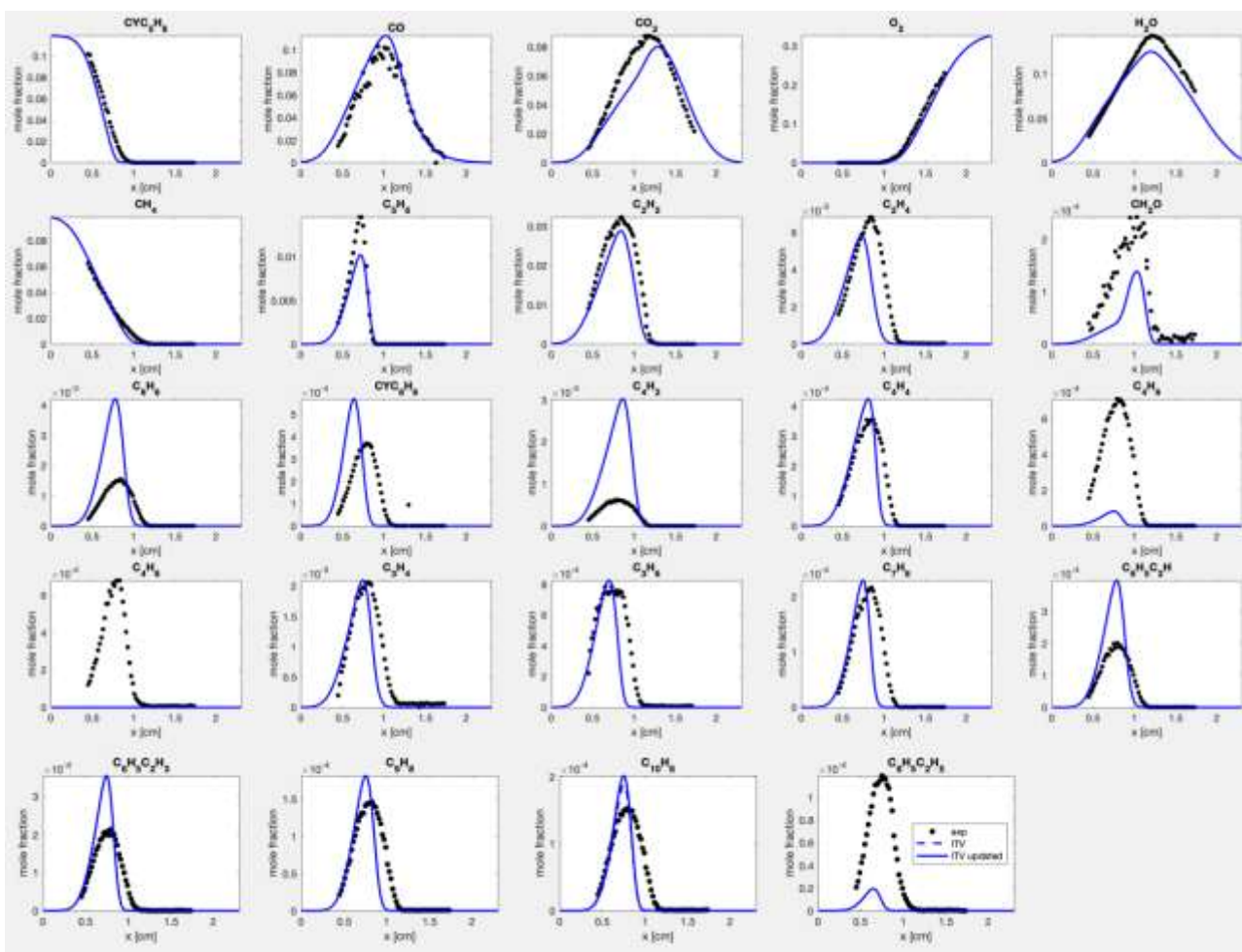
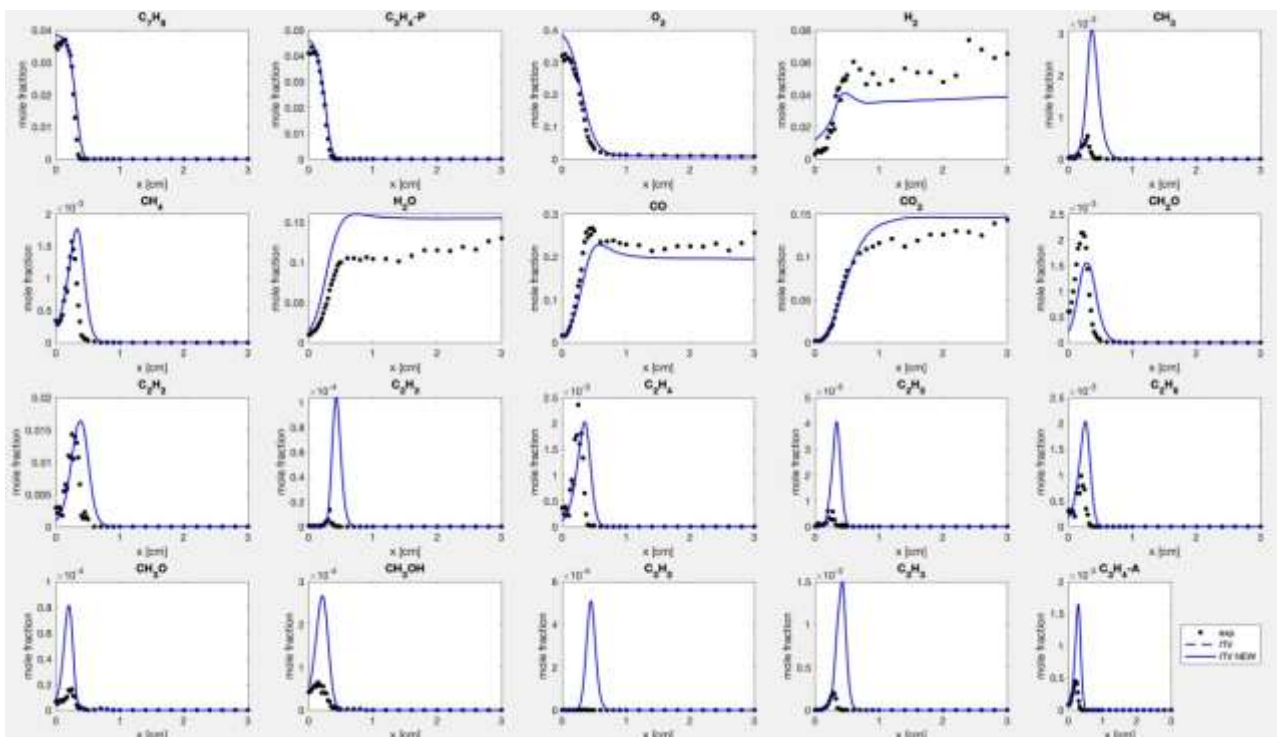
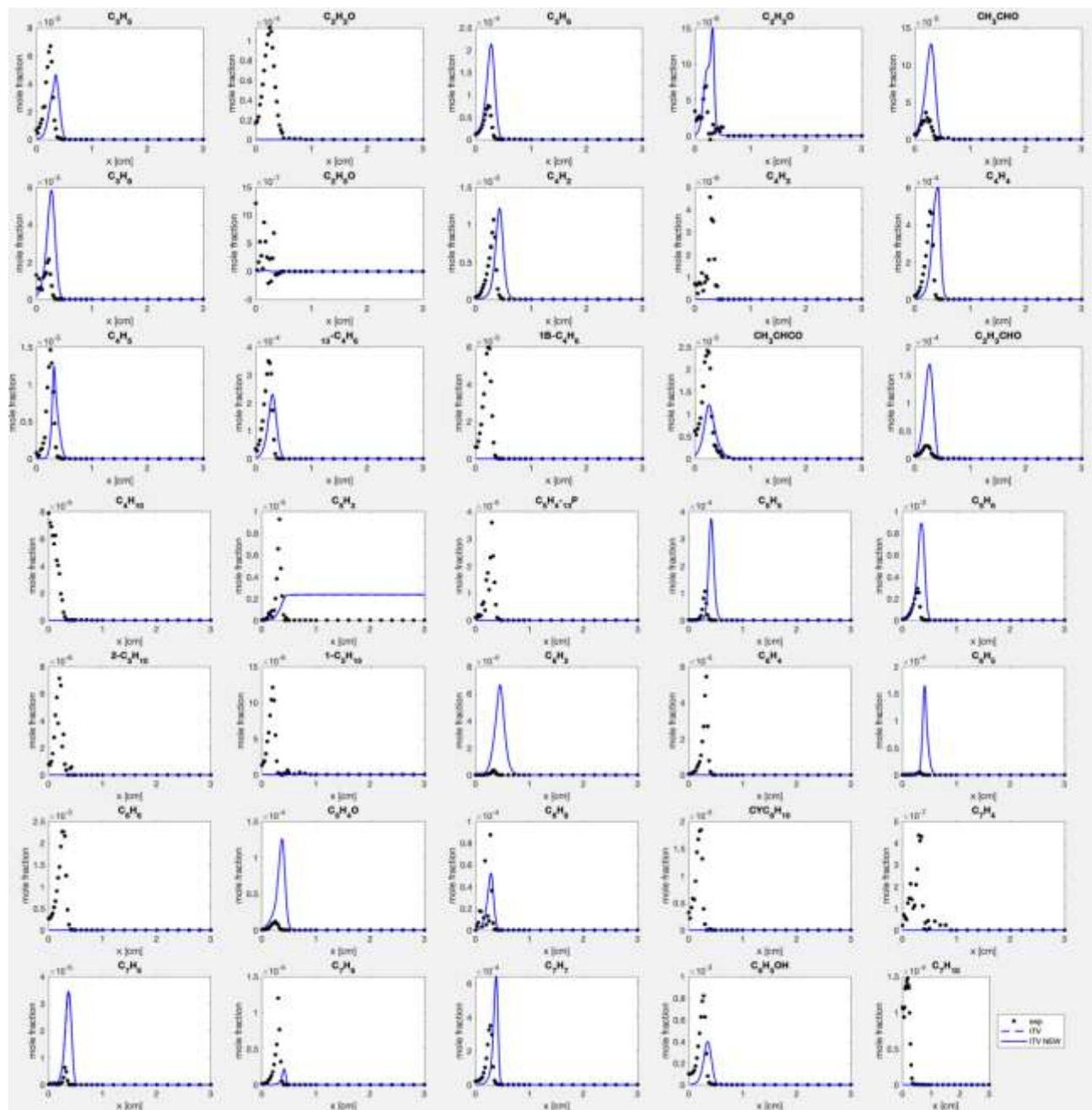


Figure S43: Experimental (points) and simulated (lines) mole fraction profiles of relevant detected products in the counterflow diffusion flame experiments of methane-doped cyclopentene oxidation of Baroncelli et al.²⁰. Dashed blue lines: starting model (ITV 2023), solid blue lines: final model with updated thermos and kinetics (ITV updated)





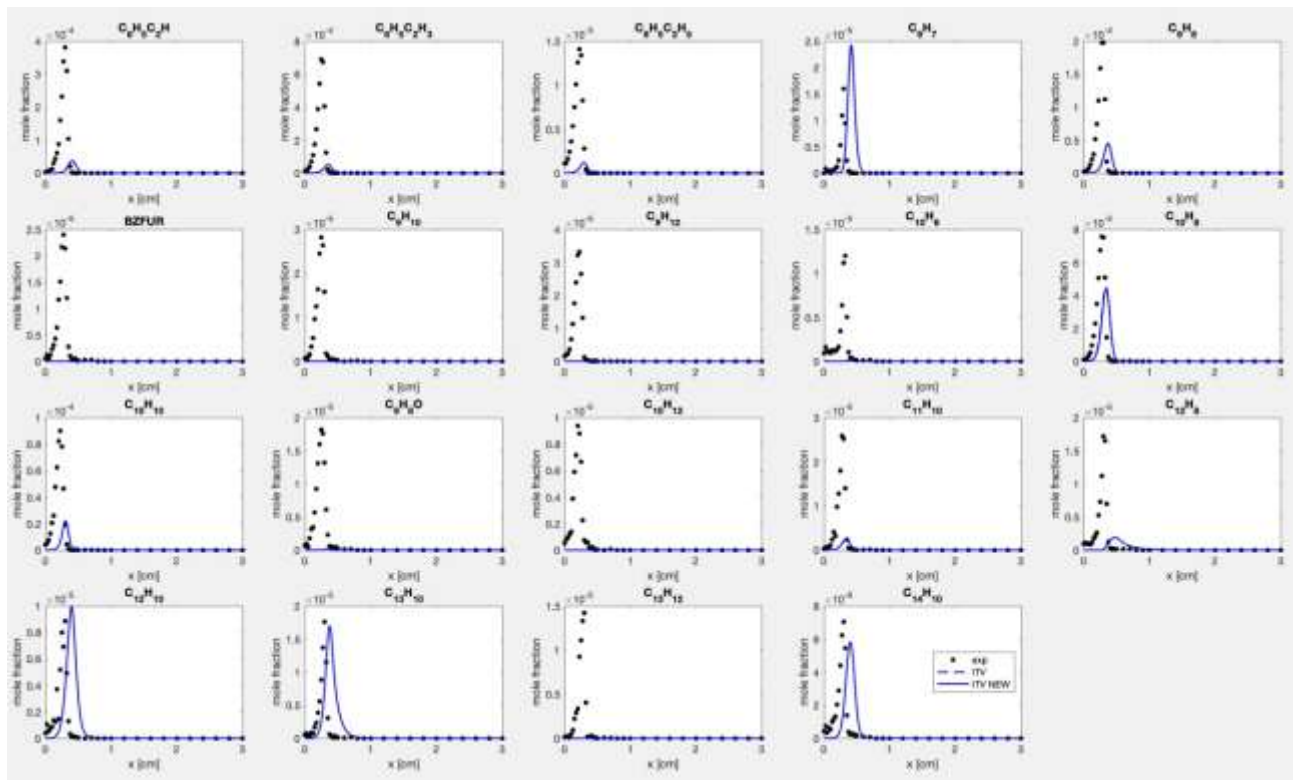


Figure S44: Experimental (points) and simulated (lines) mole fraction profiles of relevant detected products in the laminar premixed flame experiments of proyne-doped toluene oxidation of Hansen et al.²³. Dashed blue lines: starting model (ITV 2023), solid blue lines: final model with updated thermos and kinetics (ITV updated)

References

1. W. Sun, A. Hamadi , S. Abid, N. Chaumeix and A. Comandini, *Combustion and Flame*, 2021, **231**, 111485.
2. A. J. Vervust, M. R. Djokic, S. S. Merchant, H.-H. Carstensen, A. E. Long, G. B. Marin and W. H. Green, *Energy & Fuels*, 2018, **32**, 3920--3934.
3. M. R. Djokic, K. Van Geem, C. Cavallotti, A. Frassoldati, E. Ranzi and G. B. Marin, *Combustion and Flame*, 2014, **161**, 2739--2751.
4. A. Hamadi, L. Carneiro Piton, S. Abid, N. Chaumeix and A. Comandini, *Proceedings of the Combustion Institute*, 2023, **39**, 95-104.
5. W. Sun, A. Hamadi, S. Abid, N. Chaumeix and A. Comandini, *Proceedings of the Combustion Institute*, 2021, **38**, 891--900.
6. W. Sun, A. Hamadi, S. Abid , N. Chaumeix and A. Comandini *Combustion and Flame*, 2022, **236**, 111799.
7. W. Sun, A. Hamadi, S. Abid, N. Chaumeix and A. Comandini *Combustion and Flame*, 2021, **226**, 129--142.
8. W. Yuan, Y. Li , P. Dagaut, Yang, Jiuzhong and F. Qi *Combustion and Flame*, 2015, **162**, 3--21.
9. I. Meziane, N. Delort , O. Herbinet, R. Bounaceur and F. Battin-Leclerc, *Combustion and Flame*, 2023, **257**, 113046.
10. T. Bierkandt, T. Kasper, E. Akyildiz, A. Lucassen and P. Owald, *Proceedings of the Combustion Institute*, 2015, **35**, 803--811.
11. M. Baroncelli, D. Felsmann, N. Hansen and H. Pitsch, *Combustion and Flame*, 2019, **204**, 320-330.
12. Y. Li, L. Zhang, Z. Tian, T. Yuan, K. Zhang , B. Yang and F. Qi, *Proceedings of the Combustion Institute*, 2009, **32**, 1293--1300.
13. M. J. Castaldi, N. M. Marinov, C. F. Melius, J. Huang , S. M. Senkan , W. J. Pitz and C. K. Westbrook, *Symposium (International) on Combustion*, 1996, **26**, 693--702.
14. S. J. Harris, A. M. Weiner and R. J. Blint *Combustion and Flame*, 1988, **72**, 91--109.
15. F. Carbone, F. Cattaneo and A. Gomez, *Combustion and Flame*, 2015, **162**, 4138-4148.
16. N. Hansen, J. Miller, A., P. R. Westmoreland, T. Kasper, K. Kohse-Höinghaus , J. Wang and T. A. Cool, *Combustion and Flame*, 2009, **156**, 2153-2164.
17. G. Kukkadapu, S. W. Wagnon, W. J. Pitz and N. Hansen *Proceedings of the Combustion Institute*, 2021, **38**, 1477--1485.
18. J. A. Cole, J. D. Bittner , J. P. Longwell and J. B. Howard *Combustion and Flame*, 1984, **56**, 51--70.
19. N. Hansen, T. Kasper, S. J. Klippenstein , P. Westmoreland, R. M. E. Law , C. A. Taatjes, Kohse-Höinghaus, K. Wang , J. Wang and T. A. Cool, *Journal of Physical Chemistry A*, 2007, **111**, 4081-4092.
20. M. Baroncelli, Q. Mao, S. Galle, N. Hansen and H. Pitsch, *Physical Chemistry Chemical Physics*, 2020, **22**, 4699-4714.
21. Y. Li, J. Cai, L. Zhang, T. Yuan, K. Zhang and F. Qi, *Proceedings of the Combustion Institute*, 2011, **33**, 593--600.
22. Y. Li, L. Zhang, Z. Tian, T. Yuan, J. Wang, B. Yang and F. Qi *Energy and Fuels*, 2009, **23**, 1473--1485.
23. N. Hansen, B. Yang, M. Braun-Unkhoff, A. Ramirez and G. Kukkadapu, *Combustion and Flame*, 2022, **243**, 112075.